Methods to Assess Pulmonary Metabolism

Inauguraldissertation

zur

Erlangung der Würde eines Doktors der Philosophie vorgelegt der

Philosophisch-Naturwissenschaftlichen Fakultät der Universität Basel

von

Yildiz Yilmaz

aus Liestal, Baselland

Basel, 2019

Originaldokument gespeichert auf dem Dokumentenserver der Universität Basel

edoc.unibas.ch

Genehmigt von der Philosophisch-Naturwissenschaftlichen
Fakultät auf Antrag von

Prof. Dr. Stephan Krähenbühl (Fakultätsverantwortlicher)
Dr. Gian Camenisch (Dissertationsleiter)
Prof. Dr. Michael Arand (Korreferent)

Basel, den 16. Oktober 2018

Prof. Dr. Martin Spiess
(Dekan)

This work was performed in collaboration with the Clinical Pharmacology and Toxicology Department at the University of Basel and the Human ADME Biotransformation, PK Sciences group at Novartis Institutes for BioMedical Research Basel, Switzerland.

Acknowledgments

I would first like to express my thanks to Prof. Dr. Dr. med. Stephan Krähenbühl for being the academic supervisor. I highly appreciated his scientific discussions, reviews of written publications and his overall support.

A big thanks to Dr. Gian Camenisch, director of PKS ADME Biotransformation Discovery at Novartis, who contributed to the successful development of this project. Without his management and sponsorship, the project would not have been realizable as an industrial doctorate.

I address special thanks to Dr. Markus Walles, who was my industrial supervisor. He contributed a lot to my professional education and personal growth. I highly appreciated his time, support and patience for my questions.

I am very grateful to Gareth Williams supervision for his manuscript writing, finding always solutions for laboratorial issues and giving me the possibility to look at the problems from different angles. Without his contribution to the authored publications, the papers would not have been engaging.

Further, I would like to thank Dr. Kenichi Umehara for his time of industrial supervision, who educated me on how to think scientifically and how to be skeptical to science. I`m grateful for his contribution to my education in quantitative analytics. In addition, his support helped me to be an organized and structured scientist.

I would like to acknowledge Prof. Dr. Michael Arand for agreeing to be the Korreferent of my thesis.

Finally I want to extend my thanks to the former DMPK, former MAP, new ADME Biotransformation group at Novartis and my PhD colleagues in Clinical Pharmacology and Toxicology group, who contributed to the successful development of this work and for supporting me in getting through this adventure.

“Poison is in everything, and no thing is without poison.
The dosage makes it either a poison or a remedy.”

Paracelsus

Table of contents

Abbreviations

ABT	=	1-aminobenzotriazole
ADME	=	Absorption, distribution, metabolism, and excretion
AhR	=	Aryl hydrocarbon receptor
AO	=	Aldehyde oxidase
AUC	=	Area under the blood concentration-time curve
$AUC_{i.a.}$	=	AUC following intra-arterial dosing
$AUC_{0\text{-}inf}$	=	AUC from time zero to infinity
$AUC_{i.v.}$	=	AUC following intravenous dosing
CAR	=	Constitutive androstane receptors
CE	=	Collision energy
CES1	=	Carboxylesterase 1
CID	=	Collision induced dissociation
$CL_{int,\textit{in vitro}}$	=	*In vitro* intrinsic clearance
$CL_{int,organ}$	=	Intrinsic clearance of whole organ
CL_{lung}	=	Lung clearance
CL_{blood}	=	Blood clearance
COPD	=	Chronic obstructive pulmonary disease
CV	=	Cone voltage
CYP	=	Cytochrome P450
DMSO	=	Dimethyl sulfoxide
DOC	=	Dynamic organ culture
E_{lung}	=	*In vivo* extraction ratio in lung
ESI	=	Electrospray ionization
EROD	=	7-ethoxy-resorufin-O-deethylase
FMO	=	Flavin-containing monooxygenase
fu	=	Unbound fraction of the drug in plasma
fu_{inc}	=	Unbound fraction in microsomal incubations

fu_{lung}	=	Fraction unbound in lung slices incubations
GST	=	Glutathione S-transferase
HEPES	=	4-(2-hydroxyethyl)-1-piperazineethanesulfonic acid
i.a.	=	Intra-arterial
i.v.	=	Intravenous
Km	=	Michaelis-Menten constant
LC-MS/MS	=	Liquid chromatography-tandem mass spectrometry
LLQ	=	Lower Limit of Quantitation
MEM	=	Minimal essential medium
MRM	=	Multiple reaction monitoring
MRT	=	Mean residence time
NADPH	=	β nicotinamide adenine dinucleotide phosphate reduced
NAT	=	N-acetyl transferase
NCA	=	Non-compartmental analysis
PCLS	=	Precision-cut lung slices
PK	=	Pharmacokinetic
PXR	=	Pregnane X receptors
Q_{liver}	=	Liver blood flow
Q_{lung}	=	Pulmonary blood flow
$R_{b/p}$	=	Blood/plasma ratio
SD	=	Sprague Dawley
S.D.	=	Standard deviation
S.E:	=	Standard error of the mean
SDM	=	Sulfadimethoxine
SULT	=	Sulfotransferase
λz	=	Terminal disposition rate constant
UDPGA	=	Uridine-diphosphate-glucuronic acid trisodium salt
UGT	=	Uridine 5’-diphosphoglucuronosyltransferase
UPLC	=	Ultra Performance Liquid Chromatography

V_{max}	=	Maximum rate of metabolism (limiting reaction velocity)
V_{ss}	=	Volume of distribution at steady state
WH	=	Wistar Han
4-MU	=	4-Methylumbelliferone

Chapter 1. Summary

Drug metabolism involves the biochemical modification of pharmaceutical substances or xenobiotics by living organisms, usually through specialized enzymes. This process normally converts lipophilic chemicals into less potent, and more hydrophilic products that facilitates their elimination from the body (Mittal *et al.*, 2015). However, these processes may also convert the drug into more lipophilic, more potent or even toxic metabolites (Macherey and Dansette, 2015). In order to design effective and safe dosage regimens, the pharmacology, toxicology, and drug-drug interactions of the drug and its metabolites should be thoroughly understood (Tillement and Tremblay, 2007). As a result, the study of drug metabolism is vital to the pharmaceutical industry. Drug metabolism is generally divided into two distinct phases. Phase I reactions include oxidation, reduction and hydrolysis which are mediated by enzymes such as cytochrome P450 (CYPs), flavin-containing monooxygenases (FMOs), aldehyde oxidase (AO) and various hydrolases (Shehata, 2010). In phase II metabolism, enzymes such as uridine 5′-diphosphoglucuronosyltransferase (UGT), sulfotransferase, glutathione S-transferase (GST) and N-acetyl transferase (NAT) catalyze the conjugation of drugs with endogenous molecules (Testa and Clement, 2015).

Although the liver is the primary site of drug metabolism, other organs including skin, lungs, kidneys, and intestine also possess considerable metabolic capacity (Krishna and Klotz, 1994). Furthermore, drug-metabolizing enzymes are known to be expressed in the lungs, albeit to a lesser extent than in liver (Somers *et al.*, 2007). Recent reports have highlighted the metabolic role of lungs, a highly perfused organ that is in direct contact with inhaled xenobiotics and drugs (Borghardt *et al.*, 2018). In addition, phase I enzymes such as CYP1A1 may play an important role in bioactivation of inhaled procarcinogens, such as those present in tobacco smoke (Anttila *et al.*, 2011). From the perspective of pharmacotherapy, pulmonary drug metabolism may cause a first-pass effect for inhaled medicines, as well as contribute to overall clearance of systemically administered drugs (Winkler *et al.*, 2004). Frequent exposure of the lungs to environmental xenobiotics may also lead to induction of drug-metabolizing enzymes via pregnane X receptors (PXR), constitutive androstane receptors (CAR), or aryl hydrocarbon receptors (AhR), a

phenomenon that can significantly alter the rate of drug metabolism (Tolson and Wang, 2010).

Despite the potential importance of lung metabolism for respiratory therapies, relatively little is known about the actual activity and protein abundance of drug-metabolizing enzymes in lung tissue (Hukkanen *et al.*, 2002). The lack of robustness and consistency of existing experimental models of lung metabolism leads to considerable difficulties in the interpretation and prediction of drug clearance. This project was designed to address these challenges and establish a robust and predictive experimental model for rat and human pulmonary drug metabolism. Therefore the aim of this thesis was 1) to investigate the further development of a precision-cut lung slicing (PCLS) model to accurately estimate pulmonary drug clearance in rat, 2) to examine the pulmonary metabolic activity of rat and human phase I and phase II enzymes using this model, and 3) to compare the PCLS model with currently available *in vitro* and *in vivo* experimental models in order to better understand the contribution of pulmonary metabolism to drug elimination.

1) **Establish a PCLS model to accurately estimate pulmonary drug clearance in rat**

PCLS technology is a 3D organotypic tissue model which reflects the natural and relevant microanatomy and the metabolic function of the lung (Neuhaus *et al.*, 2017). Although the use of PCLS is becoming accepted as a research tool to investigate pulmonary drug metabolism, the protocols applied vary between laboratories and there is still opportunity to improve and standardize the methodology. Therefore, some of the key experimental factors used in the PCLS procedure were optimized with the aim of reducing variability and tissue damage and retaining lung metabolic activity. Due to the limited availability of fresh human lung tissue, method optimization was performed using rat lung tissue (under the assumption that rat is a suitable surrogate for human) and referring to a well-known CYP1A1 substrate, mavoglurant (AFQ056). The choice of mavoglurant as a test compound was based on two factors; 1) it is a CYP1A1 substrate and this enzyme is located primarily in extra-hepatic organs such as lung, kidney, brain and intestine (Drahushuk *et al.*, 1998, Cheung *et al.*, 1999, Paine *et al.*, 1999, Smith *et al.*, 2001)

and 2) metabolism of mavoglurant by CYP1A1 produces a specific metabolite, CBJ474, that serves as a marker for CYP1A1 metabolic activity (Walles *et al.*, 2013). During the optimization process of the PCLS model it was possible to achieve higher mavoglurant turnover by performing incubations on dynamic organ culture system. This investigation demonstrated the importance of optimization and standardization of PCLS conditions.

2) **Investigate the activity of phase I and phase II metabolic enzymes in rat and human lungs using PCLS model**

Preclinical species such as rats and mice are commonly used for the optimization of pharmacokinetic (PK) properties and for testing *in vivo* efficacy of new chemical entities. The PK data from these preclinical species is also often used for the prediction of human PK, and therefore, it is desirable that drug metabolism in these species is representative of that in human. For the comparison of enzyme activity in rat and human lungs, a selection of phase I and phase II probe substrates (please refer to chapter 3.1, Table 3 for a list of the probe substrates tested) were incubated using the optimized PCLS model. The results showed that there are remarkable differences in pulmonary metabolic activity between rat and human, reflecting species dependent expression of drug-metabolizing enzymes. CYP-mediated metabolic activity was relatively low in both species, whereas phase II enzyme activities appeared to be more significant in rat than in human. Therefore, care should be taken when extrapolating metabolism data from animal models to humans.

3) **Comparison of PCLS model with established *in vitro* and *in vivo* experimental models to be able to understand the contribution of pulmonary metabolism to drug elimination**

A variety of *in vitro* and *ex vivo* lung models such as cell culture, sub-cellular fractions, tissue slices and isolated perfused lung models have been used to investigate pulmonary metabolism. Each tool has advantages and disadvantages and can be used to answer specific scientific questions. However, due to the diversity of the cells in the lung it is difficult to obtain quantitative data. In this research project, mavoglurant and benzydamine (well-characterized FMO substrate) were incubated using rat lung microsomes (*in vitro*) and rat PCLS (*ex*

vivo) and also administered intravenously (i.v.) and intra-arterially (i.a.) to rats (*in vivo*). Previous human *in vivo* studies had indicated that extra-hepatic metabolism contributes to the elimination of mavoglurant (Novartis internal data). The goal was to use these models to understand if the lung makes a significant contribution to total body clearance. Using the well-stirred organ model, lung clearance (CL_{lung}) of mavoglurant was estimated from microsomal and PCLS data and compared to the *in vivo* data obtained from i.v. and i.a. dosing to rats. The data generated from these three experimental models were comparable and the data suggested that the contribution of pulmonary metabolism to the elimination of mavoglurant is negligible. The same experiments were also performed using benzydamine. Interestingly, calculated lung clearance from microsomal data were 8-fold higher than lung clearance estimates from the PCLS model. Hence, similar to the PCLS-derived predictions, *in vivo* data indicated very low pulmonary clearance.

Chapter 2. Introduction

The lungs are a target organ for the treatment of respiratory diseases such as asthma, chronic obstructive pulmonary disease (COPD), cystic fibrosis, and pulmonary infections. For the efficient and safe treatment of respiratory diseases, inhaled drug delivery allows the direct application of high drug concentrations to the target site. For inhaled drug delivery, the evaluation of local drug metabolism in the lung is vital in order to assess the fraction of the drug metabolized during the absorption process. Consequently, pulmonary drug metabolism is expected to exert an effect on drug bioavailability. Likewise, as lung blood flow is almost equivalent to cardiac output, drug metabolism may also be relevant for orally as well as i.v. administered drugs.

2.1. Lung anatomy

Through breathing, we inspire oxygenated air and the principal function of the lung is to distribute the oxygen to the blood and remove carbon dioxide from the body (Figure 1). Two separate systems deliver blood to the lungs, namely the bronchial and the pulmonary circulation systems (Levitzky, 2013b). The bronchial circulation system carries 1% of the cardiac output, nutrients and oxygen to the cells. It is under high pressure and a part of the general systemic circulatory system (Woo and Szmuszkovicz, 2009, Flieder, 2018). The pulmonary circulation system receives almost the entire cardiac output and carries deoxygenated blood away from the right ventricle of the heart in order to oxygenate the blood. It is under low pressure and has high flow (Lust, 2007, Sly and Collins, 2008, Culver and Glenny, 2012, Aggarwal *et al.*, 2015).

The respiratory tree can be divided into a conducting zone and a respiratory zone as shown in Figure 2 (Levitzky, 2017). The conducting zone extends from the large airways to the bronchioles and terminal bronchioles and has the function of warming, humidifying and filtering inhaled air (Barrett *et al.*, 2012). The respiratory zone includes the respiratory bronchioles, alveolar ducts, and alveolar sacs and is the site of gas exchange (Patwa and Shah, 2015).

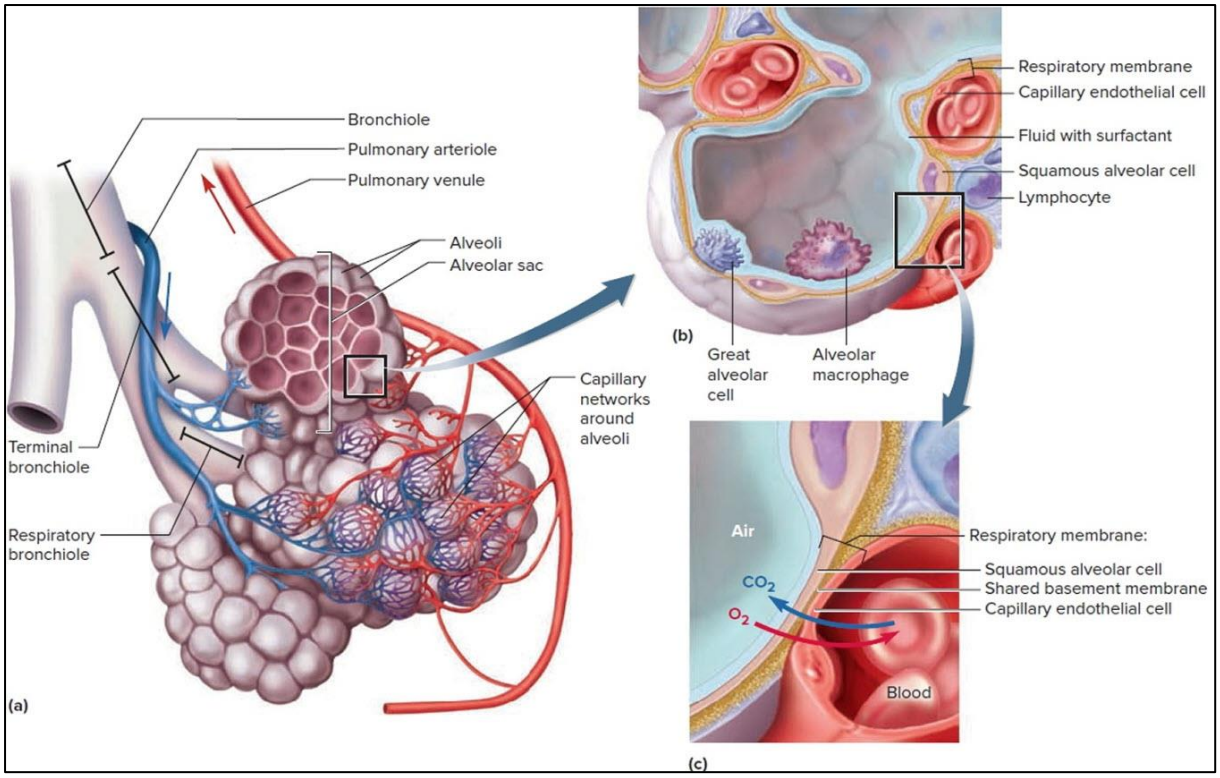

Figure 1: Illustration of pulmonary Alveoli. (a) Clusters of alveoli and their blood supply. (b) Structure of an alveolus. (c) Structure of the respiratory membrane (Saladin *et al.*, 2018)

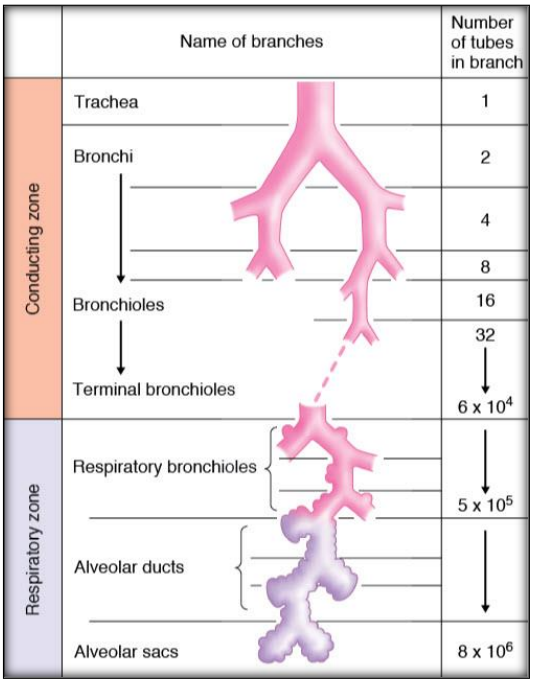

Figure 2: Conducting zone and respiratory zone of respiratory tree (Barrett *et al.*, 2012)

The area of the air-blood barrier where gas exchange occurs is composed of three

layers (Figure 1 and 3) (Horvath *et al.*, 2015). The first layer consists of alveolar epithelial cells (surface area 140 m^2), the middle layer is a thin basement membrane and the third layer is a capillary bed (surface area 130 m^2) (Simionescu, 1980). The large surface area of the air-blood barrier and its extreme thinness (0.1-0.5 µm) facilitate rapid gas exchange by passive diffusion (Plopper, 1996).

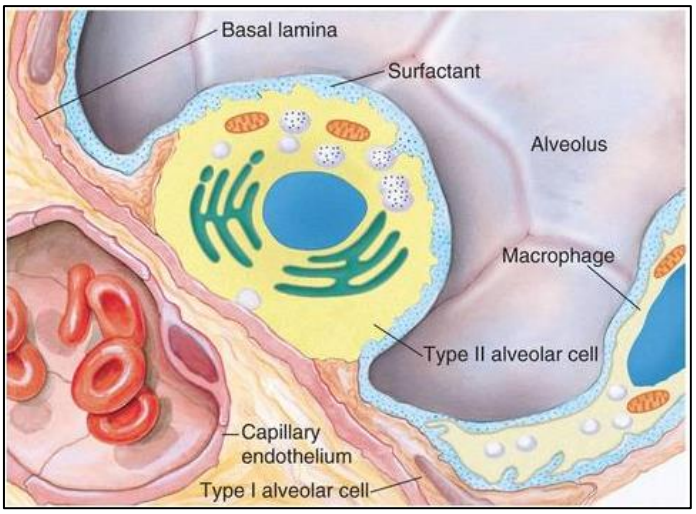

Figure 3: The air-blood barrier of the gas exchange area (Lechner and Mayo, 2015)

The anatomical structure of the lung differs in human, dogs and common laboratory rodents. This may have important implications for the deposition of drug delivered by the inhaled route. Table 1 compares the composition of the airways and gas-exchange barrier in human and rat lungs. During early drug discovery, new drug compounds are initially tested in laboratory animals. When making the translation of the measured lung clearance values from lab animals to human, so-called scaling factors are applied. These factors are species-dependent as there is considerable variability in metabolism across animals. Some possible reasons for the metabolism variability across different species are diverse enzyme isoform compositions, varying enzyme expression and catalytic activities, and lung anatomical structure differences (Tronde *et al.*, 2003, Martignoni *et al.*, 2006).

Table 1: Comparison of rat and human lung anatomical features. Data as compiled from (Crapo et al., 1982, Gehr, 1984, Berg et al., 1989, Levitzky, 2013a).

	Rat	**Human**
Lung lobes	Left lung: 1	Left lung: 2
	Right lung: 4	Right lung: 3
Branching	Strongly monopodial, very sharp	Dichotomous, symmetrical, sharp bifurcations for first ten generations
Respiratory bronchioles	Absent	Several generations
Structure of gas exchange barrier		
Average body weight (kg)	0.25	74
Thickness of gas diffusion barrier (μm)	0.38	0.62
Gas exchange surface area/unit lung volume (cm^2/cm^3)	750	371
Capillary volume/ unit lung volume (ml/cm^3)	0.092	0.057
Cellular composition in alveoli (%)		
Type I	9	8
Type II	14	16
Endothelial	46	30
Interstitial	28	36
Macrophage	3	9

2.2. Pulmonary enzyme expression

The lung has a unique anatomy and physiology with a highly complex architecture including over 40 cell types and diverse enzyme activities compared to the hepatic system (Nemery and Hoet, 1993, Zhang *et al.*, 2006, Franks *et al.*, 2008). The xenobiotic metabolizing enzymes are located in epithelial cells, namely in bronchial and bronchiolar epithelium, Clara cells, type II pneumocytes, and alveolar macrophages (Hukkanen *et al.*, 2002). Numerous studies conducted on the metabolic activity of lung show that CYP1A1, 1B1, 2A13, 2E1, 2F1, 4B1, and 3A5 are expressed in the lung (Zhang *et al.*, 2006). Pulmonary enzyme expression is affected by a variety of genetic and environmental factors, and these enzymes play a very essential role as first line defense for the inhaled endogenous toxicants (Hukkanen *et al.*, 2002, Castell *et al.*, 2005). Therefore, lung may express specific isoforms such as e.g. UGT2A1 and CYP1A1 at a greater level than in the liver (Somers *et al.*, 2007). Expression of xenobiotic-metabolizing enzymes in human lung are summarized in Table 2 (Zhang *et al.*, 2006).

Table 2: Summary of the enzymes expressed in human lung based on literature findings (Zhang et al., 2006)

Enzymes Phase I	**mRNA**	**Protein**	**Enzymes Phase II**	**mRNA**	**Protein**
1A1*	+++	+++	UGTs	+/-	+/-
1A2	+/-	+/-	SULTs	+	+
1B1	++	+/-	GSTs	++	+
2A6	++	+/-	NATs	+	+
2B6	+++	+++			
2C8	+	+/-			
2D6	+/-	+/-			
2E1	+++	+++			
2J2	+	++			
3A5	+++	++			
EHs	++	++			
FMOs	++	+			

+/- conflicting evidence, + weak positive evidence, ++ moderate positive evidence, +++ strong positive evidence, *smokers

2.3. Contribution of pulmonary metabolism to the total body clearance of drugs

Generally, if the total body clearance exceeds the liver blood flow, this can be an indication for extrahepatic metabolism (Kanto and Gepts, 1989). In addition to the fact that enzymes are expressed in lung, there are further theoretical considerations that pulmonary metabolism contributes to the total body clearance of a drug (Roth and Wiersma, 1979, Roth and Vinegar, 1990). First, the lungs receive almost entire cardiac output, which means that the circulating drugs or agents are exposed to pulmonary enzymes (Levitzky, 2013b). Furthermore, the lung is a first-pass metabolism organ for the drugs given by inhalation, intravenously, intramuscularly, subcutaneously, or topically as the drugs circulates first through the lung before reaching the liver (Boer, 2003). Moreover, due to the large vascular surface area of pulmonary veins, the compounds can circulate

efficiently to pulmonary enzymes (Levitzky, 2013a). The lung can be considered as a second-pass metabolism organ for toxic and carcinogenic metabolites as well (Roth and Wiersma, 1979). Consequently, pulmonary metabolism can lead to a decrease in the systemic availability of the drug and organ-specific toxicity (Roth and Wiersma, 1979, Hukkanen *et al.*, 2002).

2.4. Compounds metabolized by enzymes in the lung

Several drugs including resveratrol, lidocaine, midazolam, nifedipine, nilutamide, phenol, theophylline, salmeterol, isoprenaline, budesonide, and ciclesonide have been reported to undergo significant lung metabolism (Roth and Vinegar, 1990, Dickinson and Taylor, 1996, Aoki *et al.*, 2010, Joseph *et al.*, 2013). Example of phase I and phase II reactions in lung are summarized in Table 3 (Cohen, 1990, Mutch *et al.*, 2007, Nave *et al.*, 2010).

Table 3: Phase I and phase II reactions catalyzed by lung tissue

Compound	Phase I reactions	Compound	Phase II reactions
Pentobarbitone	Side-chain oxidation	4-Methylumbelliferone	Glucuronide conjugation
Benzo(a)pyrene	Aromatic hydroxylation	3-Hydroxybenzo(a)pyrene	Sulfate conjugation
Nortriptyline	N-Dealkylation	5-Hydroxytryptamine	N-Methyltransferase
N-Methylaniline	N-Hydroxylation	Phenol	O-Methyltransferase
Ethoxyresorufin	O-Dealkylation	Mercaptoethanol	S-Methyltransferase
Aldrin	Epoxidation	Isoprenaline	Catechol O-methyltransferase
Nitrazepam	Nitroreduction	Sulfanilamide	Acetylation
Acetophenone	Ketone reduction	Benz(a)anthracene 5,6-oxide	
Imipramine N-oxide	N-oxide reduction		
Ciclesonide	Ester hydroxylation		

2.5. Compound selection

Mavoglurant (AFQ056), a metabotropic glutamate receptor 5 (mGluR5) antagonist, was developed for the treatment of neurological diseases such as Fragile X syndrome and Parkinson's disease (Sourial *et al.*, 2013, Petrov *et al.*, 2014, Berry-Kravis *et al.*, 2016). The full structure of mavoglurant has been shown in a previous publication (Walles *et al.*, 2013). CYP1A1 efficiently catalyzes the oxidation of mavoglurant, leading to the formation of the metabolite CBJ474 (Walles *et al.*,

2013). In addition, other substrates, such as riluzole, gefitinib, erlotinib, granisetron and riociguat have been shown to be partly metabolized by CYP1A1 (Sanderink *et al.*, 1997, Nakamura *et al.*, 2005, Li *et al.*, 2007, Li *et al.*, 2010, Khaybullina *et al.*, 2014). The mavoglurant clinical data indicated that extra-hepatic metabolism makes a significant contribution to the elimination of this compound (Novartis internal data).

Benzydamine is a nonsteroidal anti-inflammatory drug (NSAID), that is marketed as a mouthwash solution, spray and gel for the treatment of mouth ulcers and sore throat (Segre and Hammarstrom, 1985, Quane *et al.*, 1998). Benzydamine is a well-characterized high-turnover FMO substrate (Lang and Rettie, 2000a). Further examples of FMO substrates include albendazole, clindamicyn, pargyline, itopride and cimetidine (Rawden *et al.*, 2000, Wynalda *et al.*, 2003, Cruciani *et al.*, 2014). FMOs catalyze the N-oxygenation of benzydamine while CYP3A4 is responsible for the formation of nor-benzydamine in human liver (Stormer *et al.*, 2000). Benzydamine displayed high turnover in early *in vitro* rat lung investigations and there was great interest in understanding if this would translate to significant pulmonary clearance *in vivo*.

2.5. Methods to assess lung metabolism

Several experimental methods have been described for the investigation of pulmonary drug metabolism (Woods *et al.*, 1980, Courcot *et al.*, 2012, Costa *et al.*, 2014). These include cell cultures, subcellular fractions, tissue slices, isolated perfused lungs and whole animal models (Woods *et al.*, 1980). The applications of these models and their advantages and disadvantages are summarized in Table 4.

Table 4: Lung metabolism models, their applications and pros and cons

Methods	Advantages	Disadvantages	Field of application	References
Cultured cells	Different cell lines are commercially available, easy to incubate	Enzyme abundance information is not available, difficult to make prediction for *in vivo*	Metabolite screening, species comparison, inhibition and induction studies, drug-drug interaction studies	(Castell *et al.*, 2005, Donato *et al.*, 2008, Garcia-Canton *et al.*, 2013)
Sub-cellular fractions	Easy to prepare and incubate, commercially available, long term storage is possible	Lack of membrane transport and endogenic concurrent reactions to estimate the whole organ clearance process	Metabolite screening, species comparison, inhibition and induction studies, drug-drug interaction studies	(Behera *et al.*, 2008, Ioannides, 2013)
PCLS	Intact phase I and II reactions, retaining of cell structure, cell contact and the transport process	Complex preparation process, time consuming procedure, fresh tissue is needed	Metabolite screening, species comparison, inhibition and induction studies, drug-drug interaction studies, toxicology studies	(Price *et al.*, 1995, Umachandran *et al.*, 2004, Pushparajah *et al.*, 2007, Morin *et al.*, 2013)
Isolated perfused lung	Cells are maintained in their normal anatomical and physiological association, transcellular transport and diffusion of agents are not modified	Time consuming, expensive and very complex procedure to set up the experiment, limited duration (not more than 8h), professional surgery is needed	Drug ADMET studies	(Niemeier, 1984, Powley and Carlson, 2002, Tronde *et al.*, 2003, Nave *et al.*, 2006, Nelson *et al.*, 2015, Bosquillon *et al.*, 2017)
i.v. and i.a. drug administration	Direct *in vivo* application	Expensive, technically challenging, require trained & skilled personal, special ethical approval needed	Drug ADMET studies	(Cassidy and Houston, 1984, Sharan and Nagar, 2013)

For the PCLS method the steps involved in the preparation of lung slices are illustrated in Figure 4. For more details on the method please refer to chapter 4.1.

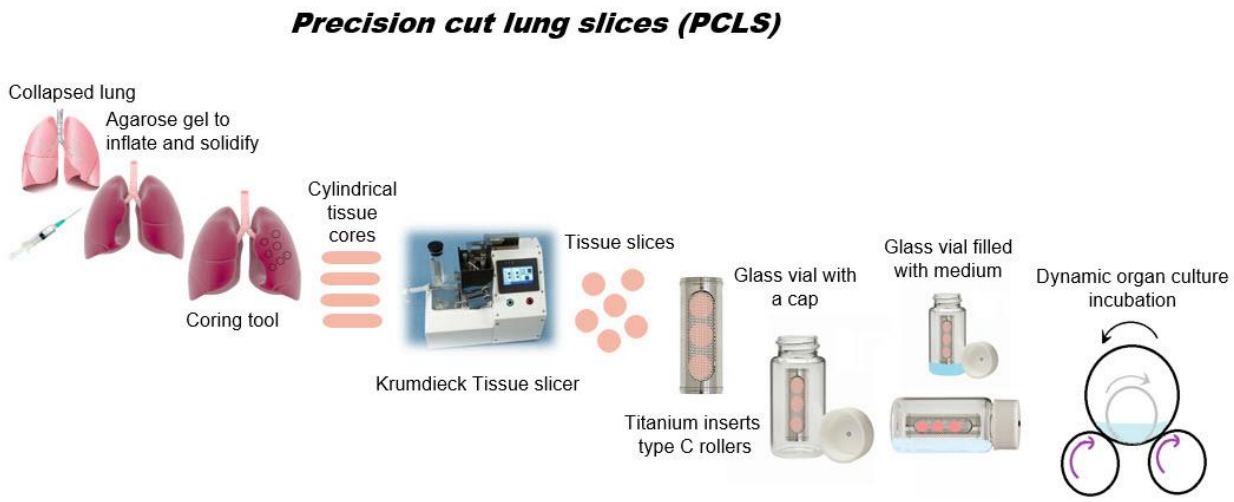

Figure 4: Preparation of lung tissue slices

2.6. Hepatic elimination models

Three models are commonly used to describe hepatic clearance: the well-stirred model, the parallel tube model and the dispersion model. The well-stirred model views the liver as a well-stirred compartment with concentration of drug in the liver in equilibrium with that in the emergent blood (Pang and Rowland, 1977, Yang *et al.*, 2007). The parallel tube model considers the liver as a number of identical tubes, where each tube has plug flow of the blood carrying the drug and the metabolites evenly around the tubes (Ridgway *et al.*, 2003, Poulin *et al.*, 2012). Finally, the dispersion model is based on the distribution of residence times of blood elements within the liver (Roberts and Rowland, 1986b). All three models assume: 1) that the drug is distributed immediately and homogenously throughout organ water, 2) that the metabolizing enzymes are equally distributed through the system and 3) that there are no limitations to drug movement within the system (Roberts and Rowland, 1986a, Chiba *et al.*, 2009). However, as previously discussed, lung tissue has intact cells with membrane, transporters, and cell-matrix interactions. Therefore, drug distribution throughout the tissue is not immediate as it has to diffuse through the cell membrane. The transport and efflux of the drug across cell membranes may be

significantly affected by its physicochemical properties. Although, it is known that Clara cells, alveolar type I and alveolar type II cells contain drug-metabolizing enzymes, those cells are not homogeneously distributed in lung (Zhang *et al.*, 2006). Hence, all three models might have similar liabilities for lung clearance predictions considering the anatomical complexity and particularities of the lung.

Chapter 3. Results

The results of this thesis were published / submitted* in the following articles:

3.1. Comparison of rat and human pulmonary metabolism using precision-cut lung slices (PCLS)*

Yilmaz et al., Drug Metabolism letters (2018)

3.2. Assessment of the pulmonary CYP1A1 metabolism of mavoglurant (AFQ056) in rat

Yilmaz et al., Xenobiotica (2017), 48:8, 793-803, DOI: 10.1080/00498254.2017.1373311

3.3. Functional assessment of rat pulmonary flavin-containingmonooxygenase activity

Yilmaz et al., Xenobiotica (2018), DOI: 10.1080/00498254.2018.1469804

3.1. Comparison of rat and human pulmonary metabolism using precision-cut lung slices (PCLS)

Yildiz Yilmaz[1], Gareth Williams[1], Markus Walles[1], Nenad Manevski[1], Stephan Krähenbühl[2] and Gian Camenisch[1]

Pharmacokinetic Sciences[1], Novartis Institutes for Biomedical Research, Basel, Switzerland

Clinical Pharmacology and Toxicology[2], University hospital Basel, Switzerland

Submitted in journal of Drug metabolism letters

Abstract

Background: Although the liver is the primary organ of drug metabolism, lungs also contain drug-metabolizing enzymes and may therefore contribute to the elimination of the drugs. In this investigation, the precision-cut lung slice (PCLS) technique was standardized with the aims of characterizing rat and comparing rat and human pulmonary drug metabolizing activity.

Method: Due to the limited availability of human lung tissue, standardization of the PCLS method was performed with rat lung tissue. Pulmonary enzymatic activity was found to vary significantly with rat age and rat strain. The dynamic organ culture (DOC) system was superior to well plates for tissue incubations, while oxygen supply appeared to have a limited impact within the 4h incubation period used here.

Results: The metabolism of a range of phase I and phase II probe substrates was assessed in rat and human lung preparations. Cytochrome P450 (CYP) activity was relatively low in both species, whereas phase II activity appeared to be more significant.

Conclusion: PCLS is a promising tool for the investigation of pulmonary drug metabolism. The data indicates that pulmonary CYP activity is relatively low and that there are significant differences in enzyme activity between rat and human lung.

1. Introduction

Although the primary function of the lung is gas exchange, it also performs several important non-respiratory functions. Through breathing, the lung is frequently exposed to environmental toxicants and carcinogens and plays an important role in their detoxification. The same enzymes that play a role in the detoxification of these environmental components may also contribute to the metabolism and elimination of inhaled, orally and intravenously administered drugs. The awareness of pulmonary diseases such as lung cancer, bronchial asthma and chronic obstructive pulmonary disease (COPD) has increased during the last twenty years (Del Donno *et al.*, 2002). Consequently, the inhaled route of drug delivery has gained more importance with the aim to treat these diseases directly. Inhaled drug delivery has several benefits including a small drug load with high local concentrations, immediate delivery of the drug to the target with a rapid onset of action and reduced systemic exposure and adverse reactions. If absorbed, inhaled compounds appear rapidly in the systemic circulation, bypassing any extensive hepatic first past effects (Rau, 2005). The lung is a complex organ containing over 40 different types of cells with varied functions and architecture (Stone *et al.*, 1992). The location of the pulmonary metabolizing enzymes has been previously discussed (Zhang *et al.*, 2006). Bronchial and bronchiolar epithelia, Clara cells, type II pneumocytes, and alveolar macrophages all express cytochrome P450 (CYP) enzymes (Devereux *et al.*, 1989, Raunio *et al.*, 1999). However, type I pneumocytes and endothelial cells, which are most directly exposed to blood flow, contain only small amounts of CYPs (Hukkanen *et al.*, 2002). Phase II enzymes such as UGT1A (glucuronyl transferase) and GST-P1 (glutathione S-transferase), which are important detoxifying enzymes, are also found in lung cells (Somers *et al.*, 2007, Olsson *et al.*, 2011). Due to this diversity of cell types and variable metabolic activity, the study of pulmonary disposition

is challenging. Therefore, suitable *in vitro* tools are required to fully understand the potential role of pulmonary metabolism in drug disposition.

Similar to the liver, pulmonary subcellular fractions such as microsomes and S9 are available from human and preclinical animal species. Although these *in vitro* systems require the addition of appropriate cofactors such as NADPH and UDPGA, they provide a convenient means for studying lung metabolism. Proteolytic enzymes are required for the preparation of subcellular fractions such as lung microsomes (Ioannides *et al.*, 2011). However, these subcellular fractions lack the architecture of the intact cells and may therefore not fully reflect the capacity of pulmonary metabolism. Precision-cut lung slices (PCLS) are an alternative tool for studying lung metabolism and have several important advantages over subcellular fractions as they possess the full range of cell types, intact tissue architecture and cofactors at physiologically relevant concentrations (De Kanter *et al.*, 1999, Umachandran and Ioannides, 2006). As a result, phase I and phase II metabolic processes are fully represented by tissue slices (Ioannides *et al.*, 2011). The use of rat PCLS for drug metabolism investigations was first reported in 1977 (O'Neil *et al.*, 1977). As an example, *in vitro* human pulmonary metabolism of ciclesonide, an inhaled corticosteroid, was investigated using PCLS (Nave *et al.*, 2006). Furthermore, PCLS have recently been used to study the metabolism of mavoglurant (Yilmaz *et al.*, 2017).

One drawback of the PCLS model is that it generally requires fresh tissue. Although this is routinely available for rodent species, its availability is limited for human and other species such as dog and monkey. Nevertheless, the use of PCLS show great promise as the methodology can be easily applied to different organs such as liver, kidney and brain and may also be used to identify potential differences in drug metabolism between human and animals used for toxicological studies (De Kanter *et al.*, 2002). Lung slices can be produced from limited amounts of tissue and, therefore, surgical waste material may be suitable for

this purpose (Kanter *et al.*, 2002). The preparation of subcellular fractions from similar amounts of tissue would typically result in poor yields of protein. Although lung microsomes and S9 are commercially available and relatively inexpensive, their preparation time is usually longer than that of tissue slices, potentially leading to loss of metabolic activity. Furthermore, enzymatic activity will be adversely affected by repeated freeze-thaw cycles and this should be avoided when using microsomes and S9. In recent years, the potential use of tissue cryopreservation has been investigated to reduce the dependence of the PCLS model on fresh material (de Graaf and Koster, 2003). Yet, a robust methodology for tissue cryopreservation has so far not been developed and, therefore, has not been used in the current investigations.

Although lung slicing technology is commonly used in metabolism studies, the protocols used vary between laboratories and there is still opportunity to improve and standardize the technique (Liberati *et al.*, 2010). Therefore, in this study, some of the key experimental factors used in the PCLS procedure were optimised with the aim of reducing tissue damage and retaining lung metabolic activity. The PCLS incubation conditions were partly optimised and fully standardized using the CYP1A1 substrate, AFQ056. CYP1A1 has previously been shown to efficiently catalyse the oxidation of AFQ056, leading to the formation of the metabolite, CBJ474 (Walles *et al.*, 2013). CYP1A1 is widely recognised as an extrahepatic enzyme that is expressed in organs including kidney, intestine and lung (Ding and Kaminsky, 2003, Nishimura and Naito, 2006, Bieche *et al.*, 2007). CYP1A1 mRNA is known to have a short half-life of approximately 2.4 h (Lekas et al., 2000) and it is therefore critical that the experimental conditions used do not adversely affect CYP1A1 activity. The pulmonary metabolism of AFQ056 is sensitive regarding the conditions used and was therefore considered to be suitable for the optimization of the PCLS conditions. Finally, the optimised and standardized PCLS parameters were used to compare rat and

human pulmonary enzyme activity. Incubations were performed with a range of substrates for enzymes including CYPs, FMOs, UGTs and SULTs and were selected based upon literature data, availability of reference standards for parent compound and metabolite quantification.

2. Materials and Methods

2.1. Reagents, chemicals, and materials

AFQ056 (mavoglurant) and NVP-CBJ474 (AFQ056-M3) were synthesized at Novartis (Basel, Switzerland). Minimal Essential Medium (MEM, without L-glutamine, HEPES, and phenol red) and agarose UltraPure™ low melting point were purchased from Life Technologies (Carlsbad, CA). 4-Methylumbelliferone, 4-methylumbelliferyl glucuronide, 4-methylumbelliferyl sulfate, benzydamine, ramipril, triclosan, carbazeran, diclofenac, diazepam, amodiaquine, sumatriptan, P-toluidine and 4-methylacetanilide were purchased from Sigma Aldrich. Benzydamine N-oxide, ramiprilat, triclosan glucuronide, triclosan sulfate, 4-hydroxycarbazeran, 4-hydroxydiclofenac, diclofenac glucuronide, midazolam, 1-hydroxymidazolam, nordiazepam and N-desethylamodiaquine were purchased from Toronto research chemicals.

2.2. Standardization of the PCLS incubation conditions

Rat lung tissue slices were performed as previously described (Yilmaz *et al.*, 2017). The impact of animal age was investigated by performing incubations with lung slices from Sprague Dawley (SD) rats aged between 6 and 12 weeks. In order to evaluate differences in enzyme activity due to rat strain, lung tissue was also obtained from 6 week old Wistar Han (WH) rats. PCLS incubations were performed using titanium (type C) roller inserts (Vitron Inc., Tucson, AZ). Three lung tissue slices (average weight 0.024 g/slice) were positioned onto the roller inserts and then placed in glass vials (Figure 1). The glass vials were prefilled with a modified dynamic organ culture medium composed of MEM, HEPES (25mM) and glucose (25 mM) (Smith *et al.*, 1985, Smith *et al.*, 1986).

Table 1: Important parameters for the tissue slice preparation

Factors	Subfactors	Comments
Animals	Strains	Sprague Dawley & Wistar Han
	Age	6-12 weeks
	Fed/fasted	Fed
Anesthesia	Drug	3-5% Isofluran
	Duration	3 min
Slice preparation	Agarose gel	Low melting point (2.5% v/v)
	Slice thickness /weight	~416 µm / ~24 mg
	Buffer	MEM, HEPES, Glucose
Medium	Volume	2mL
	Rotating frequency	4 rpm
Incubation conditions	Temperature	37 °C
	Duration of incubation	0-4 h
	Incubation system	Dynamic organ culture system & well-plate

These factors should be considered to minimize tissue damage in order to obtain an accurate and reproducible system for the determination of pulmonary drug metabolism.

During the optimization process, the DOC incubation system was compared with well-plates (Figure 2) to determine if the pulmonary activity was dependent upon the incubation device. As the primary role of the lung is gas exchange, the impact of the oxygen content in the incubation system on drug metabolism was investigated. For that, metabolic activities were compared using an oxygen rich atmosphere (75% O_2, 5% CO_2) and an atmosphere composed of 5% CO_2 and normal air (21% O_2 content).

Figure 1: Incubation vial for dynamic organ culture system

For PCLS incubations three lung tissue slices (average weight 0.024 g/slice) were positioned onto the titanium (type C) roller inserts and then placed into glass vials. The glass vials were filled with a modified medium composed of MEM, HEPES (25mM), glucose (25 mM) and compounds of interest. Each time point was carried out in duplicate comprising 3 slices for each time point, and each incubation was carried out in triplicate.

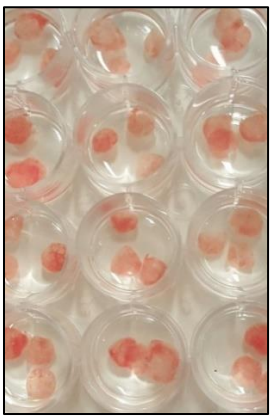

Figure 2: Precision cut lung slices incubation on well plate system

For PCLS incubations 12 well-plates were filled with 2 mL of a medium composed of MEM, HEPES (25mM), glucose (25 mM) and compounds of interest. On each plate, three lung tissue slices (average weight 0.024 g/slice) were positioned and incubated for 4h.

2.3. Preparation and incubation of lung tissue slices

Animal experiments were conducted with the approval of the Cantonal Veterinary Authority of Basel City, Switzerland (Protocol BS-2723). Male SD and WH rats, with an average age of 6 – 12 weeks and body weight of 200 – 250 g, were used in this study (Charles River Germany). Fresh rat lungs were obtained with the trachea and immediately put on ice after surgery until processing.

The use of human lung tissue was approved by the local ethics committee of Basel, Switzerland (EKNZ 2015-355) and the studies were performed in accordance with the Declaration of Helsinki (1964 and subsequent revisions). In written manner the informed consent was obtained from the study participants. Tumour-free tissue samples from different region of the lung were collected post-surgically from six patients at the Department of Thoracic Surgery, University Hospital Basel. Basic demographic information is presented in Table 2. The excised lung samples were immediately submerged in cold MEM medium. Samples were transported to our laboratories at 4 ºC within 60 min from the time of surgical excision.

Table 2: Demographic information of human lung donors

Donor	Gender	Ethnicity	Primary lung disease
1	Male	Caucasian	Bronchiectasis
2	Female	Caucasian	Lung cancer
3	Male	Caucasian	Lung cancer
4	Male	Caucasian	Lung cancer
5	Male	Caucasian	Lung cancer
6	Male	Caucasian	Lung cancer

Macroscopically healthy lung tissue surrounding the tumor or lesion was collected post-surgically from subjects aged 45 – 79 years.

Pre-warmed lung tissue (37 °C for 5 min) was inflated with a 37 °C solution of agarose (low melting point, 2.5% v/v) in MEM medium. The rat lungs were inflated *via* the trachea,

whereas human lung tissue was inflated by injecting airways using a syringe and needle. The preparation of lung slices and 4h incubations were performed as previously described (Yilmaz *et al.*, 2017). An important consideration is the slice thickness that the cut surface of the slice contains mainly damaged cells and if the slice thickness decreases then the overall slice metabolism can be affected. Furthermore, if the slice thickness increases this can lead to suboptimal metabolism due to the substrate delivery and gas diffusion difficulty (Liberati *et al.*, 2010). Slice thickness (~416 μm) was chosen in this case based on the previous findings (O'Neil *et al.*, 1977, Dogterom, 1993, Liberati *et al.*, 2010, Sanderson, 2011). The incubation reactions were stopped after 4 h by addition of 3 mL of acetonitrile. The samples were vortex mixed and stored at -80 °C until further processing.

For the enzyme activity comparison between human and rat lungs, numerous phase I and phase II enzyme substrates (listed in Table 3) were incubated and substrate concentration as well as metabolite formation were measured. The monitored metabolites are also shown in Table 3. Probe substrates for drug-metabolizing enzymes were selected based on literature reports of the specific biotransformation pathways and enzymes involved and availability of synthetic standards enabling quantification of formed metabolites. 4-Methylumbelliferone and triclosan have been described as broad substrates for human UGTs and mammalian SULTs (Wang *et al.*, 2004, Manevski *et al.*, 2013). P-Toluidine was reported to be a substrate for human N-acetyltransferases present in human skin (Gotz *et al.*, 2012, Manevski *et al.*, 2015). Midazolam hydroxylation to 1'-hydroxymidazolam is catalysed by human CYP3A4/3A5 (Yuan *et al.*, 2002). Amodiaquine N-deethylation is catalysed by CYP2C8 leading to the formation of N-desethylamodiaquine (Li *et al.*, 2002). Diclofenac hydroxylation to 4'-hydroxydiclofenac is catalysed by human CYP2C9 (Carlile *et al.*, 1999). Diazepam N-demethylation to nordiazepam is predominantly catalysed by human CYP2C19 and CYP3A (Ono *et al.*, 1996). Benzydamine is reported to be a high-

turnover substrate for human FMOs (Lang and Rettie, 2000b) and carbazeran hydroxylation to 4-hydroxycarbazeran is catalysed by human aldehyde oxidase (Kaye *et al.*, 1985, Hutzler *et al.*, 2012). Rampril hydrolysis to ramiprilat was reported to be catalyzed by human carboxyl esterase 1 (CES1) (Thomsen *et al.*, 2014).

2.4. Analytical methods

Samples were quantitatively analysed using a Triple Quadripole 6500 LC-MS/MS system (AB Sciex, Ontario, CA) coupled to a UPLC system (Waters Acquity). Separations were achieved using various reversed phase stationary phases. The analytical columns and mobile phase compositions were developed for the simultaneous quantification of substrate and metabolite and are summarised in Table 4. This analytical methods are developed based on the literature findings and for this research purpose. The columns were operated at 40 °C, and eluted with a mobile phase flow rate of 400 µL/min. The presence of metabolites were confirmed by chromatography with reference standards.

Table 3: Probe substrates and corresponding metabolites used to investigate pulmonary metabolism

Compound	Metabolic reaction	Metabolite	Responsible enzyme
Triclosan	Glucuronidation	Triclosan glucuronide	UGT
Triclosan	Sulfation	Triclosan sulfate	SULTs
4-MU	Glucuronidation	4-MUG	UGT
4-MU	Sulfation	4-MU-Sulfate	SULTs
P-Toluidine	N-Acetylation	4'-Methylacetanilide	NATs
Midazolam	Hydroxylation	1-Hydroxymidazolam	CYP3A4
Amodiaquine	N-deethylation	N-Desethylamodiaquine	CYP2C8
Diclofenac	Hydroxylation	4-Hydroxydiclofenac	CYP2C9
Diazepam	N-demethylation	Nordiazepam	CYP2C19/3A
AFQ056	4-hydroxylation	CBJ474	CYP1A1
Benzydamine	N-Oxygenation	Benzydamine-N-oxide	FMOs
Carbazeran	Hydroxylation	4-Hydroxycarbazeran	AO
Ramipril	Hydrolysis	Ramiprilat	CES1

The probe substrates used in this study, their respective metabolites and responsible enzymes are shown.

Prior to analysis, samples were prepared as follows. The samples were thawed and sonicated for 5 min and 200µL aliquots were transferred to a new tube containing 400 µL acetonitrile with internal standard, estradiol glucuronide. The diluted samples were vortex mixed and sonicated for 2 min and then centrifuged for 15 min at 15000 g. The supernatants were transferred to a new tube and evaporated to dryness under a stream of nitrogen. Finally, the samples were reconstituted in 150µL 95/5 (v/v) water/acetonitrile containing 0.1 % formic acid and analysed by LC-MS/MS. The LLQ for the metabolites were 0.001 µM.

.

Table 4: LC-MS/MS methods for the determination of probe substrates and metabolites

Analyte	Column	SRM transition	Gradient A	Gradient B	Gradient profile	Ionization mode
AFQ056	Kinetex C8, 2.6 µm, 2.1x50 mm	296/221	0.1% FA in H_2O	ACN	A	ESI $^+$
CBJ474		312/237				
4-MU	Phenomenex Luna Phenylhexyl, 3 µm, 2.0x150 mm	175/133	20 mM NH_4HCO_2 (pH 4.2) in H_2O	MeOH	B	ESI $^-$
4-MU glucuronide		351/175				
4-MU sulfate		255/175				
Benzydamine	Supelco Ascentis C18, 3 µm, 2.1x50 mm	310/265	20 mM NH_4HCO_2 (pH 4.2) in H_2O	ACN	A	ESI $^+$
Benzydamine-N-oxide		326/102				
Ramipril	Supelco Ascentis C18, 3 µm, 2.1x50 mm	417/234	20 mM NH_4HCO_2 (pH 4.2) in H_2O	ACN	A	ESI $^+$
Ramiprilat		389/156				
Triclosan	Supelco Ascentis C18, 3µm, 2.1x50 mm	289/289 287/287	0.1% FA in H_2O	ACN	B	ESI $^-$
Triclosan glucuronide		463/287				
Triclosan sulfate		367/175, 367/287				
Carbazeran	Supelco Ascentis C18, 3 µm, 2.1x50 mm	361/272	0.1% FA in H_2O	ACN	A	ESI $^+$
4-Hydroxycarbazeran		377/288				
Diclofenac	HALO C18, 3 µm, 2.1x100mm + guard	294/250, 294/214, 296/252	0.1% FA in H_2O	ACN	A	ESI $^-$
4-Hydroxydiclofenac		310/266, 312/268, 312/232				
Diclofenac glucuronide		470/193, 470/250, 470/175, 472/193				
Midazolam	Supelco Ascentis C18, 3 µm, 2.1x50 mm	326/291	20 mM NH_4HCO_2 (pH 4.2) in H_2O	ACN	A	ESI $^+$
1-Hydroxymidazolam		342/324				
Diazepam	Supelco Ascentis C18, 3 µm, 2.1x50 mm	285/193	20 mM NH_4HCO_2 (pH 4.2) in H_2O	ACN	A	ESI $^+$
Nordiazepam		271/208				
Amodiaquine	Supelco Ascentis C18, 3 µm, 2.1x50 mm	356/283	0.1% FA in H_2O	ACN	C	ESI $^+$
N-Desethylamodiaquine		328/283				
P-Toluidine	Phenomenex Luna Phenylhexyl, 3 µm, 2.0x150 mm	108/93	0.1% FA in H_2O	ACN	A	ESI $^+$
4'-Methylacetanilide		150/108				
Estradiol Glucuronide (IS)		447/271				

Gradient elution profiles
A= 0-1 min 5% B, 5 min 50% B, 10-11 min 95% B, 12-15 min 5% B
B= 0-1 min 5% B, 5 min 30% B, 6-12 min 95% B, 12.5-15 min 5% B
C= 0-1 min 5% B, 6 min 80% B, 10-13 min 95% B, 13.5-15 min 5% B

3. Results

3.1 Standardization of the PCLS assay conditions

The initial aim of this investigation was the standardization of the PCLS incubation conditions. As mentioned earlier, some of the important incubation conditions were optimized using the CYP1A1 substrate, AFQ056. Furthermore, due to the limited availability of fresh human lung tissue, the optimization process was carried out using rat tissue with the assumption that rat lung is a suitable surrogate for human lung.

The PCLS results indicated that pulmonary CYP1A1 activity varied with rat age and rat strain (Figure 3). AFQ056 turnover was approximately 1.5-fold higher in 6 week than in 12 week old SD rats. Similarly, pulmonary CYP1A1 activity in 6 week old SD rats was approximately 1.8-fold higher than in WH rats of the same age (Figure 3).

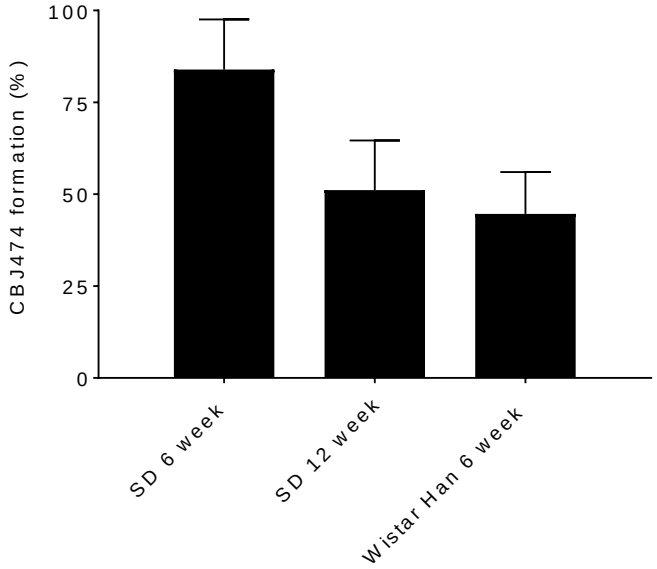

Figure 3: Age and strain dependent lung metabolism of AFQ056 in rats

AFQ056 (1 µM) was incubated for 4h with lung tissue slices obtained from 6 and 12 week old SD rats and 6 week old WH rats. The metabolite, CBJ474 formed after 4 h was quantified and expressed as a percentage of initial AFQ056. Data are presented as mean values ± S.D. (n=3). Each time point was carried out in duplicate comprising 3 slices for each time point, and each incubation was carried out in triplicate. The kinetic experiments showed linear formation of CBJ474 with time as shown in the previous investigations (Yilmaz *et al.*, 2017) *(Figure 4B).*

The choice of the incubation vessel was also found to be an important consideration when performing PCLS incubations. As shown in Figure 4, a higher CBJ474 formation was observed with the DOC incubation system than with the well plates. Although the use of the rollers was more cumbersome than a simple well plate, it is evident that they plaid a crucial role in obtaining optimum enzymatic activity.

Given that the in vivo, the lungs are directly exposed to the atmosphere, the influence of the oxygen content in the incubation buffer was investigated. The results indicated that CYP1A1 activity was not influenced by the atmospheric oxygen content during the 4h incubation period used here (Figure 4). This insensitivity to the oxygen content may have been due to the fact that the incubation buffer was routinely saturated with oxygen prior to starting the incubation. The addition of this amount of oxygen may have been sufficient to support enzyme activity during the 4 h incubation period.

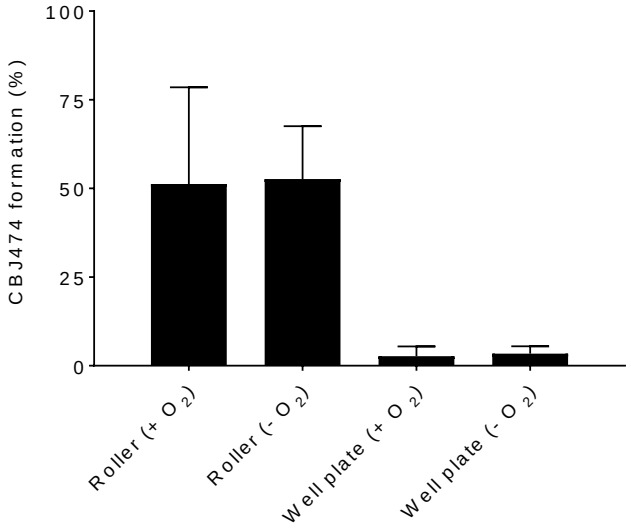

Figure 4: The impact of the incubation system on AFQ056 pulmonary metabolism

AFQ056 (1 µM) was incubated for 4h with lung tissue slices obtained from 6 week old SD rats. The impact of oxygen supply on CBJ474 formation was investigated. Dynamic organ culture (DOC) and well plate incubation systems were also compared. The metabolite, CBJ474, formed after 4 h was quantified and expressed as a percentage of initial AFQ056. Data are presented as mean values ± S.D. (n=3). Each time point was carried out in duplicate comprising 3 slices for each time point, and each incubation was carried out in triplicate.

3.2. Comparison of pulmonary enzyme activity in rats and humans

The pulmonary metabolism of a selection of phase I and II substrates in rat and human lung tissue was compared using the optimum conditions discussed above. The results suggested that there were considerable species differences with respect to the metabolism of the probe substrates tested (Figure 5). Although CYP activity was generally low in both species, activity in human lung appeared to be remarkably lower than in rat. Accordingly, with the exception of CBJ474, it was not possible to detect the CYP mediated metabolites in human lung incubations. The formation of CBJ474 is mediated by CYP1A1 (Yilmaz *et al.*, 2017), an

isoform that is thought to be expressed in extrahepatic tissues including the lung. The data shown here demonstrates the presence of CYP1A1 in lung tissue albeit to a lesser extent in human than in rat.

Similarly, remarkable benzydamine N-oxygenation was observed in rat lung, whereas activity in human lung was negligible (approximately 1 % of initial parent concentration during 4 h). The limited carbazeran hydroxylation observed in both species suggested that pulmonary aldehyde oxidase activity is low irrespective of the species.

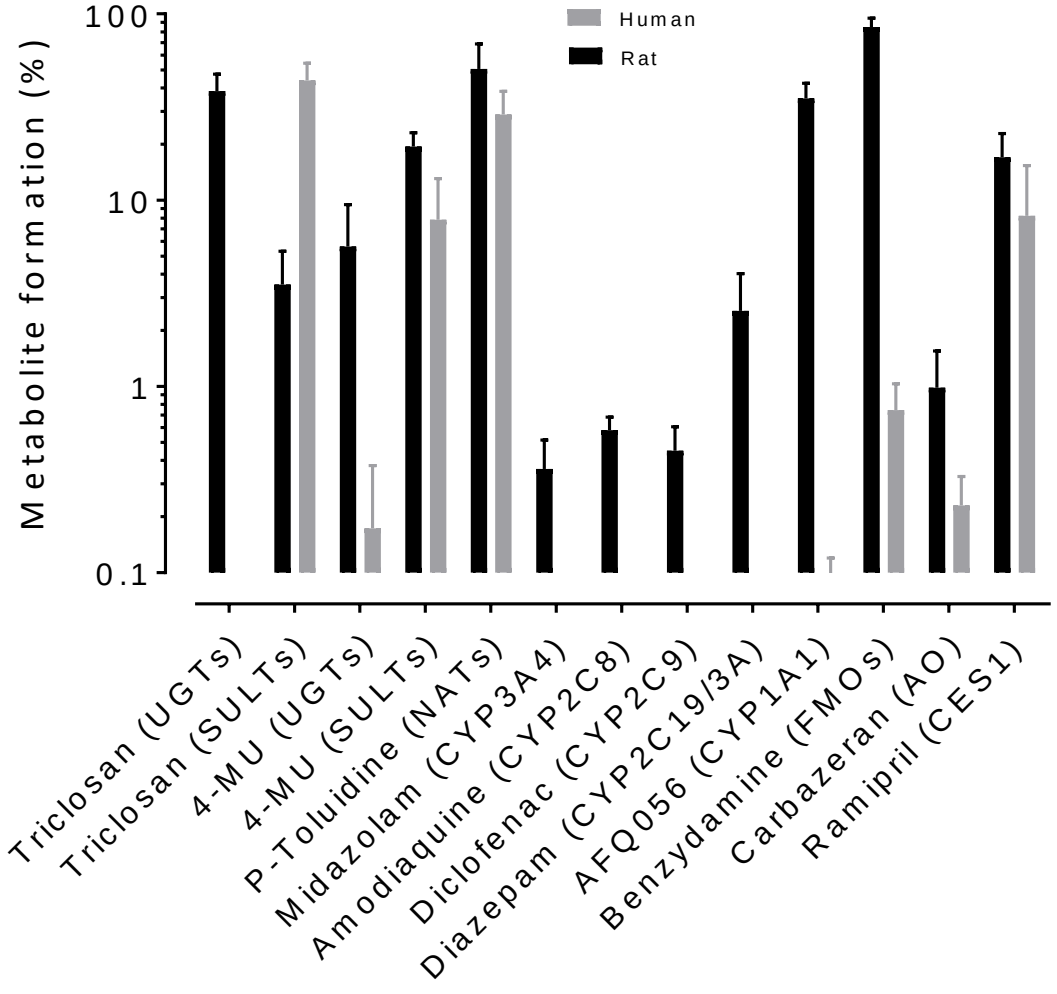

Figure 5: Comparison of rat and human pulmonary drug metabolizing activity

Substrates (1 µM) were incubated in the presence of rat and human lung PCLS for 4 h. The metabolites were quantified and are displayed as a percentage of initial substrate concentration. Data are presented as mean values ± S.D. (n=3). Each time point was carried out in duplicate comprising 3 slices for each time point, and each incubation was carried out in triplicate.

In contrast to the generally low oxidative metabolism observed here, pulmonary phase II processes appeared to be prominent. Triclosan and 4-MU underwent sulfation in rat and human lung with comparable turnover displayed in both species. Furthermore, toluidine N-acetylation also occurred in both species to a similar extent. Although glucuronidation of the UGT substrates, triclosan and 4-MU was observed in both rat and human lung, the velocity was significantly higher in rat than in human lung. CES1 mediated hydrolysis of ramipiril was comparable in rat and human lung slices.

4. Discussion

Although the liver has the highest metabolic capacity of all organs, the lung could also contribute to the total body clearance of drugs. The fact that the lungs receive 100% of the cardiac output, which means that the whole quantity of circulating compounds is exposed to pulmonary enzymes, may be a reason why lungs could contribute to total body drug clearance. Consequently, every compound given intravenously, intramuscularly, subcutaneously or topically circulates through the lung before reaching the liver. Therefore, the metabolic first-pass of the lung could be significant for drug applications bypassing intestinal absorption.

PCLS provide a great possibility to investigate *in vitro* pulmonary drug metabolism using fresh rat or human lung tissue. Since the slices contain all relevant cell and metabolite components, the results obtained *in vitro* could predict the *in vivo* pulmonary metabolism of specific drugs. Although the successful use of PCLS for drug metabolism studies has previously been demonstrated (Nave *et al.*, 2006), there is a still a need to evaluate and improve the protocols used with the aim to optimize this technique. Herein, the impact of several key factors including rat age and rat strain, incubation vessels and oxygen supply were evaluated (Table 1).

As shown in Figure 3, differences in CBJ474 formation were observed between 6 and 12 week old SD rats. These observations are consistent with the fact that in the rat, age-related changes in anatomy, morphology, biochemistry, and physiology are known to result in corresponding changes in drug metabolizing activity (Nijjar and Ho, 1980, Van Bezooijen *et al.*, 1986, Yamamoto *et al.*, 2003, McCutcheon and Marinelli, 2009, Samuel *et al.*, 2016, Bozhkov *et al.*, 2017). The age of a rat can be defined in three specific life phases: infants (<3 week), juveniles

(3-8 weeks), and adults (from 8 weeks up to 1.5 years). It appears that juvenile rats have higher pulmonary CYP1A1 activities than adult rats. Similarly, differences in CYP1A1 mRNA expression and metabolic activity among rat strains have previously reported (Nishiyama *et al.*, 2016). The impact of this strain-dependent CYP1A1 activity can be seen in Figure 3, where CBJ474 formation is shown to be greater in 6 week old SD than in WH rats of the same age. Given the age and strain differences in metabolic activity observed here, it is important that age and strain of animals used in this type of metabolic studies are standardised to obtain comparable results with a low variability. We therefore recommend that 6 week old juvenile SD rats are used wherever possible.

The choice of the incubation vessel was also found to be important as higher CBJ474 turnover was seen with the DOC system than with multi-well plates. The continuous rotation of the titanium rollers in the DOC system may result in more efficient oxygenation and optimal substrate and nutrient delivery to the tissue slices, therefore mimicking the *in vivo* situation more closely (Fisher *et al.*, 1995, Parrish *et al.*, 1995, Umachandran *et al.*, 2004, Umachandran and Ioannides, 2006, Morin *et al.*, 2013). The primary drawback of the DOC system is that the number of incubations that can be performed in parallel is limited and that a specific incubator has to be purchased. Incubations could be more efficiently performed using multi-well plates, which allow increasing the number of incubations much more easily. However, as shown in this study, the metabolic activity is compromised when well plates are used (Figure 4). Although the influence of oxygen supply on lung slice viability has been reported previously (Siminski *et al.*, 1992, Monteil *et al.*, 1999), our data suggests that oxygen supply has an only limited impact when incubation times are short (4h) and the buffer is pre-oxygenated. Based

on these results, subsequent incubations were performed using the DOC system at atmospheric oxygen tension and buffer pre-oxygenation.

The optimization process discussed here was performed with a single compound, AFQ056, a CYP1A1 substrate. While this may be considered to be a limitation, the well documented fragility of CYP1A1 (Lekas *et al.*, 2000) requires additional care to maintain the activity when performing PCLS experiments. The data shown here are consistent with previous results (Yilmaz *et al.*, 2017), reflecting the reproducibility of our procedure. We consider therefore AFQ056 a suitable compound for monitoring the performance of the PCLS procedure.

The use of human tissue in this study turned out to be difficult but nevertheless yielded valuable results. The preparation of human tissue slices was technically more challenging than rat slices and, therefore, appropriate modifications of the methodology had to be made. Rat lungs could easily be inflated with agarose via the intact trachea. However, human lung tissue was obtained as surgical waste, and airways were generally not visible. Human tissue was therefore carefully inflated via a series of small injections of agarose gel using a fine needle. Care was taken to avoid applying excessive pressure that could have caused bursting of alveoli, possibly leading to loss of metabolic activity. It is therefore possible that not only species differences, but also the quality of the lung slices has contributed to the lower enzyme activities in human compared to rat lung.

We were fortunate to obtain fresh human lung tissue from the local University Hospital. Although the availability of human tissue was limited, we aimed to reduce experimental bias by processing the human tissue samples as carefully and rapidly as possible. It can be assumed that the health status of the subjects had only a limited impact on the results as the tissue collected was not tumorous. The PCLS technique is dependent upon the availability of fresh

tissue and, therefore, samples were transported from the hospital to our laboratory within one hour of isolation. Tissue slices were then quickly prepared within 90 minutes to minimise any loss of metabolic activity.

In the past years various studies have been published on the characterization, expression levels and localization of xenobiotic metabolizing enzymes in the lung, but information about the functional aspects of these enzymes is rare (Lorenz *et al.*, 1984, Pacifici *et al.*, 1988, Zhang *et al.*, 2006). Possible reasons for this information gap may be that the activity of drug-metabolizing enzymes in lung tissue is low (in particular regarding phase I metabolism enzymes) and that suitable systems for long-term measurement of enzyme activities have not been available. PCLS may close this gap. The data of the current investigation shows that phase II activity in rat and human lung is reasonably comparable and that the activity of phase II is considerably higher than of phase I enzymes (Figure 5). This is consistent with previously published data that summarised the expression and activity of drug-metabolizing enzymes in human lung (Somers *et al.*, 2007).

Pulmonary UGT activity was assessed using the non-selective UGT substrates, triclosan and 4-MU. Although UGT activity appeared to be higher in rat than in human lung, this finding has to be interpreted with caution, since the metabolism of triclosan and 4-MU depends not on the activity of one specific UGT, but on the interplay of different UGT isoforms present in the lungs of these two species (Uchaipichat *et al.*, 2004, Jackson *et al.*, 2013).

While pulmonary CYP450 activity was low in both species, the activity in human lung appeared to be even lower than in rat lung. The low pulmonary CYP450 activity observed here is in clear contrast to the role of this enzyme family in the liver. Regarding Flavin mono-oxygenases, remarkably greater benzydamine N-oxygenation activity was observed in rat than

in human lung. The pronounced N-oxide formation observed here in rat is consistent with previously obtained data (Yilmaz *et al.*, 2018). FMOs are known to display complex species, tissue and gender dependent expression, which may account for the species difference observed here (Ripp *et al.*, 1999, Janmohamed *et al.*, 2004, Hines, 2006, Phillips and Shephard, 2017). FMO expression in human lung is low and the major pulmonary isoform, FMO2 is catalytically inactive in Caucasians (Dolphin *et al.*, 1998, Cashman and Zhang, 2006). As this study only included lung tissue from Caucasian donors, it is not surprising that limited N-oxide formation was observed. It would be interesting to explore pulmonary FMO activity from other populations, such as native Africans, where active FMO2 is expressed in lung (Cashman and Zhang, 2006). Aldehyde oxidase mediated oxidation of carbazeran was observed to a limited extent in both species. Aldehyde oxidase has been shown to be expressed in the bronchial epithelium of rats (Garattini *et al.*, 2009). The role of aldehyde oxidase in extrahepatic metabolism has so far not been fully explored and further investigations would be of interest.

5. Conclusion

Due to time constraints, only key experimental parameters were evaluated during our optimization of the PCLS technique. The study demonstrates the importance of optimization and standardization of PCLS conditions, eventually resulting in a more reliable method to determine pulmonary metabolic activity. The reason for our particular interest in the comparison of pulmonary enzymatic activity in rats and humans is that animal models are commonly used in the preclinical development of new drugs. The results show that there are remarkable differences in pulmonary metabolic activity between rats and humans, reflecting species and tissue dependent expression of drug-metabolizing enzymes. Care should therefore be taken when extrapolating metabolism data from animal models to humans. PCLS turned out to be a valuable tool for the investigation of pulmonary drug metabolism and should be developed further for assessing enzyme and metabolic activities not only in lungs but also in other organs.

List of Abbreviations

PCLS	=	Precision-cut lung slices
DOC	=	Dynamic organ culture
CYP	=	Cytochrome P450
COPD	=	Chronic obstructive pulmonary disease
UGTs	=	UDP-glucuronosyltransferase
GST	=	Glutathione S-transferase
SULTs	=	Sulfotransferases
NADPH	=	Nicotinamide adenine dinucleotide phosphate
UDPGA	=	Uridine-diphosphate-glucuronic acid trisodium salt
FMOs	=	Flavin-containing monooxygenase
SD	=	Sprague Dawley
WH	=	Wistar Han
MEM	=	Minimal Essential Medium
UPLC	=	Ultra Performance Liquid Chromatography
LLQ	=	Lower Limit of Quantitation
4-MU	=	4-Methylumbelliferone
CES1	=	Carboxylesterase 1
AO	=	Aldehyde oxidase
S.D.	=	Standard deviation

CONSENT FOR PUBLICATION

Not applicable.

CONFLICT OF INTEREST

The authors declare no conflict of interest, financial or otherwise.

ACKNOWLEDGEMENTS

The study was conducted with the great support from the PK Sciences group of Novartis institutes for biomedical research. The authors would like to acknowledge Arnold Demailly for providing support in the generation of data. Prof. Dr. Didier Lardinois and Dr. Mark Nikolaj Wiese from Basel University Hospital are acknowledged for post-surgical collection of discarded human lung samples.

References

[1] Del Donno, M.;Verduri, A.;Olivieri, D. Air pollution and reversible chronic respiratory diseases. Monaldi Arch. Chest Dis., 2002, 57, 164-166.

[2] Rau, J. L. The inhalation of drugs: advantages and problems. Respir. Care Clin. N. Am., 2005, 50, 367-382.

[3] Stone, K. C.;Mercer, R. R.;Gehr, P.;Stockstill, B.;Crapo, J. D. Allometric relationships of cell numbers and size in the mammalian lung. Am J Respir Cell Mol Biol, 1992, 6, 235-243.

[4] Zhang, J. Y.;Wang, Y.;Prakash, C. Xenobiotic-metabolizing enzymes in human lung. Curr. Drug Metab., 2006, 7, 939-948.

[5] Devereux, T. R.;Domin, B. A.;Philpot, R. M. Xenobiotic metabolism by isolated pulmonary cells. Pharmacol. Ther., 1989, 41, 243-256.

[6] Raunio, H.;Hakkola, J.;Hukkanen, J.;Lassila, A.;Päivärinta, K.;Pelkonen, O.;Anttila, S.;Piipari, R.;Boobis, A.;Edwards, R. J. Expression of xenobiotic-metabolizing CYPs in human pulmonary tissue. Experimental and Toxicologic Pathology, 1999, 51, 412-417.

[7] Hukkanen, J.;Pelkonen, O.;Hakkola, J.;Raunio, H. Expression and regulation of xenobiotic-metabolizing cytochrome P450 (CYP) enzymes in human lung. Crit. Rev. Toxicol., 2002, 32, 391-411.

[8] Olsson, B.;Bondesson, E.;Borgström, L.;Edsbäcker, S.;Eirefelt, S.;Ekelund, K.;Gustavsson, L.;Hegelund-Myrbäck, T., Pulmonary Drug Metabolism, Clearance, and Absorption In: Controlled Pulmonary Drug Delivery; Smyth, H. D. C.; Hickey, A. J., Ed.; Springer New York: New York, NY, 2011; pp. 21-50.

[9] Somers, G. I.;Lindsay, N.;Lowdon, B. M.;Jones, A. E.;Freathy, C.;Ho, S.;Woodrooffe, A. J.;Bayliss, M. K.;Manchee, G. R. A comparison of the expression and metabolizing activities of phase I and II enzymes in freshly isolated human lung parenchymal cells and cryopreserved human hepatocytes. Drug Metab. Dispos., 2007, 35, 1797-1805.

[10] Ioannides, C.;Lake, B. G.;Lyubimov, A. V., Precision-Cut Tissue Slices: A Suitable In Vitro System for the Study of the Induction of Drug-Metabolizing Enzyme Systems In: Encyclopedia of Drug Metabolism and Interactions; John Wiley & Sons, Inc.: 2011.

[11] Umachandran, M.;Ioannides, C. Stability of cytochromes P450 and phase II conjugation systems in precision-cut rat lung slices cultured up to 72 h. Toxicology, 2006, 224, 14-21.

[12] De Kanter, R.;Olinga, P.;De Jager, M. H.;Merema, M. T.;Meijer, D. K.;Groothius, G. M. Organ slices as an in vitro test system for drug metabolism in human liver, lung and kidney. Toxicol In Vitro, 1999, 13, 737-744.

[13] O'Neil, J. J.;Sanford, R. L.;Wasserman, S.;Tierney, D. F. Metabolism in rat lung tissue slices: technical factors. J. Appl. Physiol. Respir. Environ. Exerc. Physiol., 1977, 43, 902-906.

[14] Nave, R.;Fisher, R.;Zech, K. In Vitro metabolism of ciclesonide in human lung and liver precision-cut tissue slices. Biopharm. Drug Dispos., 2006, 27, 197-207.

[15] Yilmaz, Y.;Umehara, K.;Williams, G.;Faller, T.;Schiller, H.;Walles, M.;Kraehenbuehl, S.;Camenisch, G.;Manevski, N. Assessment of the pulmonary CYP1A1 metabolism of mavoglurant (AFQ056) in rat. Xenobiotica, 2017, 1-11.

[16] De Kanter, R.;De Jager, M.;Draaisma, A.;Jurva, J.;Olinga, P.;Meijer, D.;Groothuis, G. Drug-metabolizing activity of human and rat liver, lung, kidney and intestine slices. Xenobiotica, 2002, 32, 349-362.

[17] Kanter, R.;Monshouwer, M.;Meijer, D.;Groothuis, G. Precision-cut organ slices as a tool to study toxicity and metabolism of xenobiotics with special reference to non-hepatic tissues. Current drug metabolism, 2002, 3, 39-59.

[18] de Graaf, I. A. M.;Koster, H. Cryopreservation of precision-cut tissue slices for application in drug metabolism research. Toxicology in Vitro, 2003, 17, 1-17.

[19] Liberati, T. A.;Randle, M. R.;Toth, L. A. In vitro lung slices: a powerful approach for assessment of lung pathophysiology. Expert. Rev. Mol. Diagn., 2010, 10, 501-508.

[20] Walles, M.;Wolf, T.;Jin, Y.;Ritzau, M.;Leuthold, L. A.;Krauser, J.;Gschwind, H. P.;Carcache, D.;Kittelmann, M.;Ocwieja, M.;Ufer, M.;Woessner, R.;Chakraborty, A.;Swart, P. Metabolism and disposition of the metabotropic glutamate receptor 5 antagonist (mGluR5) mavoglurant (AFQ056) in healthy subjects. Drug Metab. Dispos., 2013, 41, 1626-1641.

[21] Ding, X.;Kaminsky, L. S. Human extrahepatic cytochromes P450: function in xenobiotic metabolism and tissue-selective chemical toxicity in the respiratory and gastrointestinal tracts. Annu. Rev. Pharmacol. Toxicol., 2003, 43, 149-173.

[22] Nishimura, M.;Naito, S. Tissue-specific mRNA expression profiles of human phase I metabolizing enzymes except for cytochrome P450 and phase II metabolizing enzymes. Drug Metab. Pharmacokinet., 2006, 21, 357-374.

[23] Bieche, I.;Narjoz, C.;Asselah, T.;Vacher, S.;Marcellin, P.;Lidereau, R.;Beaune, P.;de Waziers, I. Reverse transcriptase-PCR quantification of mRNA levels from cytochrome (CYP)1, CYP2 and CYP3 families in 22 different human tissues. Pharmacogenet. Genomics, 2007, 17, 731-742.

[24] Smith, P. F.;Gandolfi, A. J.;Krumdieck, C. L.;Putnam, C. W.;Zukoski, C. F., 3rd;Davis, W. M.;Brendel, K. Dynamic organ culture of precision liver slices for in vitro toxicology. Life Sci., 1985, 36, 1367-1375.

[25] Smith, P. F.;Krack, G.;McKee, R. L.;Johnson, D. G.;Gandolfi, A. J.;Hruby, V. J.;Krumdieck, C. L.;Brendel, K. Maintenance of adult rat liver slices in dynamic organ culture. In Vitro Cell Dev. Biol., 1986, 22, 706-712.

[26] Sanderson, M. J. Exploring lung physiology in health and disease with lung slices. Pulm. Pharmacol. Ther., 2011, 24, 452-465.

[27] Dogterom, P. Development of a simple incubation system for metabolism studies with precision-cut liver slices. Drug Metab. Dispos., 1993, 21, 699-704.

[28] Manevski, N.;Troberg, J.;Svaluto-Moreolo, P.;Dziedzic, K.;Yli-Kauhaluoma, J.;Finel, M. Albumin stimulates the activity of the human UDP-glucuronosyltransferases 1A7, 1A8, 1A10, 2A1 and 2B15, but the effects are enzyme and substrate dependent. PLoS One, 2013, 8, e54767.

[29] Wang, L. Q.;Falany, C. N.;James, M. O. Triclosan as a substrate and inhibitor of 3'-phosphoadenosine 5'-phosphosulfate-sulfotransferase and UDP-glucuronosyl transferase in human liver fractions. Drug Metab. Dispos., 2004, 32, 1162-1169.

[30] Gotz, C.;Pfeiffer, R.;Tigges, J.;Blatz, V.;Jackh, C.;Freytag, E. M.;Fabian, E.;Landsiedel, R.;Merk, H. F.;Krutmann, J.;Edwards, R. J.;Pease, C.;Goebel, C.;Hewitt, N.;Fritsche, E. Xenobiotic metabolism capacities of human skin in comparison with a 3D epidermis model and keratinocyte-

based cell culture as in vitro alternatives for chemical testing: activating enzymes (Phase I). Exp Dermatol, 2012, 21, 358-363.

[31] Manevski, N.;Swart, P.;Balavenkatraman, K. K.;Bertschi, B.;Camenisch, G.;Kretz, O.;Schiller, H.;Walles, M.;Ling, B.;Wettstein, R.;Schaefer, D. J.;Itin, P.;Ashton-Chess, J.;Pognan, F.;Wolf, A.;Litherland, K. Phase II metabolism in human skin: skin explants show full coverage for glucuronidation, sulfation, N-acetylation, catechol methylation, and glutathione conjugation. Drug Metab. Dispos., 2015, 43, 126-139.

[32] Yuan, R.;Madani, S.;Wei, X. X.;Reynolds, K.;Huang, S. M. Evaluation of cytochrome P450 probe substrates commonly used by the pharmaceutical industry to study in vitro drug interactions. Drug Metab. Dispos., 2002, 30, 1311-1319.

[33] Li, X. Q.;Bjorkman, A.;Andersson, T. B.;Ridderstrom, M.;Masimirembwa, C. M. Amodiaquine clearance and its metabolism to N-desethylamodiaquine is mediated by CYP2C8: a new high affinity and turnover enzyme-specific probe substrate. J. Pharmacol. Exp. Ther., 2002, 300, 399-407.

[34] Carlile, D. J.;Hakooz, N.;Bayliss, M. K.;Houston, J. B. Microsomal prediction of in vivo clearance of CYP2C9 substrates in humans. Br. J. Clin. Pharmacol., 1999, 47, 625-635.

[35] Ono, S.;Hatanaka, T.;Miyazawa, S.;Tsutsui, M.;Aoyama, T.;Gonzalez, F. J.;Satoh, T. Human liver microsomal diazepam metabolism using cDNA-expressed cytochrome P450s: role of CYP2B6, 2C19 and the 3A subfamily. Xenobiotica, 1996, 26, 1155-1166.

[36] Lang, D. H.;Rettie, A. E. In vitro evaluation of potential in vivo probes for human flavin-containing monooxygenase (FMO): metabolism of benzydamine and caffeine by FMO and P450 isoforms. Br. J. Clin. Pharmacol., 2000, 50, 311-314.

[37] Kaye, B.;Rance, D. J.;Waring, L. Oxidative metabolism of carbazeran in vitro by liver cytosol of baboon and man. Xenobiotica, 1985, 15, 237-242.

[38] Hutzler, J. M.;Yang, Y. S.;Albaugh, D.;Fullenwider, C. L.;Schmenk, J.;Fisher, M. B. Characterization of aldehyde oxidase enzyme activity in cryopreserved human hepatocytes. Drug Metab. Dispos., 2012, 40, 267-275.

[39] Thomsen, R.;Rasmussen, H. B.;Linnet, K.;Consortium, I. In vitro drug metabolism by human carboxylesterase 1: focus on angiotensin-converting enzyme inhibitors. Drug Metab. Dispos., 2014, 42, 126-133.

[40] Van Bezooijen, C. F. A.;Horbach, G. J. M. J.;Hollander, C. F., The Effect of Age on Rat Liver Drug Metabolism In: Drugs and Aging; Platt, D., Ed.; Springer Berlin Heidelberg: Berlin, Heidelberg, 1986; pp. 45-55.

[41] Bozhkov, A. I.;Nikitchenko, Y. V.;Klimova, E. M.;Linkevych, O. S.;Lebid, K. M.;Al-Bahadli, A. M. M.;Alsardia, M. M. A. Young and old rats have different strategies of metabolic adaptation to Cu-induced liver fibrosis. Advances in Gerontology, 2017, 7, 41-50.

[42] Yamamoto, Y.;Tanaka, A.;Kanamaru, A.;Tanaka, S.;Tsubone, H.;Atoji, Y.;Suzuki, Y. Morphology of aging lung in F344/N rat: Alveolar size, connective tissue, and smooth muscle cell markers. The Anatomical Record Part A: Discoveries in Molecular, Cellular, and Evolutionary Biology, 2003, 272A, 538-547.

[43] Samuel, J. J.;Nick, A.;Doug, B.;Ilaria, B.;James, G.;Lamia, H.;Alan, H.;Judy, L.;Anja, P.;Paul, P.;Andrew, R.;Alison, R.;Michelle, S.;Carol, S.;Mark, Y.;Kathryn, C. Does age matter? The impact of rodent age on study outcomes. Laboratory Animals, 2016, 51, 160-169.

[44] McCutcheon, J. E.;Marinelli, M. Age matters. The European journal of neuroscience, 2009, 29, 997-1014.

[45] Nijjar, M. S.;Ho, J. C. Isolation of plasma membranes from rat lungs: effect of age on the subcellular distribution of adenylate cyclase activity. Biochim Biophys Acta, 1980, 600, 238-243.

[46] Nishiyama, Y.;Nakayama, S. M.;Watanabe, K. P.;Kawai, Y. K.;Ohno, M.;Ikenaka, Y.;Ishizuka, M. Strain differences in cytochrome P450 mRNA and protein expression, and enzymatic activity among Sprague Dawley, Wistar, Brown Norway and Dark Agouti rats. J. Vet. Med. Sci., 2016, 78, 675-680.

[47] Morin, J. P.;Baste, J. M.;Gay, A.;Crochemore, C.;Corbiere, C.;Monteil, C. Precision cut lung slices as an efficient tool for in vitro lung physio-pharmacotoxicology studies. Xenobiotica, 2013, 43, 63-72.

[48] Parrish, A. R.;Gandolfi, A. J.;Brendel, K. Precision-cut tissue slices: applications in pharmacology and toxicology. Life Sci, 1995, 57, 1887-1901.

[49] Fisher, R. L.;Shaughnessy, R. P.;Jenkins, P. M.;Austin, M. L.;Roth, G. L.;Gandolfi, A. J.;Brendel, K. Dynamic Organ Culture is Superior to Multiwell Plate Culture for Maintaining Precision-Cut Tissue Slices: Optimization of Tissue Slice Culture, Part 1. Toxicology Methods, 1995, 5, 99-113.

[50] Umachandran, M.;Howarth, J.;Ioannides, C. Metabolic and structural viability of precision-cut rat lung slices in culture. Xenobiotica, 2004, 34, 771-780.

[51] Monteil, C.;Guerbet, M.;Le Prieur, E.;Morin, J.-P.;M Jouany, J.;Fillastre, J. P., Characterization of Precision-cut Rat Lung Slices in a Biphasic Gas/Liquid Exposure System: Effect of O2. 1999.

[52] Siminski, J. T.;Kavanagh, T. J.;Chi, E.;Raghu, G. Long-term maintenance of mature pulmonary parenchyma cultured in serum-free conditions. American Journal of Physiology-Lung Cellular and Molecular Physiology, 1992, 262, L105-L110.

[53] Lekas, P.;Tin, K. L.;Lee, C.;Prokipcak, R. D. The human cytochrome P450 1A1 mRNA is rapidly degraded in HepG2 cells. Arch. Biochem. Biophys., 2000, 384, 311-318.

[54] Lorenz, J.;Glatt, H. R.;Fleischmann, R.;Ferlinz, R.;Oesch, F. Drug metabolism in man and its relationship to that in three rodent species: monooxygenase, epoxide hydrolase, and glutathione S-transferase activities in subcellular fractions of lung and liver. Biochem. Med., 1984, 32, 43-56.

[55] Pacifici, G. M.;Franchi, M.;Bencini, C.;Repetti, F.;Di Lascio, N.;Muraro, G. B. Tissue distribution of drug-metabolizing enzymes in humans. Xenobiotica, 1988, 18, 849-856.

[56] Jackson, E. N.;Schneider, J.;Faux, L. R.;James, M. O. Isoform-selective glucuronidation of triclosan. The FASEB Journal, 2013, 27, 892.811-892.811.

[57] Uchaipichat, V.;Mackenzie, P. I.;Guo, X.-H.;Gardner-Stephen, D.;Galetin, A.;Houston, J. B.;Miners, J. O. Human UDP-Glucuronlytransferases: Isoform selectivity and kinetics of 4-Methylumbellifferone and 1-Naphtol Glucuronidation, effects of organic solvents, and inhibition by Diclofenac and Probenecid. Drug Metab. Dispos., 2004, 32, 413-423.

[58] Yilmaz, Y.;Williams, G.;Manevski, N.;Walles, M.;Krahenbuhl, S.;Camenisch, G. Functional assessment of rat pulmonary flavin-containing monooxygenase activity. Xenobiotica, 2018, 1-10.

[59] Ripp, S. L.;Itagaki, K.;Philpot, R. M.;Elfarra, A. A. Species and sex differences in expression of flavin-containing monooxygenase form 3 in liver and kidney microsomes. Drug Metab. Dispos., 1999, 27, 46-52.

[60] Hines, R. N. Developmental and tissue-specific expression of human flavin-containing monooxygenases 1 and 3. Expert Opin. Drug Metab. Toxicol., 2006, 2, 41-49.

[61] Phillips, I. R.;Shephard, E. A. Drug metabolism by flavin-containing monooxygenases of human and mouse. Expert Opin. Drug Metab. Toxicol., 2017, 13, 167-181.

[62] Janmohamed, A.;Hernandez, D.;Phillips, I. R.;Shephard, E. A. Cell-, tissue-, sex- and developmental stage-specific expression of mouse flavin-containing monooxygenases (Fmos). Biochem Pharmacol, 2004, 68, 73-83.

[63] Dolphin, C. T.;Beckett, D. J.;Janmohamed, A.;Cullingford, T. E.;Smith, R. L.;Shephard, E. A.;Phillips, I. R. The flavin-containing monooxygenase 2 gene (FMO2) of humans, but not of other primates, encodes a truncated, nonfunctional protein. J. Biol. Chem., 1998, 273, 30599-30607.

[64] Cashman, J. R.;Zhang, J. Human flavin-containing monooxygenases. Annu. Rev. Pharmacol. Toxicol., 2006, 46, 65-100.

[65] Garattini, E.;Fratelli, M.;Terao, M. The mammalian aldehyde oxidase gene family. Hum. Genomics, 2009, 4, 119-130.

3.2. Assessment of the pulmonary CYP1A1 metabolism of mavoglurant (AFQ056) in rat

Yildiz Yilmaz[1], Kenichi Umehara[1], Gareth Williams[1], Thomas Faller[1], Hilmar Schiller[1], Markus Walles[1], Stephan Krähenbühl[3], Gian Camenisch[1]and Nenad Manevski[2]

Pharmacokinetic Sciences[1], Novartis Institutes for Biomedical Research, Basel, Switzerland

Drug Metabolism and Pharmacokinetics[2], UCB, Slough, United Kingdom

Clinical pharmacology and toxicology[3], University hospital Basel, Switzerland

Published in

Journal of Xenobiotica (2017)

48:8, 793-803

DOI: 10.1080/00498254.2017.1373311

http://tandfonline.com/ixen
ISSN: 0049-8254 (print), 1366-5928 (electronic)

Xenobiotica

Xenobiotica, 2018; 48(8): 793–803
 DOI: 10.1080/00498254.2017.1373311

Taylor & Francis
Taylor & Francis Group

RESEARCH ARTICLE

Check for updates

Assessment of the pulmonary CYP1A1 metabolism of mavoglurant (AFQ056) in rat

Yildiz Yilmaz[1], Kenichi Umehara[1], Gareth Williams[1], Thomas Faller[1], Hilmar Schiller[1], Markus Walles[1], Stephan Kraehenbuehl[2], Gian Camenisch[1], and Nenad Manevski[3]

[1]Pharmacokinetic Sciences, Novartis Institutes for Biomedical Research, Basel, Switzerland, [2]Clinical Pharmacology and Toxicology, University Hospital Basel, Switzerland, and [3]Drug Metabolism and Pharmacokinetics, UCB, Slough, United Kingdom,

Abstract

1. AFQ056 phenotyping results indicate that CYP1A1 is responsible for the formation of the oxidative metabolite, M3. In line with the predominant assumption that CYP1A1 is mainly expressed in extrahepatic tissues, only traces of M3 were detected in hepatic systems. The aim of this study was to investigate the pulmonary CYP1A1 mediated metabolism of AFQ056 in rat.
2. Western blot analysis confirmed that CYP1A1 is expressed in rat lung albeit at low levels. M3 formation was clearly observed in recombinant rat CYP1A1, lung microsomes and lung tissue slices and was strongly inhibited by ketoconazole in the incubations. As CYP3A4 and CYP2C9 metabolites were only observed at trace levels, we concluded that the reduced M3 formation was due to CYP1A1 inhibition.
3. AFQ056 lung clearance (CL_{lung}) as estimated from *in vitro* data was predicted to be negligible (<1% pulmonary blood flow). This was confirmed by *in vivo* experiments where intravenous and intra-arterial dosing to rats failed to show significant pulmonary extraction.
4. While rat lung may make a contribution to the formation of M3, it is unlikely to be the only organ involved in this process and further experiments are required to investigate the potential metabolic elimination routes for AFQ056.

Keywords

AFQ056, CYP1A1, extrahepatic metabolism, lung metabolism, lung slices, rat lung clearance

History

Received 5 July 2017
Revised 25 August 2017
Accepted 26 August 2017

Introduction

AFQ056 (mavoglurant), a metabotropic glutamate receptor 5 (mGluR5) antagonist, was developed for the treatment of neurological diseases such as Parkinson's disease and Fragile X syndrome (Vranesic et al., 2014). As shown in Figure 1, a human absorption, distribution, metabolism, and excretion (ADME) study of AFQ056 identified a hydroxylated metabolite M3 and several downstream metabolites including the corresponding glucuronide M20 and sulphate conjugates M26 (Walles et al., 2013). This biotransformation pathway accounted for approximately 20% and 15% of total drug-related exposure in human plasma and excreta, respectively, and was also observed in mouse, rat, and dog ADME studies. Although found *in vivo*, the metabolite M3 was not observed during *in vitro* incubations with liver microsomes and hepatocytes, suggesting that M3 is formed extrahepatically. Preliminary assays with recombinant human CYPs revealed that AFQ056 is a high-turnover substrate for CYP1A1 and that M3 is a major product of this reaction (Walles et al., 2013). It should be noted that human CYP1A2 and CYP2C19 also catalyse the formation of M3 but to a much lesser extent. In addition, the human recombinant P450 enzymes incubations demonstrated that the oxidative metabolite M7 was formed mainly by the CYP2C family, whereas metabolites M1/M2 were formed by CYP3A4 with negligible contributions of CYP1A1 (Walles et al., 2013).

CYP1A1 is a drug-metabolising enzyme primarily expressed in extrahepatic tissues such as lungs, intestine, kidneys, and skin (Bieche et al., 2007; Ding & Kaminsky, 2003; Nishimura & Naito, 2006). The amino acid sequence of CYP1A1 is well conserved between humans and animals used in preclinical studies (80–95%) (Martignoni et al., 2006), suggesting an overlap between substrates and inhibitors. Expression of CYP1A1 can be induced via the aryl hydrocarbon receptor (AhR) by cigarette smoking (Anttila et al., 1992), air pollution (Sancini et al., 2014; Totlandsdal

Address for correspondence: Yildiz Yilmaz Pharmacokinetic Sciences, Novartis Institutes for BioMedical Research Basel, Switzerland. E-mail: yildiz.yilmaz@novartis.com

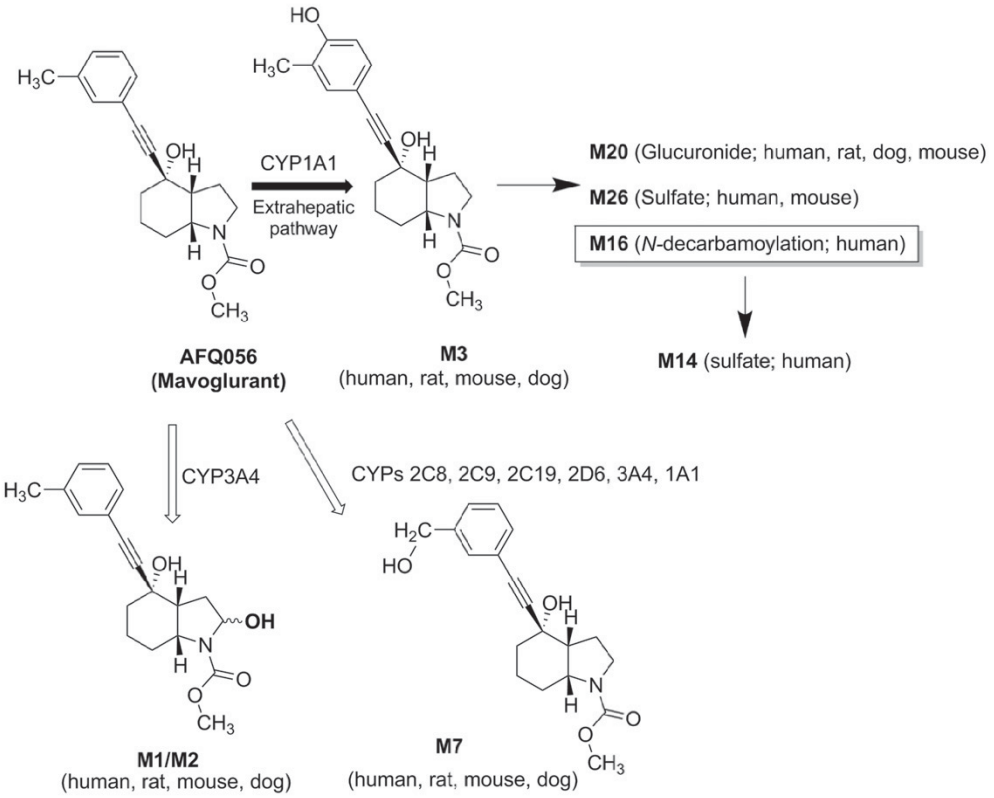

Figure 1. Biotransformation pathway of AFQ056. Following *in vivo* dosing of humans and preclinical animals, AFQ056 is metabolised to M3 by CYP1A1. Observed downstream metabolites of this biotransformation pathway are M20, M26, M16, and M14. M1/M2 is a hydroxylated metabolite formed by CYP3A4. The metabolite M7 was formed mainly by the CYP2C family with negligible contributions of CYP2D6, CYP3A4, and CYP1A1. For a detailed summary of all observed AFQ056 metabolites, see reference (Walles et al., 2013).

et al., 2010), various drugs and chemicals (Hu et al., 2007), and even dietary phytochemicals (Ito et al., 2007). Although cigarette smoking strongly induces CYP1A1 expression in the lungs, the main organ exposed to smoke (Anttila et al., 2001; Thum et al., 2006), studies have shown that heavy smoking may also induce CYP1A1 in the liver (Chang et al., 2003; Frey et al., 2016; Hussain et al., 2014) and intestine (Buchthal et al., 1995). CYP phenotyping assays have identified a number of high-turnover CYP1A1 substrates including phenacetin (Tassaneeyakul et al., 1993), riluzole (Sanderink et al., 1997), dacarbazine (Reid et al., 1999), haloperidol (Fang et al., 2001), debrisoquine (Granvil et al., 2002), granisetron (Nakamura et al., 2005), erlotinib (Li et al., 2007), dronedarone (Klieber et al., 2014), BAY 63-2521 (Frey et al., 2016) and BJ-B11 (Lu et al., 2015). However, the quantitative contribution of this enzyme to drug disposition is unknown, and it remains unclear which *in vitro* assays could be used for such predictions.

Our main objective was to confirm and evaluate the role of pulmonary CYP1A1, especially from a quantitative perspective, and to investigate experimental models suitable for prediction of its activity. As healthy human lung tissue is difficult to acquire, rat lung models have been used for method development with the assumption that rat is a suitable surrogate for human. Western blotting experiments were performed to confirm the presence of CYP1A1 in rat lung. AFQ056 biotransformation was investigated in several experimental rat models: recombinant CYP1A1, lung microsomes and lung tissue slices. Incubations with the CYP inhibitor ketoconazole were also carried out to further confirm the involvement of CYP1A1. Finally, the *in vivo* pulmonary extraction of AFQ056 was evaluated following intra-arterial (i.a.) and intravenous (i.v.) dosing to rats. The application of precision cut tissue slice technology in drug metabolism studies has been previously discussed and investigations have also included the use of tissue slices from a variety of organs including the lung (De Kanter et al., 2002). Lung slices contain all of the cofactors required for biotransformation at physiologically relevant concentrations, while retaining the cellular architecture of the tissue. Based on this, we explored the use of rat lung tissue slices to investigate the pulmonary metabolism of AFQ056.

Materials and methods

Reagents, chemicals, and materials

AFQ056 (mavoglurant), NVP-CBJ474 (AFQ056-M3), NVP-BCZ626 (AFQ056-M1/M2) and NVP-BCZ630 (AFQ056-M7), were synthesized at Novartis (Basel, Switzerland). Minimal Essential Medium (MEM, without L-glutamine, HEPES, and phenol red), UltraPure™ low melting point agarose (solution remains fluid at 37 °C and will gelatinise below 25 °C) were purchased from Life Technologies (Carlsbad, CA). β-Nicotinamide adenine dinucleotide

DOI: 10.1080/00498254.2017.1373311

phosphate reduced tetra-cyclohexylammonium salt (NADPH; ≥95%), dimethyl sulfoxide (DMSO; ≥99.7%), 4-(2-hydroxyethyl)piperazine-1-ethanesulfonic acid (HEPES; ≥99.5%), D-(+)-glucose (anhydrous; ≥99.5%), peroxyacetic acid (~39% in acetic acid), sucrose (D(+)-saccharose; ≥99.5%), ketoconazole, rabbit anti-CYP1A1 primary antibody (SAB1410273), goat anti-rabbit IgG and labetalol were purchased from Sigma-Aldrich (Buchs, Switzerland). Recombinant human and rat CYPs, expressed in baculovirus-infected insect cells (Corning Supersomes™), were obtained from BD Biosciences (Woburn, MA). For the Western blot assay XT sample buffer, dithiothreitol, Criterion XT gel, Precision Plus Protein™ All Blue, XT MES buffer, Coomassie Brilliant Blue, Trans-Blot® Turbo™ Midi PVDF membrane, Trans-Blot® Turbo™ Transfer System, milk powder, phosphate buffered saline, Tween 20, peroxidase substrate (Clarity™ Western ECL Substrate) and VersaDoc MP 4000 imager were purchased from Bio-Rad (Hercules, CA). Pooled microsomes from male Sprague–Dawley (SD) rat lungs were purchased from XenoTech (Kansas City, MO). Higher purity grade solvents water, methanol and acetonitrile used for the LC–MS were purchased from Fischer Chemicals AG (Loughborough, UK).

Rat CYP1A1 western blots

Recombinant rat CYP1A1 (0.01–0.5 pmol) and rat lung microsomes (10–50 µg total protein) were mixed with XT sample buffer supplemented with 100 mM of dithiothreitol, heated for 5 min at 95 °C and loaded on Criterion XT gel (4–12% bis-Tris precast polyacrylamide gel with a 26-well comb). Precision Plus Protein™ All Blue (10–250 kDa) was used as protein standard. The gel was run in XT MES buffer for 45 min at 200 V. Electrophoretic separation of proteins under given conditions was assessed by Coomassie Brilliant Blue gel staining. The gel was stained for 1 h at room temperature and then destained in water solution with 10% methanol and 2.5% acetic acid. Separated proteins were blotted to Trans-Blot® Turbo™ Midi PVDF membrane with Trans-Blot® Turbo™ Transfer System. To prevent non-specific antibody binding, the PVDF membrane was blocked overnight at 5 °C in 5% milk powder in phosphate buffered saline supplemented with 0.05% Tween 20. The blocked membrane was stained for 1–3 h with rabbit anti-CYP1A1 primary antibody diluted 1:250 in 5% milk powder blocking solution, and then washed 3 times for 5 min in phosphate buffered saline with 0.05% Tween 20. The secondary antibody was goat anti-rabbit IgG conjugated with horseradish peroxidase diluted 1:2000 in 5% milk powder blocking solution. Secondary staining was performed for 1 h and membrane was then washed three times for 5 min in phosphate buffered saline with 0.05% Tween 20. Peroxidase substrate was prepared by mixing equal amounts of solutions A and B (luminol and enhancer) and applied to the surface of the membrane. Spots were recorded with a VersaDoc MP 4000 imager using the Chemi Ultra Sensitivity settings.

AFQ056 enzyme kinetics with rat recombinant CYP1A1

As measured by the enzyme supplier, the 7-ethoxyresorufin deethylation activities (EROD) of human and rat CYP1A1 were 29 and 35 pmol/min/pmol of CYP1A1 protein. Prior to performing the enzyme kinetics assays, incubation time, enzyme protein amount and the reaction linearity were evaluated. Assays were performed in 100 mM sodium phosphate buffer, pH 7.4, supplemented with 5 mM $MgCl_2$ and 1.2–2 pmol/ml of recombinant CYP1A1. The AFQ056 concentration range used for rat recombinant CYP1A1 incubations was 0.1–12.5 µM. The samples were pre-incubated at 37 °C for 3 min and reactions were initiated by the addition of NADPH (1 mM). The samples were incubated for 5 min at 37 °C with mechanical shaking (500 rpm) and reactions were terminated by the addition of an equal volume of cold acetonitrile containing internal standard (labetalol; 0.25 µM). Samples were then centrifuged for 15 min at 15 000*g* and the supernatants were analysed by LC–MS/MS.

To assess AFQ056 enzyme kinetics with rat recombinant CYP1A1, experimental data were fitted to the Michaelis–Menten equation:

$$v = \frac{V_{max}[S]}{K_m + [S]} \quad (1)$$

Where v is the reaction velocity, V_{max} is the limiting reaction velocity, K_m is the Michaelis–Menten constant, and $[S]$ is the total substrate concentration. Calculations were performed using SigmaPlot Version 8.0 (S1), Enzyme Kinetics module Version 1.1 software (SPSS Science Inc., Chicago, IL).

Incubations with rat lung microsomes

Lung microsomes (1.5 mg/ml) were pre-incubated with 0.5 µM AFQ056 and 5 mM $MgCl_2$ for 3 min at 37 °C in 0.1 M sodium phosphate buffer, pH 7.4. The reactions were started by adding cofactor (1 mM NADPH). After 0, 3, 6, 9, 12, and 15 min incubations at 37 °C with mechanical shaking (500 rpm), the reactions were stopped by adding an equal volume of acetonitrile containing internal standard (labetalol; 0.25 µM). The samples were then centrifuged for 15 min at 15 000*g* and the supernatants were analysed by LC–MS/MS.

Lung tissue slice preparation and incubation

Animal experiments were conducted with the approval of the Cantonal Veterinary Authority of Basel City, Switzerland. Six-week old male Sprague–Dawley rats (Charles River; Freiburg, Germany), with an average weight of 200 g, were acclimatised for one week prior to use. Animals were sacrificed by exsanguination from the *vena cava* and cutting of the diaphragm. The lungs with trachea were immediately extracted and kept on wet water ice until processing. Rats were anaesthetised during the whole procedure with 3–5% isoflurane with O_2 as gas carrier.

Lung tissue was inflated with a pre-warmed (37 °C) agarose solution in MEM (low melting point, 2.5%, v/v) *via* the trachea. The solidified lung tissue was dissected with surgical scissors and cylindrical tissue cores were prepared with an 8 mm coring tool (Alabama Research & Development, Munford, AL). The tissue slices (8 mm in diameter, ~420 µm of thickness) were prepared using a Krumdieck tissue slicer (TSE Systems, Chesterfield, MO)

(Krumdieck, 2013) and collected in 4 °C MEM that had been previously gassed with 75% O_2 and 5% CO_2.

Briefly, three lung tissue slices (average weight 0.024 g/slice) were positioned onto titanium (type C) roller inserts (Vitron Inc., Tucson, AZ). The inserts were then placed in glass vials that had been prefilled with 2 mL of a modified dynamic organ culture Medium composed of MEM, HEPES (25 mM) and glucose (25 mM) (Smith et al., 1985, 1986). The tissue slices were pre-incubated for 30 min at 37 °C in a CO_2 incubator (Hereaus, Zurich, Switzerland) in an atmosphere of 75% O_2 and 5% CO_2. The reactions were initiated by the addition of AFQ056 (0.5 μM) and stopped after 240 min by adding 3 mL of acetonitrile containing internal standard (labetalol; 0.25 μM). While the formation of M3 has previously been shown to be predominantly catalysed by CYP1A1, CYP2C and CYP3A4 have been shown to be responsible for the formation of metabolites M7 and M1/M2, respectively (Figure 1) (Walles et al., 2013). Formation of the metabolites M1/M2 and M7 was anticipated to be low in pulmonary fractions and, therefore, additional incubations were performed for 24 h at a higher AFQ056 concentration (10 μM). Negative control incubations without tissue slices were performed in parallel to correct for non-specific binding of the substrates during the incubation period. Samples were stored at −80 °C until further analysis. Prior to analytical measurement, the samples were sonicated for 5 min, and then centrifuged for 15 min at 15 000*g* and the supernatants were analysed by LC–MS/MS.

Inhibition of AFQ056 hydroxylation by ketoconazole

Due to the lack of a selective CYP1A1 inhibitor, inhibition of AFQ056 metabolism was investigated using ketoconazole. While ketoconazole is generally considered to be a CYP3A4 inhibitor, studies have shown that it also inhibits human CYP1A1 (Paine et al., 1999). For the purposes of this investigation, we have assumed that the inhibition potential of ketoconazole on rat and human CYP1A1 is comparable, as the amino acid sequence of CYP1A1 is well conserved between humans and rats (80–95%) (Martignoni et al., 2006). Determination of the CYP1A1 inhibition constant (K_i) for ketoconazole was performed under incubation conditions similar to those used in the CYP1A1 enzyme kinetics experiments. Linearity of enzymatic reactions and approximate potency of ketoconazole inhibition were evaluated in preliminary assays. In human recombinant CYP1A1 incubations, the enzyme concentration was 1.2 pmol/mL, AFQ056 concentrations were 0.1–2.5 μM and ketoconazole concentrations were 0–2.5 μM. In rat recombinant CYP1A1 incubations, the enzyme concentration was 2 pmol/mL, AFQ056 concentrations were 0.1–20 μM and ketoconazole concentrations were 0–2.5 μM. For human and rat recombinant CYP1A1 inhibition assays, the incubation time was 5 min. Based upon ketoconazole's microsomal binding (Quinney et al., 2013) and the low total protein concentration used in our inhibition assays (0.004–0.02 mg/mL), binding of ketoconazole to recombinant CYP1A1 preparation was considered to be negligible ($fu_{inc} \approx 1$). In rat lung tissue slices, AFQ056 (1 μM) was incubated with ketoconazole (10 μM) for 4 h. Inhibition of AFQ056 hydroxylation by ketoconazole in human and rat recombinant CYP1A1 was well described by the following competitive inhibition model:

$$v = \frac{V_{max} * [S]}{[S] + K_m(1 + \frac{[I]}{K_i})} \quad (2)$$

Where K_i is the competitive inhibition constant, and $[I]$ is the total inhibitor concentration.

Analytical method

Quantitative analysis was performed using a QTRAP 5500 LC-MS/MS system (AB Sciex, Ontario, Canada) coupled to a Thermo Allegra liquid chromatograph and CTC Pal auto sampler. The analytical column was a Kinetex C8 (50 × 2.1 mm, 2.6 μm). The column flow rate and temperature were 400 μL/min and 50 °C, respectively. Eluent A was water with 0.1% (v/v) formic acid, eluent B was methanol with 0.1% (v/v) formic acid and eluent C was acetonitrile with 0.1% (v/v) formic acid. The chromatographic conditions were optimised to ensure that M3 and other oxidative metabolites, M1/M2 and M7 were sufficiently separated. Gradient elution was as follows: 0 min → 5% B, 10% C; 5 min → 49% B, 50% C; 5.95 min → 49% B, 50% C; 6 min → 5% B, 10% C; 7.5 min → 5% B, 10% C. Quantification of AFQ056, M3, M1/M2 and M7 was performed with multiple-reaction monitoring mode (positive), by detecting the following m/z transitions: AFQ056 (296 → 221, collision energy (CE); 21 eV, declustering potential (DP); 116 V), M3 (312 → 237, CE; 19 eV, DP; 111 V), M1/M2 (2 9 4 → 204, CE; 15 eV, DP; 114 V), M7 (3 1 2 → 252, CE; 15 eV, DP; 112 V) and labetalol (329 → 311, CE; 19 eV, DP; 66 V). MS data were processed with Analyst 1.6.2 software (AB Sciex, Ontario, Canada). Calibration curves for AFQ056 and M3 were prepared at a concentration range of 0.1–1000 nM.

Prediction of pulmonary clearance

AFQ056 displayed insignificant degradation in lung microsomes during the 15 min incubation and therefore, it was not possible to measure substrate depletion to calculate $CL_{int,in\ vitro}$. For this reason, the rate of M3 formation (represented by the slope, in units of concentration/time) has been used (Njuguna et al., 2016). This approach was also used for lung slices despite the fact that AFQ056 displayed measurable degradation in that system. To estimate lung organ clearance from *in vitro* incubations, the following approach was used:

$$\text{Metabolite formation} \rightarrow CL_{int,\,in\ vitro} \rightarrow CL_{int,\,lung} \rightarrow CL_{lung}$$

Where $CL_{int,in\ vitro}$ is the intrinsic clearance in the *in vitro* assay, $CL_{int,lung}$ is the intrinsic clearance in the whole rat lungs, and CL_{lung} is the lung organ clearance. The AFQ056 $CL_{int,in\ vitro}$ and $CL_{int,lung}$ were calculated using data obtained from microsomal and lung slice incubations as described in equations (3)–(6) below.

Calculation of $CL_{int,in\ vitro}$ and $CL_{int,lung}$ using lung microsomal data:

$$CL_{int,\,in\ vitro} = \frac{\text{M3 formation rate}}{(\text{mean substrate conc.}) * (\text{microsomal protein conc.})} \quad (3)$$

DOI: 10.1080/00498254.2017.1373311

$$CL_{int,lung} = \frac{CL_{int,\,in\,vitro} * (\text{microsomal contents per g lung tissue}) * (\text{g lung tissue weight per kg body weight})}{fu_{inc}} \quad (4)$$

Calculation of $CL_{int,in\ vitro}$ and $CL_{int,lung}$ using lung tissue slice data:

$$CL_{int,\,in\,vitro} = \frac{\text{M3 formation rate} * (\mu\text{L incubation volume})}{(\text{mean substrate conc.}) * (\text{mg lung tissue per sample})} \quad (5)$$

$$CL_{int,lung} = \frac{CL_{int,\,in\,vitro} * (\text{g lung tissue weight per kg body weight})}{fu_{inc}} \quad (6)$$

CL_{lung} was calculated using the well stirred organ model:

$$CL_{lung} = \frac{Q_{lung} * fu_b * Cl_{int,lung}}{Q_{lung} + fu_b * Cl_{int,lung}} \quad (7)$$

The following scaling factors used for the CL_{lung} calculation were derived from the literature: microsomal protein in lung 15 mg/g lung (Schmitz et al., 2008), rat weight 250 g, rat lung weight 1.5 g and pulmonary blood flow (Q_{lung}) 74 mL/min/rat (Davies & Morris, 1993). The free fraction in the microsomal incubations (fu_{inc}) was 0.218. This was assumed to be the same for the lung tissue slices incubations. The unbound fraction of the drug in rat blood (fu_b) was 0.036 (Novartis, unpublished data). The linear coefficients for the M3 formation rate in lung microsomes and tissue slices were 0.00140 ± 0.00020 and 0.0024 ± 0.0006 μM/min, respectively. The mean AFQ056 substrate concentrations used to calculate $CL_{int,\ in\ vitro}$ from lung microsome and tissue slice incubations were 0.477 ± 0.02 and 0.416 ± 0.05, respectively.

In vivo rat pulmonary extraction

The animal studies were approved by the Animal Care and Use Committees of the Canton Basel, Switzerland. This experiment is based on the assumption that i.v. or i.a. dosed drug will permeate or bypass lungs, respectively, before being distributed throughout the body *via* the arterial bloodstream (Cassidy & Houston, 1980, 1984). Therefore, if lung tissue distribution and the rate of pulmonary metabolism are rapid enough, a first-pass effect will occur and $AUC_{i.v.}$ will be smaller than the corresponding $AUC_{i.a.}$

To assess the first-pass effect by pulmonary CYP1A1, rats were dosed intravenously (pre-lung) and or intra-arterially (post-lungs) with 3 mg/kg of AFQ056. Male Sprague–Dawley rats were used ((SD), Charles River Germany, 9–12 weeks, 269–330 g). Prior to the study the rats were housed in standard cages at 22 °C and had free access to tap water and Kliba-Nafag food pellets No. 3890 (Provimi Kliba AG, Kaiseraugst, Switzerland). The dosing solution contained AFQ056 (1.5 mg/mL) in a vehicle of ethanol, monodispersed polyethylene glycol 200, and 5% aqueous glucose solution (5:40:55, w:w:w). For intravenous and intra-arterial drug administration, the *vena cava* and coronary artery were cannulated, respectively. The primary aim of this study was to estimate pulmonary first-pass extraction and therefore, blood vessels were selected based on proximity to the rat lungs. In addition, the femoral artery was cannulated for blood sample collection.

Rats were anaesthetized with oxygen/isoflurane mixture (97/3, v/v; Forane®; Abbott AG, Baar, Switzerland) for the cannulations and kept under anaesthesia for the complete study duration of 2 h after AFQ056 dosing. Rats were kept on a warmed plate to keep the body temperature at approximately 37 °C. While the anaesthesia is likely to have lowered the basal metabolic rate, blood flows, and blood pressure, any differences due to general anaesthesia would likely cancel out since both intravenous and intra-arterial groups were treated in the same way (Prys-Roberts et al., 1971).

After cannulation, rats were dosed with AFQ056 (3 mg/kg), either *via* the *vena cava* or the coronary artery. Blood samples (300 μL) were collected from the femoral artery at 2, 5, 10, 20, 40, 60, 90, and 120 min post-dose. The cannulas were filled with an aqueous heparin solution to avoid blood clotting. Blood samples were collected in K3-EDTA tubes and centrifuged (10 min at 3000*g*, 4 °C) to produce plasma. Plasma samples were transferred into clean centrifuge tubes and stored at –80 °C until further analysis. The rats were sacrificed after collection of the last sample. The number of animals dosed intravenously and intra-arterially was 4 and 3, respectively. For quantitative analysis, 1 volume of plasma was mixed with 9 volumes of acetonitrile. Samples were vortexed, placed in the freezer (–20 °C for 60–120 min), and then centrifuged for 20 min at 24 000*g*. The supernatants were transferred into new vials, concentrated under vacuum, and then reconstituted with mobile phase containing 15–20% of acetonitrile. For quantitative analysis by LC-MS, internal standard (500 nM) was added to samples. Calibration curves were prepared by adding AFQ056 and M3 to control rat plasma.

Pharmacokinetic parameters were calculated by non-compartmental analysis using Phoenix WinNonlin (Version 6.4; Pharsight Corporation, Mountain View, CA). I.v. and i.a. plasma clearance (CL_{plasma}) were calculated as dose/$AUC_{0\text{-inf}}$, where $AUC_{0\text{-inf}}$ is the area under the plasma concentration–time curve calculated using the trapezoidal rule and extrapolated to infinity using the apparent terminal disposition rate constant (λz). The terminal half-life was estimated from the terminal rate constant with half-life = $0.693/\lambda z$. For i.v. and i.a. dosing, the steady state volume of distribution (V_{ss}) was calculated as V_{ss} = MRT * CL_{plasma} with the mean residence time (MRT) being defined as the area under the first moment curve ($AUMC_{0\text{-inf}}$) divided by $AUC_{0\text{-inf}}$. According to the well-stirred model, the lung extraction ratio (E_{lung}) represents a function of the *in vitro* intrinsic metabolic clearance in lung $CL_{int,lung}$. E_{lung} can be calculated using the difference in observed AUC after i.a. and i.v. dosing:

$$E_{lung} = \frac{AUC_{i.a.} - AUC_{i.v.}}{AUC_{i.a.}} \quad (8)$$

Results

The CYP1A1 mediated hydroxylation of AFQ056 to form M3 has been investigated in several rat models including lung

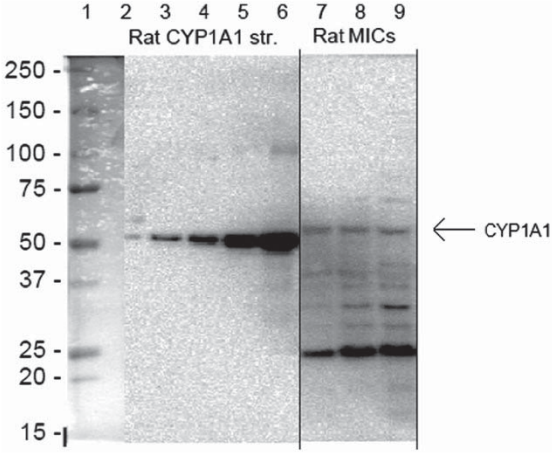

Figure 2. CYP1A1 Western blotting. Western blot of rat lung microsomes; bands 2–6 correspond to recombinant rat CYP1A1 standard (0.01–0.5 pmol). Bands 7–9 correspond to rat lung microsomes with gel loading of 10, 25, and 50 μg of total protein.

microsomes, lung tissue slices and *in vivo* following intravenous and intra-arterial dosing.

Rat CYP1A1 western blots

Western blots were carried out to confirm the presence of the enzyme CYP1A1 in rat lung (Figure 2). A polyclonal anti-CYP1A1 antibody produced in rabbits raised against an immunogen sequence with 99% identity between human and rat CYP1A1. Rat recombinant CYP1A1 protein ranging from 0.01 to 0.05 pmol was readily recognised around 50 kDa, consistent with previous literature observations (Black et al., 1998). However, blots obtained with rat lung microsomes after loading of 10, 25, and 50 μg total protein showed only faint bands at this position. The Western blots also showed numerous lighter bands recognised by the anti-CYP1A1 antibody, especially around 25 kDa.

AFQ056 enzyme kinetics with rat recombinant CYP1A1

CYP phenotyping assays have shown that in humans, metabolite M3 is predominantly formed by CYP1A1 (Walles et al., 2013). In the current study, we have compared the enzyme kinetics of AFQ056 hydroxylation by rat recombinant CYP1A1 with the previously obtained human data. The formation of M3 by rat recombinant CYP1A1 was well described by the Michaelis–Menten model and the parameters obtained are summarised in Table 1. The data indicated that AFQ056 is a high-turnover substrate for both human and rat CYP1A1 with M3 formed as the main reaction product and with only trace levels of M1/M2 and M7 detected (Figure 3). The rate of CYP1A1 mediated AFQ056 hydroxylation exceeded the reaction rates of the CYP1A1 assay using EROD as probe substrate that were reported by the supplier. The K_m obtained with rat recombinant CYP1A1 was slightly higher than that observed with human CYP1A1 whereas V_{max} was comparable. These initial experiments with rat recombinant CYP1A1 supported the use of the rat as a surrogate species to investigate pulmonary CYP1A1 activity.

Table 1. Enzyme kinetics of AFQ056 hydroxylation in recombinant rat and human CYP1A1.

Enzyme kinetic	K_m (μM)	V_{max} (pmol/min/pmol)	$CL_{int,\ in\ vitro}$ (μL/min/pmol)
Human CYP1A1	0.796 ± 0.077	45.3 ± 1.0	57.1 ± 0.2
Rat CYP1A1	1.91 ± 0.02	62.8 ± 0.71	32.8 ± 0.12

The enzyme kinetic parameters of AFQ056 hydroxylation by rat recombinant CYP1A1 (1.2–2 pmol/min) were determined. The formation rate of M3 after incubation of AFQ056 at 0.1–12.5 μM for 5 min was evaluated according to the Michaelis–Menten equation providing K_m, V_{max} and $CL_{int,in\ vitro}$. The K_m and $CL_{int,in\ vitro}$ values are based on total AFQ056 concentrations in incubations. The CYP1A1 enzyme kinetic results are expressed as mean values ± SD ($n = 2$). The human data shown in the table are taken from the previous investigations (Walles et al., 2013).

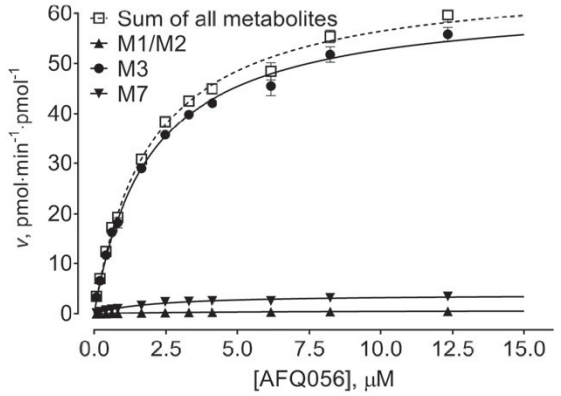

Figure 3. Rat recombinant CYP1A1 kinetics. Enzyme kinetics of AFQ056 hydroxylation by rat recombinant CYP1A1. Enzyme kinetic data are presented as mean values ± SD and were evaluated according to the Michaelis–Menten equation.

Incubations with rat lung microsomes

Linear formation of M3 was observed during the 15 min incubation period corresponding to approximately 4.6% of the initial AFQ056 concentration (Figure 4(A)). Using the rate of M3 formation as measured, the *in vitro* intrinsic clearance, $CL_{int,in\ vitro}$ was estimated to be 1.961 ± 0.20 μL/min/mg protein, resulting in an up-scaled *in vitro* intrinsic clearance $CL_{int,lung}$ of 0.808 ± 0.08 mL/min/kg. Using the well-stirred model, this was converted to the *in vivo* whole lung clearance CL_{lung} resulting in 0.029 ± 0.003 mL/min/kg (Table 2). Once again, M3 was the major product formed in lung microsomes with only traces of other oxidative metabolites (M1/M2 and M7) detected.

Incubations with rat lung slices

Significant metabolism of AFQ056 to M3 was observed during the 240 min incubation. M3 formation proceeded in a linear fashion during the incubation period and terminal M3 concentrations corresponded to approximately 82% of the initial AFQ056 concentrations. The AFQ056 disappearance rate was well-correlated with M3 formation rate during the incubation (Figure 4(B)). Based on the data at 1 μM AFQ056 for 4 h incubations time, $CL_{int,in\ vitro}$, $CL_{int,lung}$ and CL_{lung} were estimated to be 0.164 ± 0.02 μL/min/mg tissue,

DOI: 10.1080/00498254.2017.1373311

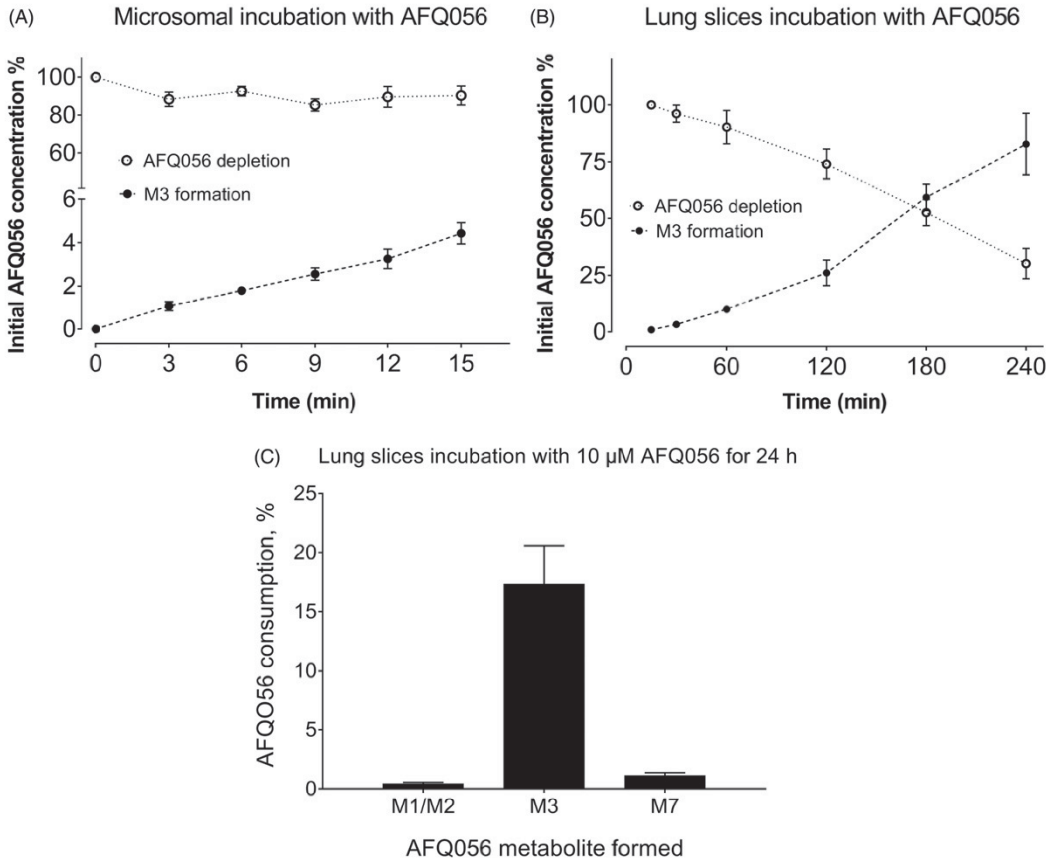

Figure 4. Metabolic stability of AFQ056 in rat lung microsomes and slices. (A) Biotransformation of AFQ056 (~0.5 µM) in lung microsomes during the 15 min incubation. (B) Biotransformation of AFQ056 (~0.5 µM) in lung slices during the 4 h incubation. Linear formation of M3 was observed during the incubation period of 15 min and 4 h corresponding to approximately 4.6% and 82% of the initial AFQ056 concentration, respectively. Open circles represent the disappearance of AFQ056 and closed circles represent the formation of metabolite M3 during the incubation. (C) Biotransformation of AFQ056 (10 µM) after incubation with rat lung tissue slices for 24 h. The main metabolite observed was M3 whereas only traces of M1/M2 and M7 were detected after 24 h. Results are presented as mean values ± SD ($n = 3$).

Table 2. Prediction of CL_{lung} of AFQ056 using the *in vitro* intrinsic metabolic clearance values.

	$CL_{int,in\ vitro}$ (µL/min/mg microsomal protein or mg slice)	$CL_{int,lung}$ (mL/min/kg)	CL_{lung} (mL/min/kg)
Rat lung microsomes	1.961 ± 0.2	0.808 ± 0.08	0.029 ± 0.003
Rat lung slices	0.164 ± 0.02	4.51 ± 0.62	0.162 ± 0.02

The *in vitro* intrinsic metabolic clearance of AFQ056 ($CL_{int,in\ vitro}$) was calculated based on the formation rate of M3 following incubation of AFQ056 (~0.5 µM) with rat lung microsomes (1.5 mg protein/mL) and tissue slices (72 mg slices/sample). The clearance values were up-scaled using the following factors: microsomal protein in lung 15 mg/g lung (Schmitz et al., 2008), rat weight 250 g and rat lung weight 1.5 g (Davies & Morris, 1993). $CL_{int,in\ vitro}$ values were converted to $CL_{int,lung}$ using fu_{inc} 0.218. The *in vivo* organ clearance (CL_{lung}) was estimated according to the well-stirred model using Q_{lung} 74 mL/min/rat (Davies & Morris, 1993) and fu_b 0.036. Results are presented as mean values ± SD ($n = 3$).

4.51 ± 0.62 mL/min/kg and 0.162 ± 0.02 mL/min/kg, respectively (Table 2). Although $CL_{int,\ lung}$ estimated from lung slices was 5.6-fold higher than the values estimated from lung microsomes, the CL_{lung} values determined from both incubations were close to zero. Only trace levels (less than 10% of M3) of other oxidative metabolites, M1/M2 and M7 were formed following incubation of AFQ056 for 24 h at 10 µM, suggesting that pulmonary CYP3A4 and CYP2C activity is low (Figure 4(C)).

Inhibition of AFQ056 hydroxylation by ketoconazole

The result show that CYP1A1-catalysed hydroxylation of AFQ056 to M3 was strongly inhibited by the ketoconazole in human and rat recombinant systems (Figure 5(A,B)). The inhibition modality was predominantly competitive and obtained K_i values are presented in Table 3. Although the potency of ketoconazole inhibition for both enzymes was in the nM range, the inhibition potency for human CYP1A1 was approximately four-fold higher compared to rat CYP1A1. M3 formation in rat lung tissue slices was almost completely inhibited by addition of ketoconazole (Figure 5(C)).

In vivo rat pulmonary extraction

To directly assess the potential pulmonary first-pass effect by CYP1A1, AFQ056 and M3 plasma concentrations were measured following intravenous and intra-arterial dosing of

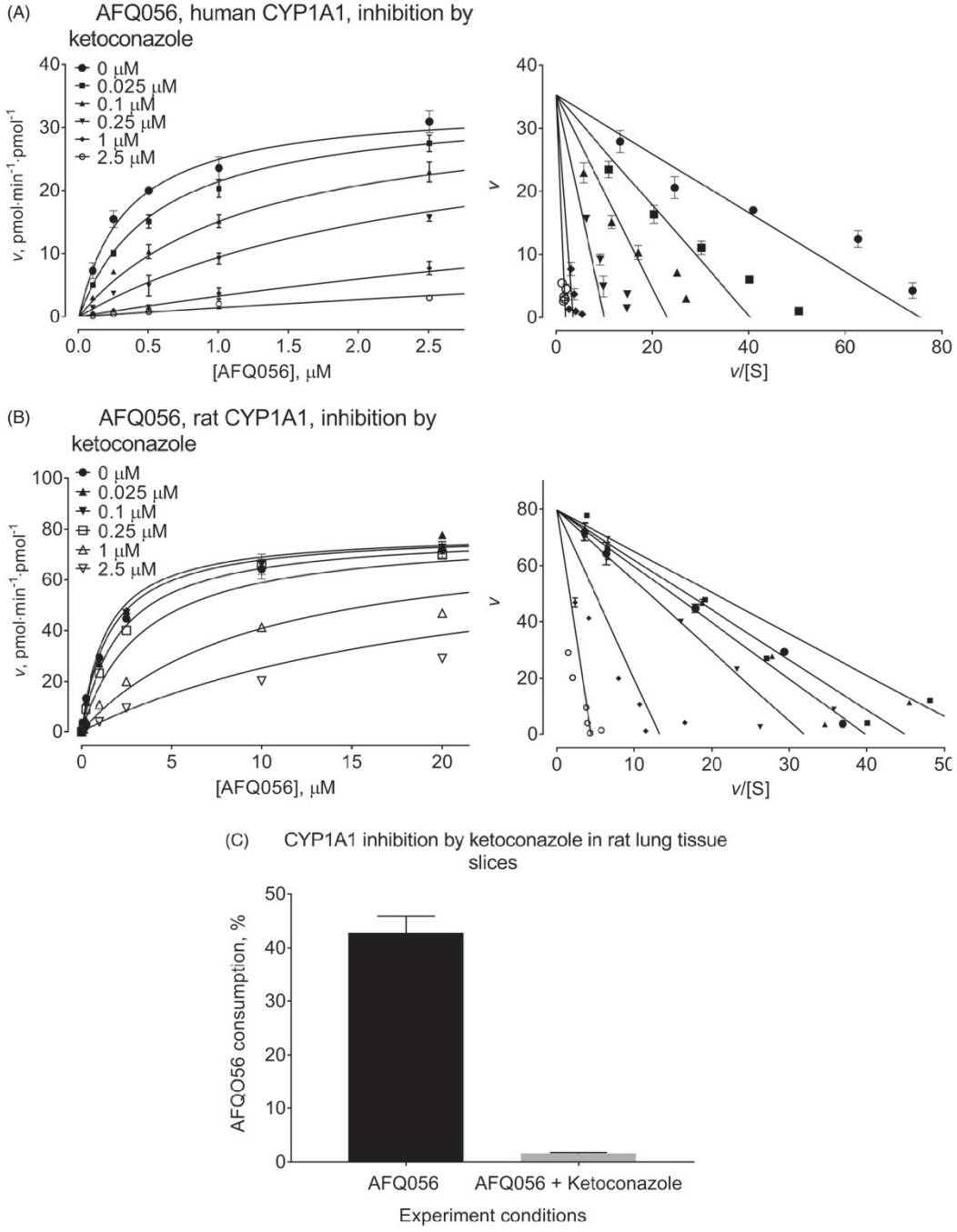

Figure 5. Inhibition of AFQ056 hydroxylation by ketoconazole. Inhibition of human (A) and rat (B) recombinant CYP1A1-catalysed AFQ056 hydroxylation by ketoconazole. Results are presented as mean values ± SD. Data were evaluated according to the competitive inhibition equation. Enzyme velocities vs. substrate concentration plots are presented. The inhibitory constants determined in this experiment are presented in Table 3. (C) Inhibition of AFQ056 metabolite M3 formation in rat lung tissue slices by ketoconazole. AFQ056 and ketoconazole concentrations were 1 and 10 μM, respectively, and the incubation time was 4 h. Results are presented as mean values ± SD ($n = 3$).

AFQ056 at 3 mg/kg to rats. The pharmacokinetic parameters obtained by non-compartmental analysis are presented in Table 4. The concentration-time profiles of AFQ056 and M3 following i.v. and i.a. administration of parent compound are shown in Figure 6. The 120 min study design and sampling protocol provided good coverage of the AFQ056 and M3 plasma exposures and was sufficient to observe differences in exposure due to pulmonary extraction. Our results show that there is no significant difference in average AFQ056 and M3 AUC_{inf} values between the two dosing groups. These results indicate that there is a negligible pulmonary first-pass effect (E_{lung}) under the specific conditions used in this experiment.

DOI: 10.1080/00498254.2017.1373311

Discussion

CYP1A1 has previously been shown to play an important role in the metabolism and disposition of AFQ056 in humans. The human phenotyping data shows that M3 formation is predominantly mediated by CYP1A1 with minor contributions of CYP2C19 and CYP1A2 (Walles et al., 2013). Enzyme kinetic experiments demonstrated that rat recombinant CYP1A1 efficiently catalyses the formation of M3 (Figure 3). In line with the predominant assumption that CYP1A1 is mainly expressed in extrahepatic tissues, only traces of M3 were detected in hepatic assays (Walles et al., 2013). In this investigation, we have used a combination of *in vitro* and *in vivo* models to investigate the pulmonary CYP1A1 metabolism of AFQ056.

Our conclusion that CYP1A1 is responsible for the formation of M3 observed in rat lung incubations is supported by several observations. First, M3 formation was clearly observed in rat lung slices during the 4 h incubation period, while only traces of the CYP3A4 metabolite, M1/M2 and CYP2C metabolite, M7 after 24 h were detected (Figure 4). Second, AFQ056 hydroxylation to M3 was strongly inhibited by ketoconazole in rat and human recombinant CYP1A1 and in rat lung slices (Figure 5). Although ketoconazole inhibits CYP1A1, CYP2C and CYP3A4 isoforms (Elsherbiny et al., 2008, Njuguna et al., 2016; Paine et al., 1999) our data indicates that pulmonary CYP2C and CYP3A4 activity is relatively low and unlikely to contribute significantly to the formation of M3 observed here (Figure 4(C)). Therefore, the reduced M3 formation in the presence of ketoconazole is likely to be due to CYP1A1 inhibition (Figure 5; Table 3).

Table 3. The inhibitory effect of ketoconazole on the oxidative metabolism of AFQ056 by human and rat CYP1A1.

Enzyme	K_i (μM)	Inhibition modality (r^2)
Human CYP1A1	0.039 ± 0.002	Competitive (0.99)
Rat CYP1A1	0.18 ± 0.018	Competitive (0.98)

The rate of M3 formation in the absence and presence of the CYP inhibitor ketoconazole (0–2.5 μM) was measured following incubation with human (0.1–2.5 μM AFQ056, 1.2 pmol/mL protein) and rat (0.1–20 μM AFQ056, 2 pmol/mL protein) recombinant CYP1A1 enzymes for 5 min. The change in the rate of M3 formation at the various inhibitor concentrations was evaluated according to the Michaelis–Menten equation with competitive-type inhibition. The estimated K_i values of ketoconazole, expressed as mean values ± SD ($n = 3$), were based on the unbound concentrations assuming no significant binding to microsomal protein ($fu_{inc} \approx 1$).

Finally, Western blot analysis clearly showed the expression of CYP1A1 in rat lung microsomes, an observation that is supported by the previous identification of CYP1A1 in rat lung (Becker et al., 2006). However, the faint bands observed corresponding to CYP1A1 suggests that the constitutive expression of CYP1A1 in rat lung is low (Figure 2). When considered together, these observations strongly support our conclusion, that the M3 formation observed in rat lung microsomes and tissue slices is mediated by CYP1A1.

Rat lung microsomes and tissue slices were tested as *in vitro* models to measure pulmonary CYP1A1 activity. While lung microsomes have the advantage of being commercially available, cryopreservable and simple to use, incubations must be supplemented with appropriate cofactors and are typically limited to approximately one hour due to a gradual decline in enzyme activity. Tissue slice technology has been used extensively for drug metabolism investigations (De Kanter et al., 2002) and has the advantage of containing a broader range of drug metabolising enzymes and necessary cofactors at physiologically relevant concentrations while retaining the architecture of the tissue (Morin et al., 2013; Stefaniak et al., 1988). Tissue slices also allow incubations to be performed for a much longer duration, a property that is particularly useful when dealing with low clearance compounds. Using the experimental design described here, we were able to maintain viability and linear activity for at least four hours.

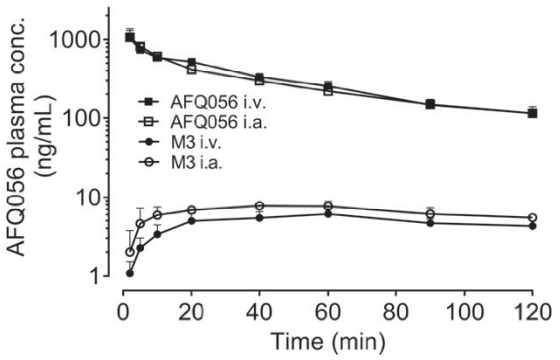

Figure 6. Plasma concentration-time profiles of AFQ056 and its oxidative metabolite M3 after intra-arterial and intravenous dosing. Mean plasma concentration-time profiles for AFQ056 following i.v. (closed squares) and i.a. (open squares) and its metabolite M3 after i.v. (closed circles) and i.a. (open circles) administration to anaesthetised male Sprague–Dawley rats. Results are shown as mean values ± SD. The number of animals in the i.v. and i.a. groups were 4 and 3, respectively.

Table 4. Pharmacokinetics of AFQ056 in rat.

Analyte		Units	AFQ056 3 mg/kg i.a. ($n = 3$)	AFQ056 3 mg/kg i.v. ($n = 4$)
AFQ056	AUC_{inf}	min*ng/mL	44 729 ± 3449	46 863 ± 5917
	CL_{plasma}	mL/min/kg	70 ± 9	72 ± 12
	V_{ss}	L/kg	5.5 ± 0.7	5.1 ± 1.2
	$T_{1/2}$	min	55 ± 8	51 ± 17
M3	AUC_{inf}	min*ng/mL	1742 ± 267	1667 ± 786

Measured plasma concentration profiles of AFQ056 over 2 h after single i.v. and i.a. dosing to male SD rats were evaluated according to the non-compartmental pharmacokinetic analysis using the trapezoidal rule. Data are presented as mean values ± SD. The numbers of animals in i.a. and i.v. group were 3 and 4, respectively.

Irrespective of the differences in the two *in vitro* assays, CL_{lung} values estimated using rat lung microsomes and slices (0.029 and 0.162 mL/min/kg, respectively; Table 2) were close to zero. These results are in agreement with our *in vivo* data, where insignificant differences in AFQ056 exposure were observed following i.v. and i.a. dosing, thus precluding a clinically important first-lung pass effect and indicating only a small contribution of pulmonary metabolism to total body clearance. The lack of significant pulmonary extraction observed here is supported by the low pulmonary CYP1A1 expression demonstrated in our Western blot analysis (Figure 2). To the best of our knowledge, this is the first time that this *in vivo* model has been used to determine CYP1A1 mediated first-pass pulmonary extraction.

Although there appears to be no significant contribution of lung metabolism to the elimination of AFQ056 in rats, the total plasma AFQ056 clearance (70–72 mL/min/kg; Table 4) was high [comparable to hepatic blood flow, which equals approximately 56 mL/min/kg (Davies & Morris, 1993)], indicating that alternative elimination pathways are responsible for AFQ056 clearance in rats.

Besides lung CYP1A1 is also expressed in other extrahepatic organs and tissues (Bieche et al., 2007; Nishimura & Naito, 2006) such as intestine, kidney, skin, spleen, and brain, and it is possible that these organs also contribute to the formation of M3. Alternatively, it remains to be explored if M3 formation in rats may be attributed to the CYP1A1 activity and/or activity of other CYPs in the liver.

CYP1A1 has previously been shown to be the major enzyme responsible for the 7-hydroxylation of the 5-HT3 receptor antagonist, granisetron (Nakamura et al., 2005). This investigation demonstrated significant variability in the granisetron 7-hydroxylation in liver microsomes prepared from 33 separate individuals (17 Caucasian, 16 Japanese). These inter-individual differences have also been confirmed in a separate investigation (Bloomer et al., 1994), where a greater than 100-fold difference in granisetron 7-hydroxylation in human hepatic samples was observed. Such extensive variability in activity may lead to significant differences in parent compound and metabolite exposures in patients. These alterations may be further exacerbated when the enzyme involved is also susceptible to induction such as CYP1A1. While constitutive expression of CYP1A1 mRNA and protein in human lung tissue from non-smokers is reported to be low, levels in smokers will be much higher due to induction (Kim et al., 2004). Furthermore, in addition to increasing lung CYP1A1 levels, smoking will also lead to increased expression in other organs and tissues including the liver.

The results of a clinical study (Novartis internal data) showed that AFQ056 C_{max} and AUC_{inf} in smokers were reduced by 41% and 46%, respectively, compared to non-smokers. This reduction in AFQ056 systemic exposure was well-correlated with elevated AUC of metabolite M3 (five-fold), and was associated with a decrease in the AUC of metabolites M1/M2 (three-fold). These results indicated that smoking induces CYP1A1 metabolism and reduces AFQ056 systemic exposure, while de-emphasising the major CYP3A4 pathway seen in non-smokers. This confirms that the *in vivo* formation of M3 can be greatly increased in heavy smokers relative to non-smoking populations, due to the induction potential.

Interestingly, Frey et al. (2016) also reported that riociguat exposure in non-smokers was higher than in smokers although total levels of the CYP1A1 metabolite, riociguat – M1, were similar in both groups. They proposed that the lower riociguat exposure in smokers was probably due to increased CYP1A1 expression and therefore, increased metabolism of the parent compound to M1.

In conclusion, our results show that AFQ056 is a high-turnover substrate for rat CYP1A1. While the *in vitro* data indicate that the lung could make a small contribution to the formation of M3, the *in vivo* data suggest that other organs must be more important in this process. There are still large gaps in our knowledge regarding the primary organs where M3 formation occurs. Further studies are required to improve our understanding of the role of hepatic and extrahepatic CYP1A1 in drug metabolism.

Acknowledgements

The study was conducted with the great support by PK Sciences group of Novartis institutes for biomedical research. The authors would like to acknowledge Marc Witschi, Laurent Hoffmann, Claudia Textor, Peter Wipfli, Werner Gertsch, Martina Suetterlin-Hachmann and Thierry Delemonte for their support in the data generation.

Declaration of interest

No potential conflict of interest was reported by the authors.

This work was supported by the Pharmacokinetic Sciences group at Novartis Institutes for Biomedical Research in Basel, Switzerland.

References

Anttila S, Tuominen P, Hirvonen A, et al. (2001). CYP1A1 levels in lung tissue of tobacco smokers and polymorphisms of CYP1A1 and aromatic hydrocarbon receptor. Pharmacogenetics 11:501–9.

Anttila S, Vainio H, Hietanen E, et al. (1992). Immunohistochemical detection of pulmonary cytochrome P450IA and metabolic activities associated with P450IA1 and P450IA2 isozymes in lung cancer patients. Environ Health Perspect 98:179–82.

Becker A, Albrecht C, Knaapen AM, et al. (2006). Induction of CYP1A1 in rat lung cells following in vivo and in vitro exposure to quartz. Arch Toxicol 80:258–68.

Bieche I, Narjoz C, Asselah T, et al. (2007). Reverse transcriptase-PCR quantification of mRNA levels from cytochrome (CYP)1, CYP2 and CYP3 families in 22 different human tissues. Pharmacogenet Genomics 17:731–42.

Black VH, Wang AF, Henry M, Shaw PM. (1998). Induction of CYP1A1, but not CYP1A2, in adrenals of 3, 3′-methylcholanthrene-treated guinea pigs. Arch Biochem Biophys 354:197–205.

Bloomer JC, Baldwin SJ, Smith GJ, et al. (1994). Characterisation of the cytochrome P450 enzymes involved in the in vitro metabolism of granisetron. Br J Clin Pharmacol 38:557–66.

Buchthal J, Grund KE, Buchmann A, et al. (1995). Induction of cytochrome P4501A by smoking or omeprazole in comparison with UDP-glucuronosyltransferase in biopsies of human duodenal mucosa. Eur J Clin Pharmacol 47:431–5.

Cassidy MK, Houston JB. (1980). In vivo assessment of extrahepatic conjugative metabolism in first pass effects using the model compound phenol. J Pharm Pharmacol 32:57–9.

Cassidy MK, Houston JB. (1984). In vivo capacity of hepatic and extrahepatic enzymes to conjugate phenol. Drug Metab Dispos 12: 619–24.

DOI: 10.1080/00498254.2017.1373311

Chang TK, Chen J, Pillay V, et al. (2003). Real-time polymerase chain reaction analysis of CYP1B1 gene expression in human liver. Toxicol Sci 71:11–19.

Davies B, Morris T. (1993). Physiological parameters in laboratory animals and humans. Pharm Res 10:1093–5.

De Kanter R, De Jager MH, Draaisma AL, et al. (2002). Drug-metabolizing activity of human and rat liver, lung, kidney and intestine slices. Xenobiotica 32:349–62.

Ding X, Kaminsky LS. (2003). Human extrahepatic cytochromes P450: function in xenobiotic metabolism and tissue-selective chemical toxicity in the respiratory and gastrointestinal tracts. Annu Rev Pharmacol Toxicol 43:149–73.

Elsherbiny ME, El-Kadi AO, Brocks DR. (2008). The metabolism of amiodarone by various CYP isoenzymes of human and rat, and the inhibitory influence of ketoconazole. J Pharm Pharm Sci 11:147–59.

Fang J, Mckay G, Song J, et al. (2001). In vitro characterization of the metabolism of haloperidol using recombinant cytochrome p450 enzymes and human liver microsomes. Drug Metab Dispos 29: 1638–43.

Frey R, Becker C, Unger S, et al. (2016). Assessment of the effects of hepatic impairment and smoking on the pharmacokinetics of a single oral dose of the soluble guanylate cyclase stimulator riociguat (BAY 63-2521). Pulm Circ 6:S5–S14.

Granvil CP, Krausz KW, Gelboin HV, et al. (2002). 4-Hydroxylation of debrisoquine by human CYP1A1 and its inhibition by quinidine and quinine. J Pharmacol Exp Ther 301:1025–32.

Hu W, Sorrentino C, Denison MS, et al. (2007). Induction of cyp1a1 is a nonspecific biomarker of aryl hydrocarbon receptor activation: results of large scale screening of pharmaceuticals and toxicants in vivo and in vitro. Mol Pharmacol 71:1475–86.

Hussain T, Al-Attas OS, Al-Daghri NM, et al. (2014). Induction of CYP1A1, CYP1A2, CYP1B1, increased oxidative stress and inflammation in the lung and liver tissues of rats exposed to incense smoke. Mol Cell Biochem 391:127–36.

Ito S, Chen C, Satoh J, et al. (2007). Dietary phytochemicals regulate whole-body CYP1A1 expression through an arylhydrocarbon receptor nuclear translocator-dependent system in gut. J Clin Invest 117:1940–50.

Kim JH, Sherman ME, Curriero FC, et al. (2004). Expression of cytochromes P450 1A1 and 1B1 in human lung from smokers, nonsmokers, and ex-smokers. Toxicol Appl Pharmacol 199:210–19.

Klieber S, Arabeyre-Fabre C, Moliner P, et al. (2014). Identification of metabolic pathways and enzyme systems involved in the in vitro human hepatic metabolism of dronedarone, a potent new oral antiarrhythmic drug. Pharmacol Res Perspect 2:e00044.

Krumdieck CL. (2013). Development of a live tissue microtome: reflections of an amateur machinist. Xenobiotica 43:2–7.

Li J, Zhao M, He P, et al. (2007). Differential metabolism of gefitinib and erlotinib by human cytochrome P450 enzymes. Clin Cancer Res 13:3731–7.

Lu D, Dong D, Liu Z, et al. (2015). Metabolism elucidation of BJ-B11 (a heat shock protein 90 inhibitor) by human liver microsomes: identification of main contributing enzymes. Expert Opin Drug Metab Toxicol 11:1029–40.

Martignoni M, Groothuis GM, De Kanter R. (2006). Species differences between mouse, rat, dog, monkey and human CYP-mediated drug metabolism, inhibition and induction. Expert Opin Drug Metab Toxicol 2:875–94.

Morin JP, Baste JM, Gay A, et al. (2013). Precision cut lung slices as an efficient tool for in vitro lung physio-pharmacotoxicology studies. Xenobiotica 43:63–72.

Nakamura H, Ariyoshi N, Okada K, et al. (2005). CYP1A1 is a major enzyme responsible for the metabolism of granisetron in human liver microsomes. Curr Drug Metab 6:469–80.

Nishimura M, Naito S. (2006). Tissue-specific mRNA expression profiles of human phase I metabolizing enzymes except for cytochrome P450 and phase II metabolizing enzymes. Drug Metab Pharmacokinet 21:357–74.

Njuguna NM, Umehara KI, Huth F, et al. (2016). Improvement of the chemical inhibition phenotyping assay by cross-reactivity correction. Drug Metab Pers Ther 31:221–8.

Paine MF, Schmiedlin-Ren P, Watkins PB. (1999). Cytochrome P-450 1A1 expression in human small bowel: interindividual variation and inhibition by ketoconazole. Drug Metab Dispos 27:360–4.

Prys-Roberts C, Meloche R, Foex P. (1971). Studies of anaesthesia in relation to hypertension. I. Cardiovascular responses of treated and untreated patients. Br J Anaesth 43:122–37.

Quinney SK, Knopp S, Chang C, et al. (2013). Integration of in vitro binding mechanism into the semiphysiologically based pharmacokinetic interaction model between ketoconazole and midazolam. CPT Pharmacometrics Syst Pharmacol 2:e75.

Reid JM, Kuffel MJ, Miller JK, et al. (1999). Metabolic activation of dacarbazine by human cytochromes P450: the role of CYP1A1, CYP1A2, and CYP2E1. Clin Cancer Res 5:2192–7.

Sancini G, Farina F, Battaglia C, et al. (2014). Health risk assessment for air pollutants: alterations in lung and cardiac gene expression in mice exposed to Milano winter fine particulate matter (PM2.5). PLoS One 9:e109685.

Sanderink GJ, Bournique B, Stevens J, et al. (1997). Involvement of human CYP1A isoenzymes in the metabolism and drug interactions of riluzole in vitro. J Pharmacol Exp Ther 282:1465–72.

Schmitz A, Portier CJ, Thormann W, et al. (2008). Stereoselective biotransformation of ketamine in equine liver and lung microsomes. J Vet Pharmacol Ther 31:446–55.

Smith PF, Gandolfi AJ, Krumdieck CL, et al. (1985). Dynamic organ culture of precision liver slices for in vitro toxicology. Life Sci 36: 1367–75.

Smith PF, Krack G, Mckee RL, et al. (1986). Maintenance of adult rat liver slices in dynamic organ culture. In Vitro Cell Dev Biol 22: 706–12.

Stefaniak MS, Gandolfi AJ, Brendel K. (1988). Adult rat lung in dynamic organ culture: a new tool in pharmacology. Proc West Pharmacol Soc 31:149–51.

Tassaneeyakul W, Birkett DJ, Veronese ME, et al. (1993). Specificity of substrate and inhibitor probes for human cytochromes P450 1A1 and 1A2. J Pharmacol Exp Ther 265:401–7.

Thum T, Erpenbeck VJ, Moeller J, et al. (2006). Expression of xenobiotic metabolizing enzymes in different lung compartments of smokers and nonsmokers. Environ Health Perspect 114: 1655–61.

Totlandsdal AI, Cassee FR, Schwarze P, et al. (2010). Diesel exhaust particles induce CYP1A1 and pro-inflammatory responses via differential pathways in human bronchial epithelial cells. Part Fibre Toxicol 7:41.

Vranesic I, Ofner S, Flor PJ, et al. (2014). AFQ056/mavoglurant, a novel clinically effective mGluR5 antagonist: identification, SAR and pharmacological characterization. Bioorg Med Chem 22:5790–803.

Walles M, Wolf T, Jin Y, et al. (2013). Metabolism and disposition of the metabotropic glutamate receptor 5 antagonist (mGluR5) mavoglurant (AFQ056) in healthy subjects. Drug Metab Dispos 41: 1626–41.

3.3. Functional assessment of rat pulmonary flavin-containingmonooxygenase activity

Yildiz Yilmaz[1], Gareth Williams[1], Nenad Manevski[1], Markus Walles[1], Stephan Kraehenbuehl[2] and Gian Camenisch[1]

Pharmacokinetic Sciences[1], Novartis Institutes for Biomedical Research, Basel, Switzerland

Clinical Pharmacology and Toxicology[2], University hospital Basel, Switzerland

Published in

Journal of Xenobiotica (2018)

DOI: 10.1080/00498254.2018.1469804

XENOBIOTICA
https://doi.org/10.1080/00498254.2018.1469804

Taylor & Francis
Taylor & Francis Group

RESEARCH ARTICLE

Functional assessment of rat pulmonary flavin-containing monooxygenase activity

Yildiz Yilmaz[a], Gareth Williams[a], Nenad Manevski[a], Markus Walles[a], Stephan Krähenbühl[b] and Gian Camenisch[a]

[a]Pharmacokinetic Sciences, Novartis Institutes for Biomedical Research, Basel, Switzerland; [b]Clinical Pharmacology and Toxicology, University Hospital, Basel, Switzerland

ABSTRACT

1. The expression of flavin-containing monooxygenase (FMO) varies extensively between human and commonly used preclinical species such as rat and mouse. The aim of this study was to investigate the pulmonary FMO activity in rat using benzydamine. Furthermore, the contribution of rat lung to the clearance of benzydamine was investigated using an *in vivo* pulmonary extraction model.
2. Benzydamine *N*-oxygenation was observed in lung microsomes and lung slices. Thermal inactivation of FMO and CYP inhibition suggested that rat pulmonary *N*-oxygenation is predominantly FMO mediated while any contribution from CYPs is negligible.
3. The predicted lung clearance (CL_{lung}) estimated from microsomes and slices was 16 ± 0.6 and 2.1 ± 0.3 mL/min/kg, respectively. The results from *in vivo* pulmonary extraction indicated no pulmonary extraction following intravenous and intra-arterial dosing to rats. Interestingly, the predicted CL_{lung} using rat lung microsomes corresponded to approximately 35% of rat CL_{liver} suggesting that the lung makes a smaller contribution to the whole body clearance of benzydamine.
4. Although benzydamine clearance in rat appears to be predominantly mediated by hepatic metabolism, the data suggest that the lung may also make a smaller contribution to its whole body clearance.

ARTICLE HISTORY
Received 21 March 2018
Revised 23 April 2018
Accepted 24 April 2018

KEYWORDS
Pulmonary metabolism; flavin-containing monooxygenases (FMO); benzydamine; rat pumonary FMO metabolism; benzydamine noxygenation

Introduction

The flavin-containing monooxygenases (FMOs) are a family of enzymes that typically catalyze the oxygenation of substrates containing a soft nucleophilic heteroatom such as nitrogen or sulfur. Human FMO5 has recently also been shown to behave as a Baeyer–Villiger monooxygenase, catalyzing the conversion of a lactone or ketone to an ester (Fiorentini et al., 2017; Lai et al., 2010; Meng et al., 2015). In humans, the FMO family is relatively small and only five functional genes (FMO1–5) have been identified (Lawton et al., 1994; Phillips et al., 1995). FMO substrates include dietary compounds, insecticides and drugs such as trimethylamine (Dolphin et al., 1997), phorate and disulfoton (Henderson et al., 2004), imipramine (Furnes & Schlenk, 2004), clozapine (Tugnait et al., 1997) and ethionamide (Henderson et al., 2008).

Cytochrome P450 enzymes (CYPs) and FMOs are both located in the microsomal compartment and are dependent on NADPH as a cofactor (Cashman, 2005; Hutzler & Zientek, 2016). However, CYP-mediated oxidative reactions proceed via two sequential one-electron transfer and require an oxidoreductase to facilitate electron transfer from NADPH. FMOs are not dependent on a coenzyme and substrates undergo a one-step two-electron oxygenation. While CYPs display optimum activity at physiological pH, FMOs display optimum catalytic activity in the pH range from 8 to 10 (Cashman, 2005; Hutzler & Zientek, 2016).

The expression of FMOs varies markedly with species, tissue, age and also gender (Hines, 2006; Phillips & Shephard, 2017; Ripp et al., 1999). For example, the major FMO isoforms expressed in adult human liver are FMO3 and FMO5 (Cashman & Zhang, 2006; Dolphin et al., 1991; Janmohamed et al., 2004; Koukouritaki et al., 2002). Hepatic expression of FMO1 in human stops after birth, but it is still expressed in extrahepatic tissues including kidney (Dolphin et al., 1996; Zhang & Cashman, 2005). On the other hand, FMO1 and FMO3 are both expressed in rat (Itoh et al., 1993; Lattard et al., 2002a; Moroni et al., 1995) and mouse liver albeit in a gender dependent manner (Cherrington et al., 1998; Falls et al., 1995; Janmohamed et al., 2004). Such differences in enzyme expression between preclinical species and human may lead to significant differences in metabolism, clearance

CONTACT Yildiz Yilmaz yildiz.yilmaz@novartis.com Novartis Institute for Biomedical Research Pharmacokinetic Sciences, Fabrikstrasse 14-1, Novartis Pharma AG, CH-4002 Basel, Switzerland

and exposure of parent compound and metabolites, and may alter efficacy and toxicity of drugs.

The liver is known to be the major site of drug metabolism in the body. Yet, drug metabolizing enzymes such as CYPs, uridine 5′diphosphoglucuronosyltransferases (UGT) and FMOs are also expressed in the lung (Ding & Kaminsky, 2003; Gundert-Remy et al., 2014; Jhajra et al., 2012; Rettie et al., 1995). The major FMO isoform expressed in the lungs of most mammals is FMO2 (Dolphin et al., 1998; Krueger et al., 2001). Caucasians and Asians possess the FMO2*2 allele that codes for a non-functional, truncated protein. On the other hand, 27% and 5% of African and Hispanic populations, respectively, possess the FMO2*1 allele and express the full length, functional active protein (Dolphin et al., 1998; Krueger et al., 2004; Whetstine et al., 2000). Similarly, the FMO2 gene in commonly used laboratory rat strains has also been shown to encode a truncated, inactive protein (Lattard et al., 2002b), whereas full-length functional FMO2 is expressed in mouse lung (Karoly and Rose, 2001). FMO1 has also been shown to be expressed in both mouse and rat lung (Janmohamed et al., 2004; Lattard et al., 2001). Despite these species differences in pulmonary expression, it can be anticipated that in rats and mice, FMO substrates will be subject to lung metabolism. However, pulmonary metabolism of FMO substrates in humans will depend upon the population involved.

Metabolism in organs such as the lung may also contribute to systemic clearance and elimination of compounds. Given that the lung is a well-perfused organ that receives a blood flow equivalent to cardiac output (Davies & Morris, 1993), it is reasonable to assume that it may play a role in extrahepatic metabolism. Indeed, *in vivo* pulmonary metabolism has been demonstrated in rodents for lidocaine, midazolam and nifedipine (Aoki et al., 2010), resveratrol (Sharan & Nagar, 2013) and phenol (Cassidy & Houston, 1980). Although FMOs are known to be expressed in the lungs of rodents, the contribution of pulmonary metabolism to the clearance of FMO substrates *in vivo* is yet to be explored.

The aim of this investigation was to evaluate pulmonary FMO activity in rats using the anti-inflammatory drug, benzydamine, a well characterized, high-turnover FMO substrate (Capolongo et al., 2010; Lang & Rettie, 2000; Störmer et al., 2000; Taniguchi-Takizawa et al., 2015). FMO catalyzes the *N*-oxygenation of benzydamine as shown in Figure 1 (Störmer et al., 2000). In this study, the enzyme kinetics of benzydamine *N*-oxygenation in rat lung microsomes and rat lung slices were compared. The precision cut lung slices incubation system described in this investigation has previously been used to investigate pulmonary CYP1A1 activity (Yilmaz et al., 2017). Although lung tissue slices are not commonly used in drug metabolism, they have the advantage of containing a variety of different cell types with differing metabolic activity. They also retain the complex cellular architecture of the tissue and are therefore a suitable system for the investigation of pulmonary metabolism. In humans, benzydamine *N*-oxygenation has been shown to be mediated by FMO1 and FMO3 with a minor contribution from CYPs (Lang & Rettie, 2000). In order to determine the contribution of FMOs and CYPs to benzydamine *N*-oxygenation in rat lung microsomes, experiments using thermal inactivation and the non-specific irreversible CYP inhibitor, 1-aminobenzotriazole (ABT) was performed. FMOs are known to be thermally labile in the absence of NADPH and are readily deactivated, whereas CYP activity is reported to be relatively unaffected (Ziegler, 1980). However, FMO2 has been shown to be less labile to heat inactivation than other isoforms such as FMO3 (Cashman, 2005; Hutzler & Zientek, 2016). This heat lability has often been exploited to understand the relative contributions of FMOs and CYPs (Cashman, 2005; Fisher et al., 2002; Rawden et al., 2000; Yanni et al., 2008). The *in vivo* clearance of benzydamine in rat has previously been shown to be well predicted by liver microsomes and hepatocytes, suggesting that its elimination is mainly driven by hepatic metabolism in this species (Fisher et al., 2002). Yet, no attempt has previously been made to determine if the lung also contributes to the whole body clearance of benzydamine in rats. Herein, *in vitro* data and the well-stirred model have been used to predict lung clearance (CL_{lung}). Finally, this predicted CL_{lung} has been compared to *in vivo* pulmonary extraction of benzydamine following intra-arterial (i.a.; post-lungs) and intravenous (i.v.; pre-lungs) dosing to rats.

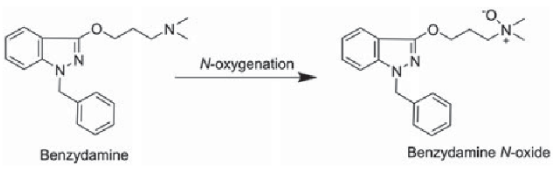

Figure 1. Benzydamine *N*-oxygenation and *N*-demethylation. For a full overview of the biotransformation pathway of benzydamine, refer to (Fisher et al., 2002).

Materials and methods

Reagents, chemicals and materials

Benzydamine hydrochloride, benzydamine *N*-oxide maleate, NADPH, sulfadimethoxine (SDM) and 1-aminobenzotriazole were purchased from Sigma-Aldrich (Poole, UK). HPLC grade water and acetonitrile were purchased from VWR (Leicestershire, UK). Sprague-Dawley rat (pool of 299) lung microsomes were obtained from Xenotech (Kansas City, MO). Lung microsomes were not further characterized with regard to CYP and FMO protein content.

Benzydamine N-oxygenation enzyme kinetics in rat lung microsomes

Rat lung microsomal incubations (0.3 mL total volume) were conducted at 37 °C in 100 mM potassium phosphate buffer, pH 7.4, supplemented with 5 mM $MgCl_2$ and 1 mM NADPH. FMOs are known to display optimum catalytic activity within the pH range from 8 to 10 (Cashman, 2005; Hutzler & Zientek, 2016) and the impact of higher pH on benzydamine *N*-oxygenation has previously been demonstrated (Kawaji et al., 1993). However, for the purposes of this investigation, we decided that it was more appropriate to perform the incubations at physiological pH (7.4), which reflects the

in vivo situation. For all experiments, microsomes were preincubated for 5 min with NADPH and reactions were started by addition of benzydamine. Initial studies were performed to establish conditions for linear product (benzydamine *N*-oxide) formation with respect to incubation time and microsomal protein concentration. In these experiments, benzydamine (1–200 μM) was incubated with rat lung (0.05 mg/mL microsomal protein) microsomes for 10 min. Benzydamine stock solutions were prepared in methanol/water (1:1, v/v) at appropriate concentrations and the concentration of organic solvent in incubations was <0.5%. Reactions were terminated by addition of ice-cold acetonitrile containing internal standard, SDM. Samples were centrifuged and the supernatants were analyzed by liquid chromatography-tandem mass spectrometry (LC-MS/MS).

Enzyme kinetic parameters were calculated by the Michaelis–Menten equation:

$$v = \frac{V_{max}[S]}{K_m + [S]} \quad (1)$$

where v and V_{max} are the reaction and limiting reaction velocities, respectively, K_m is the Michaelis–Menten constant and $[S]$ is the total substrate concentration. Prism 7.0 (GraphPad Software, San Diego, CA) was used for data processing and the determination of kinetic parameters.

Benzydamine N-oxygenation in rat lung slices

Rat lung slice preparation and rat lung slicing incubations were performed as previously described (Yilmaz et al., 2017). Benzydamine (1 μM) was incubated with lung tissue slices for 30 min to 4 h. The incubation volume was 2 mL. Negative control incubations without tissue slices were performed in parallel. Incubations were stopped with 3 mL of ice-cold acetonitrile containing internal standard. The samples were thoroughly mixed and transferred to 5 mL Eppendorf tubes. The samples were stored at −80 °C until further analysis.

Benzydamine lung tissue binding

Rapid equilibrium dialysis (RED) was used to investigate the binding of benzydamine to rat lung tissue. Tissue homogenate was prepared from rat lungs that had been exsanguinated and perfused by cardiac puncture with 10 mL Dulbecco's Phosphate-Buffered Saline (DPBS) to avoid the plasma binding bias. Rat lung homogenate (0.9 g tissue in 2 mL of DPBS) was diluted with 2 mL of DPBS. Three hundred micro liter of tissue homogenate containing 5 μM benzydamine and 500 mL of 100 mM of phosphate buffer (pH 7.4) were added to the homogenate and buffer chambers of the RED devices, respectively. The chambers were covered with a gas permeable membrane and incubated for 4 h at 37 °C with 5% of CO_2 on a shaker (750 rpm). Experiments were performed in triplicate. Equal volumes of homogenate and buffer were then taken from the chambers and transferred to a 96-deep-well plate for LC-MS/MS analysis.

The unbound fraction of benzydamine in diluted lung homogenate ($f_{u,hD}$) was calculated as shown in the below equation.

$$f_{u,hD} = \frac{C_{buffer}}{C_{homoganate}} \quad (2)$$

$f_{u,hD}$ was then scaled to undiluted lung homogenate ($f_{u,lung}$) using the below equation.

$$f_{u,lung} = \frac{1}{1 + D\left(\frac{1}{f_{u,hD}} - 1\right)} \quad (3)$$

where D is the dilution factor that was used.

Prediction of pulmonary clearance

The pulmonary microsomal $CL_{int,in\text{-}vitro}$ (V_{max}/K_m) value, 332 ± 14 μL/min/mg determined in the enzyme kinetics experiment, was used to calculate $CL_{int,lung}$ as described in Equation (4).

$CL_{int,in\text{-}vitro}$ obtained from the lung slices experiment was calculated using the rate of benzydamine *N*-oxide formation as represented by the slope (Njuguna et al., 2016). Lung organ clearance ($CL_{int,lung}$) was calculated using Equations (5) and (6):

Calculation of $CL_{int,lung}$ using lung microsomal data:

$$CL_{int,lung} = \frac{CL_{int,in\ vitro} \times \begin{array}{c}(\text{microsomal content per g tissue}) \\ \times(\text{g tissue per kg body weight})\end{array}}{fu_{inc}} \quad (4)$$

Calculation of $CL_{int,in\text{-}vitro}$ and $CL_{int,lung}$ using lung tissue slice data:

$$CL_{int,\ in-vitro} = \frac{\begin{array}{c}(N\text{-Oxygenation formation rate}) \\ \times(\mu\text{L incubation volume})\end{array}}{\begin{array}{c}(\text{mean substrate conc.}) \\ \times\ (\text{mg lung tissue per sample})\end{array}} \quad (5)$$

$$CL_{int,lung} = \frac{(CL_{int,in\ vitro}) \times \begin{pmatrix}\text{g lung tissue weight} \\ \text{per kg body weight}\end{pmatrix}}{fu_{lung}} \quad (6)$$

CL_{lung} values were then calculated using the well-stirred organ model as shown in the below:

$$CL_{lung} = \frac{Q_{lung} \times Cl_{int,lung} \times fu/R_{b/p}}{Q_{lung} + Cl_{int,lung} \times fu/R_{b/p}} \quad (7)$$

where fu_{inc} is the fraction unbound in microsomal incubations, fu_{lung} is the fraction unbound in lung tissue, fu is the plasma protein binding and $R_{b/p}$ is the blood to plasma ratio.

The following scaling factors derived from the literature were used to calculate lung CL_{lung}: microsomal protein in lung 15 mg/g lung (Schmitz et al., 2008), rat weight 250 g, rat lung weight 1.5 g and pulmonary blood flow (Q_{lung}) 74 mL/min/rat (Davies & Morris, 1993). In the absence of rat experimental data, human fu_{inc}, fu and $R_{b/p}$ values of 0.35, 0.148 and 0.76 were used (Jones et al., 2017). The fu_{lung} for rat lung homogenate was measured as 0.03. The mean linear coefficient for benzydamine *N*-oxide formation rate in lung tissue slices was 0.003 ± 0.0004 μM/min ($n = 3$).

Thermal inactivation/chemical inhibition

Heat inactivation and the non-specific CYP inhibitor, ABT was used to investigate the contribution of CYP and FMO to benzydamine *N*-oxygenation in rat lung microsomes (Cassidy & Houston, 1980; Fisher et al., 2002; Taniguchi-Takizawa et al., 2015). In the control experiment, lung microsomal incubations containing 0.05 mg/mL of microsomal protein were preincubated with NADPH (1 mM), for 10 min at 37 °C. To investigate the effect of CYP inhibition, microsomal mixtures were preincubated with 1 mM of NADPH and 2 mM of ABT, which is a pan-CYP inhibitor for 10 min prior to starting the reactions. To determine the impact of thermal inactivation, microsomes were incubated at 45 °C for 5 min in the absence of NADPH. These preparations were then cooled on ice for 10 min prior to being preincubated with NADPH for 10 min at 37 °C. Finally, to assess the combined effect of thermal inactivation and CYP inhibition, heat-inactivated microsomes were preincubated with NADPH and ABT (2 mM) for 10 min at 37 °C. In all experiments, reactions were started by the addition of benzydamine (1 μM) and terminated at 10 min by the addition of ice-cold acetonitrile containing internal standard, SDM. It has been indicated previously that the *N*-oxide is stable under similar conditions to those used here and that autoxidation was negligible in liver microsomal experiments where comparable conditions were used (Yamazaki et al., 2014). Similarly, there was no indication of autoxidation in the lung incubations described in the current investigation.

For qualitative analysis of benzydamine metabolite patterns in rat lung microsomes, incubations were performed as described for the control incubation above but using higher benzydamine and microsomal protein concentrations of 5 μM and 0.25 mg/mL, respectively. Once again, reactions were started by the addition of benzydamine and terminated at 10 min by the addition of ice-cold acetonitrile.

Estimation of in vivo pulmonary extraction ratios in rat

Studies were conducted using male Sprague-Dawley rats aged 8–9 weeks (300–350 g) supplied by Charles River Labs, Margate, Kent. Rat pharmacokinetic studies were conducted by the UK Metabolism and Pharmacokinetics group. Experimental procedures were performed according to the animal welfare regulations effective in the UK (Scientific Procedures Act, 1986).

In vivo experiments to estimate the pulmonary first pass extraction of benzydamine in rat were performed as described previously (Yilmaz et al., 2017). Briefly, under anesthesia, the carotid artery and vena cava of the rats ($n = 3$) were cannulated for intra-arterial (i.a.) or intravenous (i.v.) administration, respectively. A temporary in-dwelling tail vein cannula was inserted into the tail vein of each rat for serial blood sampling. A 1 mg/kg bolus dose of benzydamine dissolved in 5% of dextrose was administered via the carotid artery or vena cava cannulas. Serial blood samples were then taken at 3, 6, 15, 45, 90, 150 and 240 min post-administration and collected into vials containing EDTA and 50 μl of the samples were then transferred to vials and protein precipitation immediately carried out by addition of 150 μL acetonitrile containing SDM. Samples were stored at −80 °C until the day of analysis. Calibration curves for benzydamine and benzydamine *N*-oxide were prepared in control rat blood. The samples were thoroughly mixed, centrifuged (3500 rpm, 10 min, 20 °C) and the supernatant transferred to a 96-plate containing an equal volume of water. Samples were analyzed by LC-MS/MS as described below. The *N*-oxide was stable under the conditions used here and there was no indication of significant reduction during sample preparation and analysis.

Non-compartmental pharmacokinetic analysis

Benzydamine and benzydamine *N*-oxide pharmacokinetic parameters were calculated by non-compartmental analysis (NCA) using Phoenix WinNonlin (Version 6.4, Pharsight Corporation, Mountain View, CA). The trapezoidal rule was used to calculate the area under the blood concentration–time curve (AUC) which was extrapolated to infinity ($AUC_{0\text{-inf}}$) using the apparent terminal disposition rate constant (λ_z). Blood clearance (CL_{blood}) values were calculated as $CL_{blood} = dose/AUC_{0\text{-inf}}$ and the half-life was estimated from the terminal rate constant using $half\text{-}life = 0.693/\lambda_z$. The mean residence time (MRT, defined as the area under the first moment curve ($AUMC_{0\text{-inf}}$) divided by $AUC_{0\text{-inf}}$ was used to calculate the steady-state volume of distribution (V_{ss}) using $V_{ss} = MRT \times CL_{blood}$.

Quantitative LC-MS/MS

Quantitative analysis was performed on an LC-MS/MS system consisting of a Waters Acquity UPLC coupled to a Quattro Premier (Waters Corporation, Milford, MA) triple quadrupole mass spectrometer with an electrospray ionization (ESI) source operated in positive ionization mode. Chromatography was performed using a Waters Acquity UPLC BEH C18 column (2.1 mm × 500 mm, 1.7 mm (Waters Corporation) maintained at 45 °C with a flow rate of 0.5 mL/min. The mobile phase consisted of solvent A (0.1% of formic acid in water) and solvent B (acetonitrile). The chromatographic gradient was optimized to provide baseline separation between benzydamine and benzydamine *N*-oxide. Gradient elution was as follows: 0 min → 5% B; 0.8 min → 5% B; 3.3 min → 50% B; 3.8 min → 50% B; 7.4 min → 5% B. Analytes were detected using multiple reaction monitoring (MRM) mode and the following transitions, cone voltage (CV) and collision energy (CE) settings: benzydamine (*m/z* 310 → 86; CV, 30 V; CE, 18 eV), benzydamine-*N*-oxide (*m/z* 326 → 102; CV, 30 V; CE, 15 eV) and the internal standard, SDM (*m/z* 311 → 156; CV, 30 V; CE, 30 eV). Desolvation, cone (both nitrogen) and collision (argon) gases were set at 750 L/h, 50 L/h $2.5 \times 10 - 3$ mbar, respectively. The source and desolvation temperatures were 120 and 300 °C, respectively. Five micro liter of sample was injected into the LC-MS/MS system.

MassLynx software (Waters Corporation) was used for the analysis of chromatograms. The processing of MS data was performed using QuanLynx software (Waters Corporation).

Qualitative LC-MS/MS

Qualitative analysis was performed using a Thermo LTQ Orbitrap XL hybrid mass spectrometer (Thermo Finnigan, UK) interfaced with an Accela HPLC system (Thermo Finnigan). Mass spectral data were acquired in positive ESI mode with full-scan MS spectra obtained from *m/z* 100 to 1300 with a mass resolution of 30,000. Collision induced dissociation (CID) was performed at a normalized CE of 35. Accurate measurement of *m/z* values and data processing of extracted ion chromatograms (EICs) were carried out using Xcalibur 2.1 (Thermo Fisher Scientific, Waltham, MA, USA). Chromatographic separation was achieved on an Acquity BEH C18 column (150 × 2.1 mm i.d., 1.7 µm, Waters Corporation). The reversed-phase gradient LC-MS experiments were performed using a mobile phase A of 0.1% of formic acid (aqueous) and a mobile phase B of acetonitrile at a flow rate of 0.3 mL/min. The HPLC gradient started with 5% B (0–1 min) and linearly increased to 90% B in 18 min, followed by a decrease to 40% B in 5 min prior to column re-equilibration.

Results

Benzydamine N-oxygenation enzyme kinetics in rat lung microsomes

Linear formation of benzydamine *N*-oxide was observed during the 10 min incubation period. Pulmonary benzydamine *N*-oxygenation appeared to be well described by the Michaelis–Menten model and the calculated kinetic parameters (V_{max}, K_m) are summarized in Figure 2 and Table 1. Enzyme kinetics of benzydamine *N*-oxygenation in rat liver microsomes has been previously determined and the values are also shown in Table 1 (Taniguchi-Takizawa et al., 2015). Although hepatic K_m and V_{max} values were higher than those obtained with lung microsomes, $CL_{int,in\text{-}vitro}$ (V_{max}/K_m) values were reasonably comparable (280 and 332 µL/min/mg for the rat liver and lung microsomes, respectively).

Benzydamine N-oxygenation in rat lung slices

Benzydamine *N*-oxide formation was linear during the 4 h incubation and terminal concentrations corresponded to approximately 61% of the initial benzydamine concentration (Figure 3). The rate of benzydamine *N*-oxide formation in lung slices (represented by the slope, in units of concentration/time) was used to calculate $CL_{int,in\text{-}vitro}$ (Njuguna et al., 2016). The *in vitro* intrinsic clearance, $CL_{int,\ in\ vitro}$ was 0.069 ± 0.01 µL/min/mg slice, resulting in an up-scaled *in vitro* lung clearance $CL_{int,lung}$ of 14.0 ± 2.0 mL/min/kg. The well-stirred model was then used to calculate *in vivo* whole lung clearance CL_{lung} (2.1 ± 0.3 mL/min/kg, Table 2).

Thermal inactivation/CYP inhibition

The *in vitro* data obtained using heat inactivation and the non-specific CYP inhibitor, ABT is summarized in Figure 4. Pulmonary benzydamine *N*-oxide formation in incubations containing ABT was comparable to that observed in the control incubation and there was no indication inhibition. Conversely, heat treatment resulted in a significant reduction

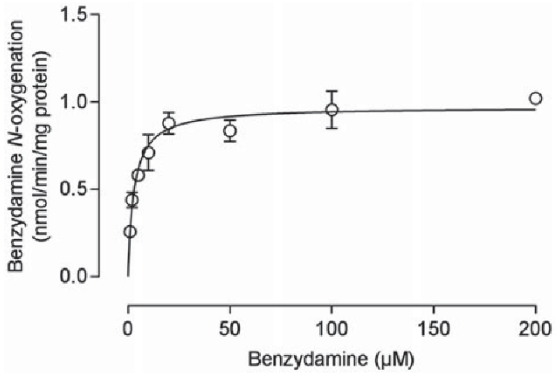

Figure 2. Kinetic parameters for benzydamine *N*-oxygenation by rat lung microsomes. Enzyme kinetics of benzydamine *N*-oxygenation by rat lung microsomes. Enzyme kinetic data were fitted to the Michaelis–Menten equation and are presented as mean values ± S.D. ($n = 3$).

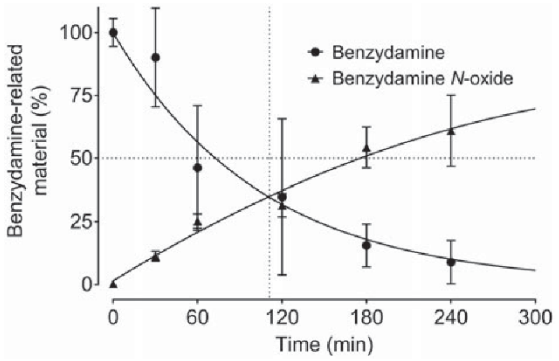

Figure 3. Incubation of benzydamine in rat lung slices. Dissapearance of benzydamine (circles) and formation of benzydamine *N*-oxide (triangles) during the 4 h incubation with rat lung slices. Results are shown as mean values ± S.D. ($n = 3$).

Table 1. Kinetic parameters for benzydamine *N*-oxygenation mediated by rat liver and lung microsomes.

	K_m (µM)	V_{max} (nmol/min/mg)	V_{max}/K_m (µL/min/mg)
Rat liver (Taniguchi-Takizawa et al., 2015)	22	6.1	280
Rat lung	2.9 ± 0.2	1.0 ± 0.03	332 ± 14

The rate of benzydamine *N*-oxide formation was measured following incubation of benzyadamine (1–1000 µM) with rat liver and (1–200 µM) lung microsomes (0.050 mg/mL microsomal protein) for 30 and 10 min, respectively. The values calculated in rat liver microsomes for benzydamine were obtained from a previous study (Taniguchi-Takizawa et al., 2015). Data were fitted according to the Michaelis–Menten equation. The estimated K_m, V_{max} and V_{max}/K_m ($CL_{int,in\text{-}vitro}$) values are expressed as mean values ± S.D. ($n = 3$).

Table 2. Prediction of rat CL_{organ} for benzydamine.

Organ	$CL_{int,organ}$ (mL/min/kg)	CL_{organ} (mL/min/kg)
Liver (microsomal)	1365 ± 175	46 ± 1.1
Lung (microsomal)	85 ± 3.5	16 ± 0.6
Lung (slices)	13.9 ± 2.0	2.1 ± 0.3

Benzydamine CL_{organ} (CL_{lung} and CL_{liver}) values were predicted using the pulmonary and hepatic V_{max}/K_m ($CL_{int,in\text{-}vitro}$) values determined in the enzyme kinetics experiments. Previously determined benzydamine *N*-oxygenation values obtained with rat liver microsomes are also shown. Scaling factors were used as follows: microsomal protein in lung 15 mg/g (Schmitz et al., 2008) and liver 45 mg/g (Obach, 2001), rat body weight 250 g, rat lung weight 1.5 g, rat liver weight 10 g, pulmonary blood flow (Q_{lung}) 296 mL/min/kg rat and hepatic blood flow (Q_{liver}) 55.2 mL/min/kg (Davies and Morris, 1993). In the absence of rat experimental data, human fu_{inc}, fu_{lung} (internal rat data), fu and $R_{b/p}$ values of 0.35, 0.03, 0.148 and 0.76 were used (Jones et al., 2017). Results are presented as mean values ± S.D. ($n = 3$).

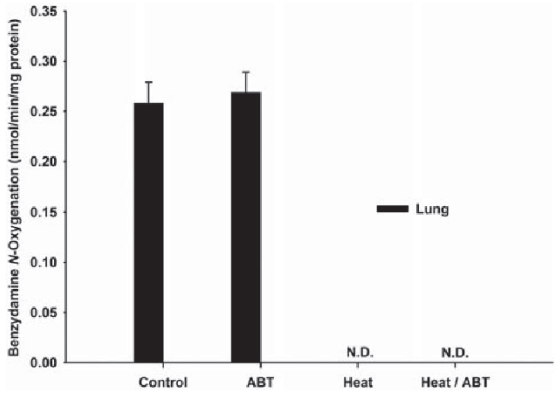

Figure 4. Effect of heat treatment and ABT-mediated CYP inhibition on benzydamine *N*-oxygenation in rat lung microsomes. The effect of thermal inactivation and the non-specific CYP inhibitor, ABT on benzydamine *N*-oxygenation by rat lung microsomes. Results are shown as mean values ± S.D. ($n = 3$). N.D. indicates that the *N*-oxide metabolite was not detected.

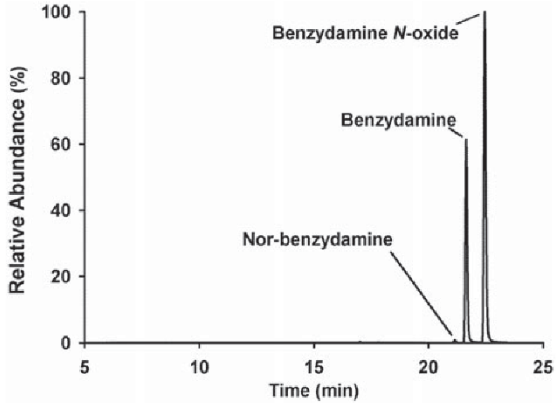

Figure 5. Metabolism of benzyadamine in rat lung microsomes. Selected ion chromatogram showing benzydamine and oxidative metabolites obtained following incubation of benzydamine with rat lung microsomes. Selected masses include 310.191 (benzydamine), 326.186 and 296.176 (nor-benzydamine).

of benzydamine *N*-oxide formation in lung fractions. Conversely, heat treatment resulted the complete abolishment of benzydamine *N*-oxide formation in lung fractions. There was no indication of autoxidation in the lung incubations described in the current investigation.

The major metabolite detected in lung microsomal incubations was benzydamine *N*-oxide while only low levels of the CYP-mediated metabolite, nor-benzydamine, were observed. The partial biotransformation pathway and selected ion chromatogram are shown in Figures 1 and 5, respectively. A more detailed investigation of the biotransformation of benzydamine in rat and human has previously been performed (Fisher et al., 2002).

Estimation of in vivo *pulmonary extraction in rat*

Benzydamine and benzydamine *N*-oxide blood concentrations were quantified following i.v. and i.a. administration of benzydamine to Sprague-Dawley rats and the pharmacokinetic parameters and concentration-time profiles are shown in Figure 6 and Table 3, respectively. Benzydamine was rapidly eliminated following i.v. and i.a. with blood clearances estimated to be 173 and 182 mL/min/kg, respectively (approximately three-fold higher than hepatic blood flow). The data showed that the benzydamine exposures achieved via the two administration routes were comparable and that there was no indication of significant pulmonary extraction under the conditions described here. The mean benzydamine *N*-oxide exposure obtained following i.v. dosing was slightly higher than after i.a. dosing (72 ± 4 and 61 ± 7 h × ng/mL respectively). However, this may likely be due to analytical or inter-animal variability rather than a reflection of pulmonary extraction.

Discussion

Preclinical species such as rats and mice are commonly used for the optimization of pharmacokinetic properties and for testing the *in vivo* efficacy of new compounds. The pharmacokinetic data from these preclinical species are often used for the prediction of human pharmacokinetics. Therefore, it is desirable that drug metabolism in these species is representative of that in human. However, the complex species dependent expression displayed by FMOs (Hines, 2006) may result in marked differences in metabolism and pharmacokinetics in preclinical species and human. For example, the absence of FMO1 in adult human liver but expression in rat (Itoh et al., 1993) and mouse liver (Cherrington et al., 1998; Janmohamed et al., 2004) means that these species may not be entirely representative for humans concerning FMO1 substrates. Similarly, the pulmonary expression of functional FMO2 in preclinical species and humans is complex. The full-length functional protein is expressed in mouse lung (Karoly & Rose, 2001), but not in the lungs of commonly used laboratory rat strains such as Sprague-Dawley and Wistar (Lattard et al., 2002b). Furthermore, 27% and 5% of people of African descent and Hispanic populations, respectively, possess the FMO2*1 allele that encodes for the full-length, functional, FMO2 protein whereas in Caucasians and Asians, FMO2 is absent (Dolphin et al., 1998; Krueger et al., 2004; Whetstine et al., 2000).

The impact of this variability in pulmonary expression of functional FMO2 in humans has been demonstrated using the antibiotic, ethionamide (Henderson et al., 2008). Ethionamide has been shown to undergo significantly higher

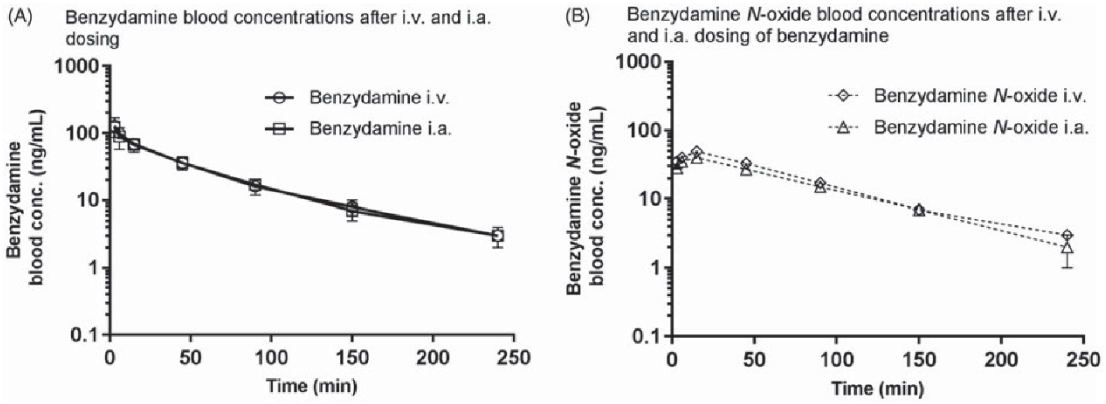

Figure 6. Blood concentration-time profiles of benzydamine and its metabolite benzydamine *N*-oxide after intra-arterial and intravenous dosing. Mean blood concentration-time profiles for benzydamine (A) following i.v. (circles) and i.a. (squares) administration and its metabolite benzydamine *N*-oxide (B) after i.v. (diamonds) and i.a. (triangles) administration to anesthetized male Sprague-Dawley rats. Results are shown as mean values ± S.D. ($n = 3$).

Table 3. Pharmacokinetics of benzydamine in rat.

Analyte		Units	Benzydamine, 1 mg/kg i.a. ($n = 3$)	Benzydamine, 1 mg/kg i.v. ($n = 3$)
Benzydamine	AUC_{inf}	h × ng/mL	93 ± 15	98 ± 15
	CL_{blood}	mL/min/kg	182 ± 31	173 ± 28
	V_{ss}	L/kg	11 ± 2.4	12 ± 3.1
	$T_{1/2}$	h	0.9 ± 0.1	1.1 ± 0.2
Benzydamine *N*-oxide	AUC_{inf}	h × ng/mL	61 ± 7	72 ± 4

Measured blood concentration profiles over time of benzydamine after single i.v. and i.a. dosing to male Sprague-Dawley rats were analyzed by non-compartmental pharmacokinetic analysis. Data are presented as mean values ± S.D. ($n = 3$).

FMO2-mediated S-oxygenation in human lung microsomes obtained from individuals expressing the functional protein than in lung microsomes where the truncated protein was expressed (Henderson et al., 2008). The authors also suggested that the expression of functional FMO2 in African and Hispanic populations may have important implications with respect to efficacy and toxicity. For instance, an FMO2 substrate that is intended for inhaled delivery may undergo metabolism in the lungs of these individuals, potentially leading to inactivation and therefore reduced efficacy. Alternatively, it may lead to the formation of a metabolite that causes local pulmonary toxicity.

The aim of this study was to investigate pulmonary FMO activity in rats using the anti-inflammatory drug, benzydamine. Furthermore, *in vivo* experiments were performed to understand if the rat lung makes a contribution to the whole body clearance of benzydamine. Benzydamine *N*-oxygenation was efficiently catalyzed by rat lung microsomes and lung slices (Figures 2 and 3, Tables 1 and 2). While calculated lung K_m and V_{max} values were lower than previously determined liver values (Taniguchi-Takizawa et al., 2015; Yamazaki et al., 2014), $CL_{int,in\text{-}vitro}$ (V_{max}/K_m) values were reasonably comparable (280 and 332 µL/min/mg for the rat liver and lung microsomes, Table 1).

CL_{organ} predicted from lung slices was approximately eight-fold lower than the value calculated with lung microsomes (2.1 and 16 mL/min/kg, respectively, Table 2). One of the potential drawbacks of the use of tissue slices is that this technique often underestimates metabolic clearance. This underprediction has previously been attributed to poor tissue penetration, diffusion and distribution of the drugs within the tissue slice during the incubation (de Graaf et al., 2006; Ekins et al., 1995; Worboys et al., 1997). The lung is a highly complex organ consisting more than 40 different types of cells. Therefore, a further cause of underprediction may be the limited number of cells in the slices that contain drug metabolizing enzymes (Carlile et al., 1999). Although CL_{lung} predicted with tissue slices is lower than the value obtained with microsomes (2.1 ± 0.3 and 16 ± 0.6 mL/min/kg, respectively) both methods suggest that the contribution of the rat lung to the whole body clearance of benzydamine is negligible (less than 5% pulmonary blood flow).

The significant rat pulmonary activity observed in lung microsomes experiments raised the question as to whether this *N*-oxygenation was catalyzed by FMOs, CYPs or a combination of both. FMOs are known to be thermally labile (Ziegler, 1980) and therefore, care should be taken when performing *in vitro* incubations to avoid loss of activity. As shown in Figure 4, heat treatment of lung microsomes at 45 °C for 5 min completely abolished benzydamine *N*-oxygenation in rat lung. Conversely, incubation with only ABT appeared to have no significant impact (Figure 4). As shown previously (Taniguchi-Takizawa et al., 2015), heat treatment of rat liver microsomes in the absence of NADPH results in a marked but incomplete reduction of benzydamine *N*-oxygenation. The data obtained in this study suggest that in rat, pulmonary benzydamine *N*-oxygenation is predominantly catalyzed by FMO while the contribution from CYPs is negligible.

The full-scan MS data obtained from the analysis of rat lung microsomal samples are shown in Figure 5. The metabolite pattern in rat lung was relatively simple and only

benzydamine *N*-oxide and low levels of nor-benzydamine were detected. The formation of nor-benzydamine has been shown to be catalyzed by CYP (Taniguchi-Takizawa et al., 2015) and the limited formation of nor-benzydamine observed here is consistent with the predominant assumption that the expression of CYPs in lung is generally low.

From these *in vitro* data, we concluded that, in rat, pulmonary benzydamine *N*-oxygenation is mainly catalyzed by FMO with no significant contribution of CYPs. It should be noted that although the involvement of FMO has been confirmed here, no attempt has been made to identify the specific isoforms responsible for the pulmonary *N*-oxygenation of benzydamine. FMO1 is known to be expressed in rat liver (Itoh et al., 1993) and lung (Lattard et al., 2001) and therefore, we may assume that this isoform contributes to the observed pulmonary *N*-oxygenation. FMO3 expression in rat lung has been shown to be relatively low and as a result, may not play a large role in the activity observed here (Lattard et al., 2001). While pulmonary FMO is commonly associated with the oxygenation of sulfur containing compounds, benzydamine has been shown to undergo complete *N*-oxygenation following incubation for 16 h with *Escherichia coli* expressing the full-length functional FMO2 protein (Geier et al., 2015). Although it has been reported that functional FMO2 is not expressed in the lungs of commonly used laboratory strains (Lattard et al., 2002b), we cannot rule out its potential involvement in the *N*-oxygenation observed here. However, FMO2 is known to be less vulnerable to heat inactivation than other isoforms (Cashman, 2005; Hutzler & Zientek, 2016) and the complete abolishment of *N*-oxygenation in heat treated lung microsomes observed in this study suggests that FMO2 was not involved. However, this would have to be confirmed with additional experiments.

Similarly to the liver, *in vitro* pulmonary intrinsic clearance values and the well-stirred model may be used to predict *in vivo* lung clearance. However, the well-stirred model depends on the assumption that the cells and their metabolic activities are homogeneously distributed in the system, which may not be the case for the lung (with 40 different cell types). Furthermore, appropriate scaling factors are not as well established as those used for the liver and further work is certainly required in this area. The validity of such predictions can be tested using rodent *in vivo* pulmonary extraction models where the compound of interest is dosed both pre- (i.v.) and post-lung (i.a.). This approach has been previously used to successfully demonstrate the impact of CYP, UGT and sulfotransferase-mediated lung metabolism (Aoki et al., 2010; Cassidy & Houston, 1980; Sharan & Nagar, 2013).

CL_{lung} estimated using rat lung microsomes was low (16 ± 0.6 mL/min/kg; Table 2) and equated to approximately 5% of pulmonary blood flow. The detection of such a low first pass extraction *in vivo* may be confounded by analytical and inter-animal variability and as such, the *in vivo* data obtained following i.a and i.v. dosing failed to show a significant difference in benzydamine exposure (Figure 6 and Table 3). Although the mean benzydamine *N*-oxide exposure observed after i.v. dosing was slightly higher than after i.a. dosing, the variability in the data preclude a confident attribution to pulmonary metabolism. The predicted CL_{liver} estimated from *in vitro* data was 46 ± 1.1 mL/min/kg, equivalent to approximately 83% hepatic blood flow (Table 2). This suggests that, in rat, benzydamine clearance is predominantly mediated by hepatic metabolism. The predicted CL_{lung} using rat lung microsomes corresponded to approximately 35% of rat CL_{liver}, also suggesting that the lung makes only a small contribution to the whole body clearance of benzydamine. Despite these findings, there may still be value in investigating the pulmonary metabolism of further FMO substrates.

In summary, benzydamine was used as a general FMO substrate to observe pulmonary FMO activity in rat and to determine the contribution of the rat lung to the whole body clearance of this compound. Although the data indicate that clearance of benzydamine in rats is mainly due to hepatic metabolism, the *in vitro* results also suggest that the lung makes a small contribution to systemic clearance of benzydamine. However, this failed to translate into a measurable pulmonary extraction *in vivo* (Figure 6), at least under the conditions used here. The route of administration may also be an important factor to consider and it is possible that a compound administered via inhalation may be subject to greater first pass lung extraction than a drug administered orally or intravenously. However, this is speculative and would need to be confirmed via appropriate experiments.

Acknowledgements

The authors would like to acknowledge Jon Rose, Arnold Demailly, Gaelle Chenal, Hazel Smulders and Asadh Miah for their support in the generation of data.

Disclosure statement

No potential conflict of interest was reported by the authors.

Funding

This work was supported by the Pharmacokinetic Sciences group at Novartis Institutes for Biomedical Research, Basel, Switzerland and Horsham, UK.

References

Aoki M, Okudaira K, Haga M, et al. (2010). Contribution of rat pulmonary metabolism to the elimination of lidocaine, midazolam, and nifedipine. Drug Metab Dispos 38:1183–8.

Capolongo F, Santi A, Anfossi P, Montesissa C. (2010). Benzydamine as a useful substrate of hepatic flavin-containing monooxygenase activity in veterinary species. J Vet Pharmacol Ther 33:341–6.

Carlile DJ, Hakooz N, Houston JB. (1999). Kinetics of drug metabolism in rat liver slices: IV. Comparison of ethoxycoumarin clearance by liver slices, isolated hepatocytes, and hepatic microsomes from rats pretreated with known modifiers of cytochrome P-450 activity. Drug Metab Dispos 27:526–32.

Cashman JR. (2005). Some distinctions between flavin-containing and cytochrome P450 monooxygenases. Biochem Biophys Res Commun 338:599–604.

Cashman JR, Zhang J. (2006). Human flavin-containing monooxygenases. Annu Rev Pharmacol Toxicol 46:65–100.

Cassidy MK, Houston JB. (1980). In vivo assessment of extrahepatic conjugative metabolism in first pass effects using the model compound phenol. J Pharm Pharmacol 32:57–9.

Cherrington NJ, Cao Y, Cherrington JW, et al. (1998). Physiological factors affecting protein expression of flavin-containing monooxygenases 1, 3 and 5. Xenobiotica 28:673–82.

Davies B, Morris T. (1993). Physiological parameters in laboratory animals and humans. Pharm Res 10:1093–5.

De Graaf IA, De Kanter R, De Jager MH, et al. (2006). Empirical validation of a rat in vitro organ slice model as a tool for in vivo clearance prediction. Drug Metab Dispos 34:591–9.

Ding X, Kaminsky LS. (2003). Human extrahepatic cytochromes P450: function in xenobiotic metabolism and tissue-selective chemical toxicity in the respiratory and gastrointestinal tracts. Annu Rev Pharmacol Toxicol 43:149–73.

Dolphin C, Shephard EA, Povey S, et al. (1991). Cloning, primary sequence, and chromosomal mapping of a human flavin-containing monooxygenase (FMO1). J Biol Chem 266:12379–85.

Dolphin CT, Beckett DJ, Janmohamed A, et al. (1998). The flavin-containing monooxygenase 2 gene (FMO2) of humans, but not of other primates, encodes a truncated, nonfunctional protein. J Biol Chem 273:30599–607.

Dolphin CT, Cullingford TE, Shephard EA, et al. (1996). Differential developmental and tissue-specific regulation of expression of the genes encoding three members of the flavin-containing monooxygenase family of man, FMO1, FMO3 and FMO4. Eur J Biochem 235:683–9.

Dolphin CT, Janmohamed A, Smith RL, et al. (1997). Missense mutation in flavin-containing mono-oxygenase 3 gene, FMO3, underlies fish-odour syndrome. Nat Genet 17:491–4.

Ekins S, Murray GI, Burke MD, et al. (1995). Quantitative differences in phase I and II metabolism between rat precision-cut liver slices and isolated hepatocytes. Drug Metab Dispos 23:1274–9.

Falls JG, Blake BL, Cao Y, et al. (1995). Gender differences in hepatic expression of flavin-containing monooxygenase isoforms (FMO1, FMO3, and FMO5) in mice. J Biochem Toxicol 10:171–7.

Fiorentini F, Romero E, Fraaije MW, et al. (2017). Baeyer–Villiger monooxygenase FMO5 as entry point in drug metabolism. ACS Chem Biol 12:2379–87.

Fisher MB, Yoon K, Vaughn ML, et al. (2002). Flavin-containing monooxygenase activity in hepatocytes and microsomes: in vitro characterization and in vivo scaling of benzydamine clearance. Drug Metab Dispos 30:1087–93.

Furnes B, Schlenk D. (2004). Evaluation of xenobiotic N- and S-oxidation by variant flavin-containing monooxygenase 1 (FMO1) enzymes. Toxicol Sci 78:196–203.

Geier M, Bachler T, Hanlon SP, et al. (2015). Human FMO2-based microbial whole-cell catalysts for drug metabolite synthesis. Microbial Cell Fact 14:82.

Gundert-Remy U, Bernauer U, Blömeke B, et al. (2014). Extrahepatic metabolism at the body's internal–external interfaces. Drug Metab Rev 46:291–324.

Henderson MC, Krueger SK, Siddens LK, et al. (2004). S-oxygenation of the thioether organophosphate insecticides phorate and disulfoton by human lung flavin-containing monooxygenase 2. Biochem Pharmacol 68:959–67.

Henderson MC, Siddens LK, Morré JT, et al. (2008). Metabolism of the anti-tuberculosis drug ethionamide by mouse and human FMO1, FMO2 and FMO3 and mouse and human lung microsomes. Toxicol Appl Pharmacol 233:420–7.

Hines RN. (2006). Developmental and tissue-specific expression of human flavin-containing monooxygenases 1 and 3. Expert Opin Drug Metab Toxicol 2:41–9.

Hutzler JM, Zientek MA. (2016). Non-cytochrome P450 enzymes and glucuronidation. In New horizons in predictive drug metabolism and pharmacokinetics. Washington (DC): The Royal Society of Chemistry, 79–130.

Itoh K, Kimura T, Yokoi T, et al. (1993). Rat liver flavin-containing monooxygenase (FMO): cDNA cloning and expression in yeast. Biochim Biophys Acta 1173:165–71.

Janmohamed A, Hernandez D, Phillips IR, Shephard EA. (2004). Cell-, tissue-, sex- and developmental stage-specific expression of mouse flavin-containing monooxygenases (FMOs). Biochem Pharmacol 68:73–83.

Jhajra S, Ramesh Varkhede N, Suresh Ahire D, et al. (2012). Extrahepatic drug-metabolizing enzymes and their significance. Encyclopedia Drug Metab Interact. [Epub ahead of print]. doi:10.1002/9780470921920.edm028.

Jones BC, Srivastava A, Colclough N, et al. (2017). An investigation into the prediction of in vivo clearance for a range of flavin-containing monooxygenase substrates. Drug Metab Dispos 45:1060–7.

Karoly ED, Rose RL. (2001). Sequencing, expression, and characterization of cDNA expressed flavin-containing monooxygenase 2 from mouse. J Biochem Molecul Toxicol 15:300–8.

Kawaji A, Ohara K, Takabatake E. (1993). An assay of flavin-containing monooxygenase activity with benzydamine N-oxidation. Anal Biochem 214:409–12.

Koukouritaki SB, Simpson P, Yeung CK, et al. (2002). Human hepatic flavin-containing monooxygenases 1 (FMO1) and 3 (FMO3) developmental expression. Pediatr Res 51:236–43.

Krueger SK, Siddens LK, Martin SR, et al. (2004). Differences in FMO2*1 allelic frequency between Hispanics of Puerto Rican and Mexican descent. Drug Metab Dispos 32:1337–40.

Krueger SK, Yueh M-F, Martin SR, et al. (2001). Characterization of expressed full-length and truncated FMO2 from rhesus monkey. Drug Metab Dispos 29:693–700.

Lai WG, Farah N, Moniz GA, Wong YN. (2010). A Baeyer–Villiger oxidation specifically catalyzed by human flavin-containing monooxygenase 5. Drug Metab Dispos 39:61–70.

Lang DH, Rettie AE. (2000). In vitro evaluation of potential in vivo probes for human flavin-containing monooxygenase (FMO): metabolism of benzydamine and caffeine by FMO and P450 isoforms. Br J Clin Pharmacol 50:311–4.

Lattard V, Buronfosse T, Lachuer J, et al. (2001). Cloning, sequencing, tissue distribution, and heterologous expression of rat flavin-containing monooxygenase 3. Arch Biochem Biophys 391:30–40.

Lattard V, Lachuer J, Buronfosse T, et al. (2002a). Physiological factors affecting the expression of FMO1 and FMO3 in the rat liver and kidney. Biochem Pharmacol 63:1453–64.

Lattard V, Longin-Sauvageon C, Krueger SK, et al. (2002b). The FMO2 gene of laboratory rats, as in most humans, encodes a truncated protein. Biochem Biophys Res Commun 292:558–63.

Lawton MP, Cashman JR, Cresteil T, et al. (1994). A nomenclature for the mammalian flavin-containing monooxygenase gene family based on amino acid sequence identities. Arch Biochem Biophys 308:254–7.

Meng J, Zhong D, Li L, et al. (2015). Metabolism of MRX-I, a novel antibacterial oxazolidinone, in humans: the oxidative ring opening of 2,3-dihydropyridin-4-one catalyzed by non-P450 enzymes. Drug Metab Dispos 43:646–59.

Moroni P, Longin-Sauvageon C, Benoit E. (1995). The flavin-containing monooxygenases in rat liver: evidence for the expression of a second form different from FMO1. Biochem Biophys Res Commun 212:820–6.

Njuguna NM, Umehara KI, Huth F, et al. (2016). Improvement of the chemical inhibition phenotyping assay by cross-reactivity correction. Drug Metab Pers Ther 31:221–8.

Obach RS. (2001). The prediction of human clearance from hepatic microsomal metabolism data. Curr Opin Drug Discov Dev 4:36–44.

Phillips IR, Dolphin CT, Clair P, et al. (1995). The molecular biology of the flavin-containing monooxygenases of man. Chem Biol Interact 96:17–32.

Phillips IR, Shephard EA. (2017). Drug metabolism by flavin-containing monooxygenases of human and mouse. Expert Opin Drug Metab Toxicol 13:167–81.

Rawden HC, Kokwaro GO, Ward SA, Edwards G. (2000). Relative contribution of cytochromes P-450 and flavin-containing monoxygenases to the metabolism of albendazole by human liver microsomes. Br J Clin Pharmacol 49:313–22.

Rettie AE, Meier GP, Sadeque AJ. (1995). Prochiral sulfides as in vitro probes for multiple forms of the flavin-containing monooxygenase. Chem Biol Interact 96:3–15.

Ripp SL, Itagaki K, Philpot RM, Elfarra AA. (1999). Species and sex differences in expression of flavin-containing monooxygenase form 3 in liver and kidney microsomes. Drug Metab Dispos 27:46–52.

Schmitz A, Portier CJ, Thormann W, et al. (2008). Stereoselective biotransformation of ketamine in equine liver and lung microsomes. J Vet Pharmacol Ther 31:446–55.

Scientific Procedures Act. (1986). Animals (Scientific Procedures) Act 1986. Available at: https://www.legislation.gov.uk/ukpga/1986/14/contents.

Sharan S, Nagar S. (2013). Pulmonary metabolism of resveratrol: in vitro and in vivo evidence. Drug Metab Dispos 41:1163–9.

Störmer E, Roots I, Brockmöller J. (2000). Benzydamine N-oxidation as an index reaction reflecting FMO activity in human liver microsomes and impact of FMO3 polymorphisms on enzyme activity. Br J Clin Pharmacol 50:553–61.

Taniguchi-Takizawa T, Shimizu M, Kume T, Yamazaki H. (2015). Benzydamine N-oxygenation as an index for flavin-containing monooxygenase activity and benzydamine N-demethylation by cytochrome P450 enzymes in liver microsomes from rats, dogs, monkeys, and humans. Drug Metab Pharmacokin 30:64–9.

Tugnait M, Hawes EM, Mckay G, et al. (1997). N-oxygenation of clozapine by flavin-containing monooxygenase. Drug Metab Dispos 25:524–7.

Whetstine JR, Yueh MF, Hopp KA, et al. (2000). Ethnic differences in human flavin-containing monooxygenase 2 (FMO2) polymorphisms: detection of expressed protein in African-Americans. Toxicol Appl Pharmacol 168:216–24.

Worboys PD, Bradbury A, Houston JB. (1997). Kinetics of drug metabolism in rat liver slices: III. Relationship between metabolic clearance and slice uptake rate. Drug Metab Dispos 25:460–7.

Yamazaki M, Shimizu M, Uno Y, Yamazaki H. (2014). Drug oxygenation activities mediated by liver microsomal flavin-containing monooxygenases 1 and 3 in humans, monkeys, rats, and minipigs. Biochem Pharmacol 90:159–65.

Yanni SB, Annaert PP, Augustijns P, et al. (2008). Role of flavin-containing monooxygenase in oxidative metabolism of voriconazole by human liver microsomes. Drug Metab Dispos 36:1119–25.

Yilmaz Y, Umehara K, Williams G, et al. (2017). Assessment of the pulmonary CYP1A1 metabolism of mavoglurant (AFQ056) in rat. Xenobiotica, 1–11. [Epub ahead of print]. doi:10.1080/00498254.2017.1373311.

Zhang J, Cashman JR. (2005). Quantitative analysis of fmo gene mrna levels in human tissues. Drug Metab Dispos 34:19–26.

Ziegler DM. (1980). Microsomal flavin-containing monooxygenase: oxygenation of nucleophilic nitrogen and sulfur compounds A2. In: Jakoby WB, ed. Enzymatic basis of detoxication. New York (NY): Academic Press, 201–227.

Chapter 4. Discussion and outlook

In recent years, the use of PCLS has increased for industrial applications such as testing of chemicals and xenobiotics as it offers advantages over cell-lines and subcellular fractions (as discussed in chapter 4). In addition to drug metabolism, PCLS is used for toxicology and biomarker studies (Lauenstein *et al.*, 2014, Hess *et al.*, 2016, Hesse *et al.*, 2016). PCLS model facilitates the investigation of drug metabolism, as the method is applicable to healthy and diseased lung tissue from different species by retaining both anatomical and physiological conditions. Another advantage of precision-cut tissue slicing is that hepatic and extra-hepatic drug-metabolizing enzymes can be induced by this technique (Price *et al.*, 2004).

4.1. Optimization of the PCLS model for more accurate estimation of pulmonary drug clearance

In order to optimize the PCLS model, different incubation conditions were tested and it was possible to achieve higher turnover using a dynamic organ culture system. Oxygen supply appeared to have negligible effect on metabolic turnover in incubations of 4 h duration. However, oxygen supply might be an essential parameter for incubations of longer duration in order to maintain the slice viability. This work clearly showed the importance of optimization and standardization of PCLS conditions for the metabolism studies. However, supplementary experiments using a broader range of probe substrates could be of interest to further evaluate the PCLS model. The in-house application of the PCLS model may also be extended to toxicology investigations.

4.2. Comparison of phase I and phase II metabolic activity in rat and human lungs

This study demonstrated that there are significant differences in pulmonary enzyme activity between rats and humans, which is due to the species and tissue dependent expression of these enzymes. Our results indicate that phase II activity appears to be more prevalent in rat than in human lung and that phase II activity is considerably higher than that of phase I enzymes. This work highlights the differences in pulmonary

metabolic activity between rat and human and emphasizes the importance of critically evaluating data derived from animal models. In order to answer the question: to what extend does lung metabolism in rat reflects the situation in the human lung, yet extensive research will be required for a statistical analysis using a broader range of specific probe substrates.

4.3. Comparison of PCLS, *in vitro* and *in vivo* experimental models for the investigation of pulmonary contribution to drug metabolic clearance

4.3.1. Mavoglurant and CYP1A1

Experiments were performed to determine if pulmonary metabolism contributed to the total body elimination of mavoglurant. Our data suggests that the lungs make a negligible contribution to mavoglurant elimination in rat. It remains unclear which other organs may contribute to the total body clearance of this compound. Previous investigations regarding mavoglurant CYP1A1-mediated elimination by kidney demonstrated negligible contribution (Novartis internal data). The contribution of brain and intestinal CYP1A1 to the metabolism of mavoglurant should be further investigated.

Although there was conflicting evidence for the expression of CYP1A1 protein in liver, current studies indicate that CYP1A1 expression in human liver is low. (Drahushuk *et al.*, 1998, Nakamura *et al.*, 2005). CYP1A1 is regulated by the AhR and is highly inducible by some PAHs, such as those found in cigarette smoke (Nebert *et al.*, 2004, Elsherbiny and Brocks, 2011, Klingbeil *et al.*, 2014, Moorthy *et al.*, 2015, Wohak *et al.*, 2016). The results of a clinical study (Novartis internal data) showed that mavoglurant C_{max} and AUC_{inf} in smokers were reduced by 41% and 46%, respectively, compared to nonsmokers. These results indicate that smoking induces CYP1A1 expression in the body and consequently reduces systemic exposure of mavoglurant. Therefore, the potential of CYP1A1 induction should not be underestimated. It is speculated that once the induction is initiated, CYP1A1 becomes highly efficient in all organs such as lung, brain, kidney, intestine and liver (van de Kerkhof *et al.*, 2008, Walsh *et al.*, 2013). Therefore, following CYP1A1 induction the level of hepatic and extrahepatic

metabolism can be significantly altered.

Likewise, for other CYP1A1 substrates such as riluzole, gefitinib, erlotinib, granisetron and riociguat, marked differences in systemic exposure have been reported in smokers and non-smokers. (Sanderink *et al.*, 1997, Corrigan *et al.*, 1999, Nakamura *et al.*, 2005, Li *et al.*, 2007, Li *et al.*, 2010, Khaybullina *et al.*, 2014, Frey *et al.*, 2016, Saleh *et al.*, 2016). These findings support the assumptions described above. Therefore, further investigations using the tissue slice model following CYP1A1 induction could potentially help to understand the importance of hepatic and extra-hepatic CYP1A1 drug metabolism.

4.3.2. Benzydamine and FMO

In the present work, we have also investigated the pulmonary metabolism of benzydamine. Benzydamine N-oxygenation is catalyzed by FMO1 and FMO3 in human (Lang and Rettie, 2000a). The expression of FMO enzymes is complex and varies extensively with species, tissue, age and gender (Ripp *et al.*, 1999, Hines, 2006, Phillips and Shephard, 2017). In our experiments using rat lung microsomes, rat lung tissue and after i.v. and i.a. administration, we could detect formation of the benzydamine N-oxide metabolite. In microsomes the calculated organ clearance for lung was approximately 35% of the liver clearance. The estimated lung clearance with PCLS model was very low. Furthermore, benzydamine clearance values obtained following i.v. and i.a. drug administration were comparable, indicating that *in vivo*, rat pulmonary metabolism of benzydamine was negligible. Although FMO3 expression is high in rat liver, in rat lung its expression is limited (Lattard *et al.*, 2002a, Lattard *et al.*, 2002c). FMO1 expression in rat lung is known to be greater than FMO3 expression (Lattard *et al.*, 2002c). Therefore, observed benzydamine N-oxide formation in lung is likely the result of metabolism by FMO1. It has previously been reported that FMO isoforms are thermally labile in the absence of NADPH (Fisher *et al.*, 2002). The contribution of FMO and CYPs to benzydamine N-oxygenation in rat lung microsomes was determined using thermal inactivation and the nonspecific irreversible CYP inhibitor (ABT). Heat treatment led to the total abolishment of benzydamine N-oxide formation in rat lung microsomes whereas ABT had no impact. These results indicated

that, benzydamine N-oxygenation is predominantly catalyzed by FMO.

The FMO2 isoenzyme is a special case among FMO isoenzymes. Although functional FMO2 enzyme is expressed in mouse lung, it is catalytically inactive in rat lung (Karoly and Rose, 2001, Lattard *et al.*, 2002b). Interestingly, in human, FMO2 is not active in Caucasians and Asians as these populations possess the FMO2*2 allele that codes for a non-functional, truncated protein (Dolphin *et al.*, 1998, Whetstine *et al.*, 2000, Krueger *et al.*, 2004). Conversely, 27% of African and 5% of Hispanic populations possess the FMO2*1 allele that codes for the full length, functional active enzyme (Henderson *et al.*, 2008). Furthermore, FMO2 has been reported to be less heat labile compare to other FMO isoforms (Cashman, 2005, Hutzler and Zientek, 2016). Therefore, depending on the target population for the drug under investigation, care should be taken when predicting PK parameters for drugs that are primarily FMO substrate.

4.3.3. Scaling parameters

While hepatic scaling factors are well defined, the availability of similar information for the lung is relatively limited. For example, in the current study the microsomal protein content in rat lung was assumed to be 15 mg/g lung (one third of that in rat liver (45 mg/g)), which is the only information found in the literature (Houston, 1994, Lakritz *et al.*, 2000, Schmitz *et al.*, 2008). Investigations into lung metabolism would benefit greatly from the development of pulmonary scaling factors in all relevant species. The abundance of metabolic enzymes can be measured by either immunochemistry techniques (if specific antibodies are available), gene expression (mRNA), or can be estimated by the use of specific enzyme substrates and inhibitors. Correct information about abundance of the enzymes will certainly provide more accurate *in vitro* clearance estimates. Furthermore, an *in vitro in vivo* extrapolation (IVIVE) method for metabolic clearance in lung needs to be established.

4.3.4. Relevance of pulmonary metabolism

At the end of the research project, it is important to answer the question “when is pulmonary metabolism relevant and when should we use the optimized PCLS model”.

The liver is the primary organ of metabolism and the lung metabolic functionality and capacity rarely exceed the hepatic function. However, if the total body clearance exceeds the liver blood flow, this can be an indication for extrahepatic metabolism (Kanto and Gepts, 1989). Inhaled compounds such as anesthesia drugs are more likely to be metabolized by pulmonary enzymes, as they are directly exposed to the lungs. Hence, lung tissue could have a significant impact on the disposition of inhaled drugs.

Pulmonary metabolism may have several consequences including decreased systemic exposure to the drug and the generation of site-specific reactive metabolites, which may lead to organ specific toxicity. Therefore, the investigation of pulmonary metabolism is relevant for the evaluation of safety and efficacy in drug discovery and development. Some prodrugs such as the inhaled corticosteroid, ciclesonide are designed to be metabolized in the lung tissue to yield an active metabolite (Nave *et al.*, 2006, Nave *et al.*, 2010). Investigations into pulmonary metabolism are crucial in cases such as these and PCLS is an appropriate model for the assessment of compounds developed for inhaled administration. For example, PCLS has previously been used to demonstrate that ciclesonide undergoes hydrolysis and reversible conjugation with fatty acids (FA) such as oleic acid in human lung (Nave *et al.*, 2006, Nave *et al.*, 2010)

The time course of drug response for dosing regimens can be estimated using physiologically based pharmacokinetic (PBPK) models combined with pharmacodynamic (PD) models (Jones *et al.*, 2015). Although the application of PBPK modelling to orally inhaled drugs has strongly increased in recent years, they currently concerned with understanding the absorption process (Borghardt *et al.*, 2015). For example, to what extent do factors such as regional lung particle deposition and drug disposition processes influence free tissue drug concentrations (Backman *et al.*, 2018). However, these models currently ignore the issue of pulmonary metabolism and its potential impact on safety and efficacy. Further investment is required in this area and the PCLS model may be a suitable system to support the development of mechanistic PBPK models for this purpose.

Chapter 5. References

Aggarwal, S., Gross, C.M., Porcelli, R.J. & Black, S.M., 2015. Chapter 14 - Pulmonary Hemodynamics A2 - Parent, Richard A. *Comparative Biology of the Normal Lung (Second Edition).* San Diego: Academic Press, 205-243.

Anttila, S., Raunio, H. & Hakkola, J., 2011. Cytochrome P450-mediated pulmonary metabolism of carcinogens: regulation and cross-talk in lung carcinogenesis. *Am J Respir Cell Mol Biol,* 44**,** 583-90.

Aoki, M., Okudaira, K., Haga, M., Nishigaki, R. & Hayashi, M., 2010. Contribution of Rat Pulmonary Metabolism to the Elimination of Lidocaine, Midazolam, and Nifedipine. *Drug Metabolism and Disposition,* 38**,** 1183-1188.

Backman, P., Arora, S., Couet, W., Forbes, B., De Kruijf, W. & Paudel, A., 2018. Advances in experimental and mechanistic computational models to understand pulmonary exposure to inhaled drugs. *Eur J Pharm Sci,* 113**,** 41-52.

Barrett, K.E., Boitano, S., Barman, S.M. & Brooks, H.L., 2012. Chapter 34. Introduction to Pulmonary Structure and Mechanics. *Ganong's Review of Medical Physiology, 24e.* New York, NY: The McGraw-Hill Companies.

Behera, D., Damre, A., Varghese, A. & Addepalli, V., 2008. In vitro evaluation of hepatic and extra-hepatic metabolism of coumarins using rat subcellular fractions: correlation of in vitro clearance with in vivo data. *Drug Metabol Drug Interact,* 23**,** 329-50.

Berg, M.M., Kim, K.J., Lubman, R.L. & Crandall, E.D., 1989. Hydrophilic solute transport across rat alveolar epithelium. *J Appl Physiol (1985),* 66**,** 2320-7.

Berry-Kravis, E., Des Portes, V., Hagerman, R., Jacquemont, S., Charles, P., Visootsak, J., Brinkman, M., Rerat, K., Koumaras, B., Zhu, L., Barth, G.M., Jaecklin, T., Apostol, G. & Von Raison, F., 2016. Mavoglurant in fragile X syndrome: Results of two randomized, double-blind, placebo-controlled trials. *Sci Transl Med,* 8**,** 321ra5.

Bieche, I., Narjoz, C., Asselah, T., Vacher, S., Marcellin, P., Lidereau, R., Beaune, P. & De Waziers, I., 2007. Reverse transcriptase-PCR quantification of mRNA levels from cytochrome (CYP)1, CYP2 and CYP3 families in 22 different human tissues. *Pharmacogenet. Genomics,* 17**,** 731-42.

Boer, F., 2003. Drug handling by the lungs. *BJA: British Journal of Anaesthesia,* 91**,** 50-60.

Borghardt, J.M., Kloft, C. & Sharma, A., 2018. Inhaled Therapy in Respiratory Disease: The Complex Interplay of Pulmonary Kinetic Processes. *Canadian Respiratory Journal,* 2018**,** 2732017.

Borghardt, J.M., Weber, B., Staab, A. & Kloft, C., 2015. Pharmacometric Models for Characterizing the Pharmacokinetics of Orally Inhaled Drugs. *AAPS J,* 17**,** 853-70.

Bosquillon, C., Madlova, M., Patel, N., Clear, N. & Forbes, B., 2017. A Comparison of Drug Transport in Pulmonary Absorption Models: Isolated Perfused rat Lungs, Respiratory Epithelial Cell Lines and Primary Cell Culture. *Pharm Res,* 34**,** 2532-2540.

Bozhkov, A.I., Nikitchenko, Y.V., Klimova, E.M., Linkevych, O.S., Lebid, K.M., Al-Bahadli, A.M.M. & Alsardia, M.M.A., 2017. Young and old rats have different strategies of metabolic adaptation to Cu-induced liver fibrosis. *Advances in Gerontology,* 7**,** 41-50.

Carlile, D.J., Hakooz, N., Bayliss, M.K. & Houston, J.B., 1999. Microsomal prediction of in vivo clearance of CYP2C9 substrates in humans. *Br. J. Clin. Pharmacol.,* 47**,** 625-35.

Cashman, J.R., 2005. Some distinctions between flavin-containing and cytochrome P450 monooxygenases. *Biochem Biophys Res Commun,* 338**,** 599-604.

Cashman, J.R. & Zhang, J., 2006. Human flavin-containing monooxygenases. *Annu. Rev. Pharmacol. Toxicol.,* 46**,** 65-100.

Cassidy, M.K. & Houston, J.B., 1984. In vivo capacity of hepatic and extrahepatic enzymes to conjugate phenol. *Drug Metab Dispos,* 12**,** 619-24.

Castell, J.V., Donato, M.T. & Gomez-Lechon, M.J., 2005. Metabolism and bioactivation of toxicants in the lung. The in vitro cellular approach. *Exp Toxicol Pathol,* 57 Suppl 1**,** 189-204.

Cheung, Y.-L., Kerr, A.C., Mcfadyen, M.C.E., Melvin, W.T. & Murray, G.I., 1999. Differential expression of CYP1A1, CYP1A2, CYP1B1 in human kidney tumours. *Cancer Letters,* 139**,** 199-205.

Chiba, M., Ishii, Y. & Sugiyama, Y., 2009. Prediction of hepatic clearance in human from in vitro data for successful drug development. *AAPS J,* 11**,** 262-76.

Cohen, G.M., 1990. Pulmonary metabolism of foreign compounds: its role in metabolic activation. *Environ Health Perspect,* 85**,** 31-41.

Corrigan, B.W., Nicholls, B., Thakrar, B., Lam, R., Grosse, C., Alianti, J. & Palmer, J.L., 1999. Heterogeneity in Systemic Availability of Ondansetron and Granisetron following Oral Administration. *Drug Metabolism and Disposition,* 27**,** 110-112.

Costa, A., Sarmento, B. & Seabra, V., 2014. An evaluation of the latest in vitro tools for drug metabolism studies. *Expert Opin Drug Metab Toxicol,* 10**,** 103-19.

Courcot, E., Leclerc, J., Lafitte, J.-J., Mensier, E., Jaillard, S., Gosset, P., Shirali, P., Pottier, N., Broly, F. & Lo-Guidice, J.-M., 2012. Xenobiotic Metabolism and Disposition in Human Lung Cell Models: Comparison with In Vivo Expression Profiles. *Drug Metabolism and Disposition,* 40**,** 1953-1965.

Crapo, J.D., Barry, B.E., Gehr, P., Bachofen, M. & Weibel, E.R., 1982. Cell number and cell characteristics of the normal human lung. *Am Rev Respir Dis,* 126**,** 332-7.

Cruciani, G., Valeri, A., Goracci, L., Pellegrino, R.M., Buonerba, F. & Baroni, M., 2014. Flavin monooxygenase metabolism: why medicinal chemists should matter. *J Med Chem,* 57**,** 6183-96.

Culver, B.H. & Glenny, R.W., 2012. Chapter 4 - Pulmonary Circulation A2 - Spiro, Stephen G. *In* G.A. Silvestri & A. Agustí (eds.) *Clinical Respiratory Medicine (Fourth Edition).* Philadelphia: W.B. Saunders, 29-36.

De Graaf, I.a.M. & Koster, H., 2003. Cryopreservation of precision-cut tissue slices for application in drug metabolism research. *Toxicology in Vitro,* 17**,** 1-17.

De Kanter, R., De Jager, M., Draaisma, A., Jurva, J., Olinga, P., Meijer, D. & Groothuis, G., 2002. Drug-metabolizing activity of human and rat liver, lung, kidney and intestine slices. *Xenobiotica,* 32**,** 349-362.

De Kanter, R., Olinga, P., De Jager, M.H., Merema, M.T., Meijer, D.K. & Groothius, G.M., 1999. Organ slices as an in vitro test system for drug metabolism in human liver, lung and kidney. *Toxicol In Vitro,* 13**,** 737-44.

Del Donno, M., Verduri, A. & Olivieri, D., 2002. Air pollution and reversible chronic respiratory diseases. *Monaldi Arch. Chest Dis.,* 57**,** 164-6.

Devereux, T.R., Domin, B.A. & Philpot, R.M., 1989. Xenobiotic metabolism by isolated pulmonary cells. *Pharmacol. Ther.,* 41**,** 243-56.

Dickinson, P.A. & Taylor, G., 1996. Pulmonary first-pass and steady-state metabolism of phenols. *Pharm Res,* 13**,** 744-8.

Ding, X. & Kaminsky, L.S., 2003. Human extrahepatic cytochromes P450: function in xenobiotic metabolism and tissue-selective chemical toxicity in the respiratory and gastrointestinal tracts. *Annu. Rev. Pharmacol. Toxicol.,* 43**,** 149-73.

Dogterom, P., 1993. Development of a simple incubation system for metabolism studies with precision-cut liver slices. *Drug Metab. Dispos.,* 21**,** 699-704.

Dolphin, C.T., Beckett, D.J., Janmohamed, A., Cullingford, T.E., Smith, R.L., Shephard, E.A. & Phillips, I.R., 1998. The flavin-containing monooxygenase 2 gene (FMO2) of humans, but not of other primates, encodes a truncated, nonfunctional protein. *J. Biol. Chem.,* 273**,** 30599-607.

Donato, M.T., Lahoz, A., Castell, J.V. & Gomez-Lechon, M.J., 2008. Cell lines: a tool for in vitro drug metabolism studies. *Curr Drug Metab,* 9**,** 1-11.

Drahushuk, A.T., Mcgarrigle, B.P., Larsen, K.E., Stegeman, J.J. & Olson, J.R., 1998. Detection of CYP1A1 protein in human liver and induction by TCDD in precision-cut liver slices incubated in dynamic organ culture. *Carcinogenesis,* 19**,** 1361-8.

Elsherbiny, M.E. & Brocks, D.R., 2011. The ability of polycyclic aromatic hydrocarbons to alter physiological factors underlying drug disposition. *Drug Metab Rev,* 43**,** 457-75.

Fisher, M.B., Yoon, K., Vaughn, M.L., Strelevitz, T.J. & Foti, R.S., 2002. Flavin-containing monooxygenase activity in hepatocytes and microsomes: in vitro characterization and in vivo scaling of benzydamine clearance. *Drug Metab Dispos,* 30**,** 1087-93.

Fisher, R.L., Shaughnessy, R.P., Jenkins, P.M., Austin, M.L., Roth, G.L., Gandolfi, A.J. & Brendel, K., 1995. Dynamic Organ Culture is Superior to Multiwell Plate Culture for Maintaining Precision-Cut Tissue Slices: Optimization of Tissue Slice Culture, Part 1. *Toxicology Methods,* 5**,** 99-113.

Flieder, D.B., 2018. 1 - Normal Anatomy, Tissue Artifacts, and Incidental Structures A2 - Zander, Dani S. *In* C.F. Farver (ed.) *Pulmonary Pathology (Second Edition).* Philadelphia: Content Repository Only!, 1-7.

Franks, T.J., Colby, T.V., Travis, W.D., Tuder, R.M., Reynolds, H.Y., Brody, A.R., Cardoso, W.V., Crystal, R.G., Drake, C.J., Engelhardt, J., Frid, M., Herzog, E., Mason, R., Phan, S.H., Randell, S.H., Rose, M.C., Stevens, T., Serge, J., Sunday, M.E., Voynow, J.A., Weinstein, B.M., Whitsett, J. & Williams, M.C., 2008. Resident cellular components of the human lung: current knowledge and goals for research on cell phenotyping and function. *Proc Am Thorac Soc,* 5**,** 763-6.

Frey, R., Becker, C., Unger, S., Schmidt, A., Wensing, G. & Mück, W., 2016. Assessment of the effects of hepatic impairment and smoking on the pharmacokinetics of a single oral dose of the soluble guanylate cyclase stimulator riociguat (BAY 63-2521). *Pulmonary Circulation,* 6**,** S5-S14.

Garattini, E., Fratelli, M. & Terao, M., 2009. The mammalian aldehyde oxidase gene family. *Hum. Genomics,* 4**,** 119-30.

Garcia-Canton, C., Minet, E., Anadon, A. & Meredith, C., 2013. Metabolic characterization of cell systems used in in vitro toxicology testing: lung cell system BEAS-2B as a working example. *Toxicol In Vitro,* 27**,** 1719-27.

Gehr, P., 1984. Respiratory tract structure and function. *J Toxicol Environ Health,* 13**,** 235-49.

Gotz, C., Pfeiffer, R., Tigges, J., Blatz, V., Jackh, C., Freytag, E.M., Fabian, E., Landsiedel, R., Merk, H.F., Krutmann, J., Edwards, R.J., Pease, C., Goebel, C., Hewitt, N. & Fritsche, E., 2012. Xenobiotic metabolism capacities of human skin in comparison with a 3D epidermis model and keratinocyte-based cell culture as in vitro alternatives for chemical testing: activating enzymes (Phase I). *Exp Dermatol,* 21**,** 358-63.

Henderson, M.C., Siddens, L.K., Morre, J.T., Krueger, S.K. & Williams, D.E., 2008. Metabolism of the anti-tuberculosis drug ethionamide by mouse and human FMO1, FMO2 and FMO3 and mouse and human lung microsomes. *Toxicol Appl Pharmacol,* 233**,** 420-7.

Hess, A., Wang-Lauenstein, L., Braun, A., Kolle, S.N., Landsiedel, R., Liebsch, M., Ma-Hock, L., Pirow, R., Schneider, X., Steinfath, M., Vogel, S., Martin, C. & Sewald, K., 2016. Prevalidation of the ex-vivo model PCLS for prediction of respiratory toxicity. *Toxicol In Vitro,* 32**,** 347-61.

Hesse, C., Mang, S., Hoymann, H.-G., Niehof, M., Braubach, P., Jonigk, D., Warnecke, G., Pfennig, O., Fieguth, H.-G., Braun, A. & Sewald, K., 2016. Induction of pro-fibrotic biomarkers in precision-cut lung slices (PCLS). *European Respiratory Journal,* 48.

Hines, R.N., 2006. Developmental and tissue-specific expression of human flavin-containing monooxygenases 1 and 3. *Expert Opin. Drug Metab. Toxicol.,* 2**,** 41-9.

Horvath, L., Umehara, Y., Jud, C., Blank, F., Petri-Fink, A. & Rothen-Rutishauser, B., 2015. Engineering an in vitro air-blood barrier by 3D bioprinting. *Sci Rep,* 5**,** 7974.

Houston, J.B., 1994. Utility of in vitro drug metabolism data in predicting in vivo metabolic clearance. *Biochem Pharmacol,* 47**,** 1469-79.

Hukkanen, J., Pelkonen, O., Hakkola, J. & Raunio, H., 2002. Expression and regulation of xenobiotic-metabolizing cytochrome P450 (CYP) enzymes in human lung. *Crit. Rev. Toxicol.,* 32**,** 391-411.

Hutzler, J.M., Yang, Y.S., Albaugh, D., Fullenwider, C.L., Schmenk, J. & Fisher, M.B., 2012. Characterization of aldehyde oxidase enzyme activity in cryopreserved human hepatocytes. *Drug Metab. Dispos.,* 40**,** 267-75.

Hutzler, J.M. & Zientek, M.A., 2016. CHAPTER 5 Non-Cytochrome P450 Enzymes and Glucuronidation. *New Horizons in Predictive Drug Metabolism and Pharmacokinetics.* The Royal Society of Chemistry, 79-130.

Ioannides, C., 2013. Up-regulation of cytochrome P450 and phase II enzymes by xenobiotics in precision-cut tissue slices. *Xenobiotica,* 43**,** 15-28.

Ioannides, C., Lake, B.G. & Lyubimov, A.V., 2011. Precision-Cut Tissue Slices: A Suitable In Vitro System for the Study of the Induction of Drug-Metabolizing Enzyme Systems. *Encyclopedia of Drug Metabolism and Interactions.* John Wiley & Sons, Inc.

Jackson, E.N., Schneider, J., Faux, L.R. & James, M.O., 2013. Isoform-selective glucuronidation of triclosan. *The FASEB Journal,* 27**,** 892.11-892.11.

Janmohamed, A., Hernandez, D., Phillips, I.R. & Shephard, E.A., 2004. Cell-, tissue-, sex- and developmental stage-specific expression of mouse flavin-containing monooxygenases (Fmos). *Biochem Pharmacol,* 68**,** 73-83.

Jones, H.M., Chen, Y., Gibson, C., Heimbach, T., Parrott, N., Peters, S.A., Snoeys, J., Upreti, V.V., Zheng, M. & Hall, S.D., 2015. Physiologically based pharmacokinetic modeling in drug discovery and development: a pharmaceutical industry perspective. *Clin Pharmacol Ther,* 97**,** 247-62.

Joseph, D., Puttaswamy, R.K. & Krovvidi, H., 2013. Non-respiratory functions of the lung. *Continuing Education in Anaesthesia Critical Care & Pain,* 13**,** 98-102.

Kanter, R., Monshouwer, M., Meijer, D. & Groothuis, G., 2002. Precision-cut organ slices as a tool to study toxicity and metabolism of xenobiotics with special reference to non-hepatic tissues. *Current drug metabolism,* 3**,** 39-59.

Kanto, J. & Gepts, E., 1989. Pharmacokinetic implications for the clinical use of propofol. *Clin Pharmacokinet,* 17**,** 308-26.

Karoly, E.D. & Rose, R.L., 2001. Sequencing, expression, and characterization of cDNA expressed flavin-containing monooxygenase 2 from mouse. *J Biochem Mol Toxicol,* 15**,** 300-8.

Kaye, B., Rance, D.J. & Waring, L., 1985. Oxidative metabolism of carbazeran in vitro by liver cytosol of baboon and man. *Xenobiotica,* 15**,** 237-42.

Khaybullina, D., Patel, A. & Zerilli, T., 2014. Riociguat (adempas): a novel agent for the treatment of pulmonary arterial hypertension and chronic thromboembolic pulmonary hypertension. *P T,* 39**,** 749-58.

Klingbeil, E.C., Hew, K.M., Nygaard, U.C. & Nadeau, K.C., 2014. Polycyclic aromatic hydrocarbons, tobacco smoke, and epigenetic remodeling in asthma. *Immunologic research,* 58**,** 369-373.

Krishna, D.R. & Klotz, U., 1994. Extrahepatic Metabolism of Drugs in Humans. *Clinical Pharmacokinetics,* 26**,** 144-160.

Krueger, S.K., Siddens, L.K., Martin, S.R., Yu, Z., Pereira, C.B., Cabacungan, E.T., Hines, R.N., Ardlie, K.G., Raucy, J.L. & Williams, D.E., 2004. Differences in FMO2*1 allelic frequency between Hispanics of Puerto Rican and Mexican descent. *Drug Metab Dispos,* 32**,** 1337-40.

Lakritz, J., Winder, B.S., Noorouz-Zadeh, J., Huang, T.L., Buckpitt, A.R., Hammock, B.D. & Plopper, C.G., 2000. Hepatic and pulmonary enzyme activities in horses. *Am J Vet Res,* 61**,** 152-7.

Lang, D.H. & Rettie, A.E., 2000a. In vitro evaluation of potential in vivo probes for human flavin-containing monooxygenase (FMO): metabolism of benzydamine and caffeine by FMO and P450 isoforms. *Br J Clin Pharmacol,* 50**,** 311-4.

Lang, D.H. & Rettie, A.E., 2000b. In vitro evaluation of potential in vivo probes for human flavin-containing monooxygenase (FMO): metabolism of benzydamine and caffeine by FMO and P450 isoforms. *Br. J. Clin. Pharmacol.,* 50**,** 311-4.

Lattard, V., Lachuer, J., Buronfosse, T., Garnier, F. & Benoit, E., 2002a. Physiological factors affecting the expression of FMO1 and FMO3 in the rat liver and kidney. *Biochem Pharmacol,* 63**,** 1453-64.

Lattard, V., Longin-Sauvageon, C., Krueger, S.K., Williams, D.E. & Benoit, E., 2002b. The FMO2 gene of laboratory rats, as in most humans, encodes a truncated protein. *Biochem Biophys Res Commun,* 292**,** 558-63.

Lattard, V., Longin-Sauvageon, C., Lachuer, J., Delatour, P. & Benoit, E., 2002c. Cloning, sequencing, and tissue-dependent expression of flavin-containing monooxygenase (FMO) 1 and FMO3 in the dog. *Drug Metab Dispos,* 30**,** 119-28.

Lauenstein, L., Switalla, S., Prenzler, F., Seehase, S., Pfennig, O., Forster, C., Fieguth, H., Braun, A. & Sewald, K., 2014. Assessment of immunotoxicity induced by chemicals in human precision-cut lung slices (PCLS). *Toxicol In Vitro,* 28**,** 588-99.

Lechner, A.J. & Mayo, M.M., 2015. Surfactant Biology and Lung Compliance. *In* A.J. Lechner, G.M. Matuschak & D.S. Brink (eds.) *Respiratory: An Integrated Approach to Disease.* New York, NY: McGraw-Hill Education.

Lekas, P., Tin, K.L., Lee, C. & Prokipcak, R.D., 2000. The human cytochrome P450 1A1 mRNA is rapidly degraded in HepG2 cells. *Arch. Biochem. Biophys.,* 384**,** 311-8.

Levitzky, M.G., 2013a. Chapter 1. Function and Structure of the Respiratory System. *Pulmonary Physiology, 8e.* New York, NY: The McGraw-Hill Companies.

Levitzky, M.G., 2013b. Chapter 4. Blood Flow to the Lung. *Pulmonary Physiology, 8e.* New York, NY: The McGraw-Hill Companies.

Levitzky, M.G., 2017. Function and Structure of the Respiratory System. *Pulmonary Physiology, 9e.* New York, NY: McGraw-Hill Education.

Li, J., Zhao, M., He, P., Hidalgo, M. & Baker, S.D., 2007. Differential metabolism of gefitinib and erlotinib by human cytochrome P450 enzymes. *Clin Cancer Res,* 13**,** 3731-7.

Li, X., Kamenecka, T.M. & Cameron, M.D., 2010. Cytochrome P450-Mediated Bioactivation of the Epidermal Growth Factor Receptor Inhibitor Erlotinib to a Reactive Electrophile. *Drug Metabolism and Disposition,* 38**,** 1238-1245.

Li, X.Q., Bjorkman, A., Andersson, T.B., Ridderstrom, M. & Masimirembwa, C.M., 2002. Amodiaquine clearance and its metabolism to N-desethylamodiaquine is mediated by CYP2C8: a new high affinity and turnover enzyme-specific probe substrate. *J. Pharmacol. Exp. Ther.,* 300**,** 399-407.

Liberati, T.A., Randle, M.R. & Toth, L.A., 2010. In vitro lung slices: a powerful approach for assessment of lung pathophysiology. *Expert. Rev. Mol. Diagn.,* 10**,** 501-8.

Lorenz, J., Glatt, H.R., Fleischmann, R., Ferlinz, R. & Oesch, F., 1984. Drug metabolism in man and its relationship to that in three rodent species: monooxygenase, epoxide hydrolase, and glutathione S-transferase activities in subcellular fractions of lung and liver. *Biochem. Med.,* 32**,** 43-56.

Lust, R.M., 2007. Pulmonary and Bronchial Circulation. *xPharm: The Comprehensive Pharmacology Reference.* New York: Elsevier, 1-8.

Macherey, A.-C. & Dansette, P.M., 2015. Chapter 25 - Biotransformations Leading to Toxic Metabolites: Chemical Aspects. *In* C.G. Wermuth, D. Aldous, P. Raboisson & D. Rognan (eds.) *The Practice of Medicinal Chemistry (Fourth Edition).* San Diego: Academic Press, 585-614.

Manevski, N., Swart, P., Balavenkatraman, K.K., Bertschi, B., Camenisch, G., Kretz, O., Schiller, H., Walles, M., Ling, B., Wettstein, R., Schaefer, D.J., Itin, P., Ashton-Chess, J., Pognan, F., Wolf, A. & Litherland, K., 2015. Phase II metabolism in human skin: skin explants show full coverage for glucuronidation, sulfation, N-acetylation, catechol methylation, and glutathione conjugation. *Drug Metab. Dispos.,* 43**,** 126-39.

Manevski, N., Troberg, J., Svaluto-Moreolo, P., Dziedzic, K., Yli-Kauhaluoma, J. & Finel, M., 2013. Albumin stimulates the activity of the human UDP-glucuronosyltransferases 1A7, 1A8, 1A10, 2A1 and 2B15, but the effects are enzyme and substrate dependent. *PLoS One,* 8**,** e54767.

Martignoni, M., Groothuis, G.M. & De Kanter, R., 2006. Species differences between mouse, rat, dog, monkey and human CYP-mediated drug metabolism, inhibition and induction. *Expert Opin Drug Metab Toxicol,* 2**,** 875-94.

Mccutcheon, J.E. & Marinelli, M., 2009. Age matters. *The European journal of neuroscience,* 29**,** 997-1014.

Mittal, B., Tulsyan, S., Kumar, S., Mittal, R.D. & Agarwal, G., 2015. Chapter Four - Cytochrome P450 in Cancer Susceptibility and Treatment. *In* G.S. Makowski (ed.) *Advances in Clinical Chemistry.* Elsevier, 77-139.

Monteil, C., Guerbet, M., Le Prieur, E., Morin, J.-P., M Jouany, J. & Fillastre, J.P., 1999. *Characterization of Precision-cut Rat Lung Slices in a Biphasic Gas/Liquid Exposure System: Effect of O2*.

Moorthy, B., Chu, C. & Carlin, D.J., 2015. Polycyclic Aromatic Hydrocarbons: From Metabolism to Lung Cancer. *Toxicological Sciences,* 145**,** 5-15.

Morin, J.P., Baste, J.M., Gay, A., Crochemore, C., Corbiere, C. & Monteil, C., 2013. Precision cut lung slices as an efficient tool for in vitro lung physio-pharmacotoxicology studies. *Xenobiotica,* 43**,** 63-72.

Mutch, E., Nave, R., Mccracken, N., Zech, K. & Williams, F., 2007. *The role of esterases in the metabolism of ciclesonide to desisobutyryl-ciclesonide in human tissue*.

Nakamura, H., Ariyoshi, N., Okada, K., Nakasa, H., Nakazawa, K. & Kitada, M., 2005. CYP1A1 is a major enzyme responsible for the metabolism of granisetron in human liver microsomes. *Curr Drug Metab,* 6**,** 469-80.

Nave, R., Fisher, R. & Zech, K., 2006. In Vitro metabolism of ciclesonide in human lung and liver precision-cut tissue slices. *Biopharm. Drug Dispos.,* 27**,** 197-207.

Nave, R., Watz, H., Hoffmann, H., Boss, H. & Magnussen, H., 2010. Deposition and metabolism of inhaled ciclesonide in the human lung. *Eur Respir J,* 36**,** 1113-9.

Nebert, D.W., Dalton, T.P., Okey, A.B. & Gonzalez, F.J., 2004. Role of aryl hydrocarbon receptor-mediated induction of the CYP1 enzymes in environmental toxicity and cancer. *J Biol Chem,* 279**,** 23847-50.

Nelson, K., Bobba, C., Eren, E., Spata, T., Tadres, M., Hayes, D., Jr., Black, S.M., Ghadiali, S. & Whitson, B.A., 2015. Method of isolated ex vivo lung perfusion in a rat model: lessons learned from developing a rat EVLP program. *J Vis Exp*.

Nemery, B. & Hoet, P.H., 1993. Use of isolated lung cells in pulmonary toxicology. *Toxicol In Vitro,* 7**,** 359-64.

Neuhaus, V., Schaudien, D., Golovina, T., Temann, U.A., Thompson, C., Lippmann, T., Bersch, C., Pfennig, O., Jonigk, D., Braubach, P., Fieguth, H.G., Warnecke, G., Yusibov, V., Sewald, K. & Braun, A., 2017. Assessment of long-term cultivated human precision-cut lung slices as an ex vivo system for evaluation of chronic cytotoxicity and functionality. *J Occup Med Toxicol,* 12**,** 13.

Niemeier, R.W., 1984. The isolated perfused lung. *Environ Health Perspect,* 56**,** 35-41.

Nijjar, M.S. & Ho, J.C., 1980. Isolation of plasma membranes from rat lungs: effect of age on the subcellular distribution of adenylate cyclase activity. *Biochim Biophys Acta,* 600**,** 238-43.

Nishimura, M. & Naito, S., 2006. Tissue-specific mRNA expression profiles of human phase I metabolizing enzymes except for cytochrome P450 and phase II metabolizing enzymes. *Drug Metab. Pharmacokinet.,* 21**,** 357-74.

Nishiyama, Y., Nakayama, S.M., Watanabe, K.P., Kawai, Y.K., Ohno, M., Ikenaka, Y. & Ishizuka, M., 2016. Strain differences in cytochrome P450 mRNA and protein expression, and enzymatic activity among Sprague Dawley, Wistar, Brown Norway and Dark Agouti rats. *J. Vet. Med. Sci.,* 78**,** 675-80.

O'neil, J.J., Sanford, R.L., Wasserman, S. & Tierney, D.F., 1977. Metabolism in rat lung tissue slices: technical factors. *J. Appl. Physiol. Respir. Environ. Exerc. Physiol.,* 43**,** 902-6.

Olsson, B., Bondesson, E., Borgström, L., Edsbäcker, S., Eirefelt, S., Ekelund, K., Gustavsson, L. & Hegelund-Myrbäck, T., 2011. Pulmonary Drug Metabolism, Clearance, and Absorption. *In* H.D.C. Smyth & A.J. Hickey (eds.) *Controlled Pulmonary Drug Delivery.* New York, NY: Springer New York, 21-50.

Ono, S., Hatanaka, T., Miyazawa, S., Tsutsui, M., Aoyama, T., Gonzalez, F.J. & Satoh, T., 1996. Human liver microsomal diazepam metabolism using cDNA-expressed cytochrome P450s: role of CYP2B6, 2C19 and the 3A subfamily. *Xenobiotica,* 26**,** 1155-66.

Pacifici, G.M., Franchi, M., Bencini, C., Repetti, F., Di Lascio, N. & Muraro, G.B., 1988. Tissue distribution of drug-metabolizing enzymes in humans. *Xenobiotica,* 18**,** 849-56.

Paine, M.F., Schmiedlin-Ren, P. & Watkins, P.B., 1999. Cytochrome P-450 1A1 expression in human small bowel: interindividual variation and inhibition by ketoconazole. *Drug Metab Dispos,* 27**,** 360-4.

Pang, K.S. & Rowland, M., 1977. Hepatic clearance of drugs. I. Theoretical considerations of a "well-stirred" model and a "parallel tube" model. Influence of hepatic blood flow, plasma and blood cell binding, and the hepatocellular enzymatic activity on hepatic drug clearance. *J Pharmacokinet Biopharm,* 5**,** 625-53.

Parrish, A.R., Gandolfi, A.J. & Brendel, K., 1995. Precision-cut tissue slices: applications in pharmacology and toxicology. *Life Sci,* 57**,** 1887-901.

Patwa, A. & Shah, A., 2015. Anatomy and physiology of respiratory system relevant to anaesthesia. *Indian J Anaesth,* 59**,** 533-41.

Petrov, D., Pedros, I., De Lemos, M.L., Pallas, M., Canudas, A.M., Lazarowski, A., Beas-Zarate, C., Auladell, C., Folch, J. & Camins, A., 2014. Mavoglurant as a treatment for Parkinson's disease. *Expert Opin Investig Drugs,* 23**,** 1165-79.

Phillips, I.R. & Shephard, E.A., 2017. Drug metabolism by flavin-containing monooxygenases of human and mouse. *Expert Opin. Drug Metab. Toxicol.,* 13**,** 167-181.

Plopper, C.G., 1996. Structure and Function of the Lung. *In* T.C. Jones, D.L. Dungworth & U. Mohr (eds.) *Respiratory System.* Berlin, Heidelberg: Springer Berlin Heidelberg, 135-150.

Poulin, P., Kenny, J.R., Hop, C.E. & Haddad, S., 2012. In vitro-in vivo extrapolation of clearance: modeling hepatic metabolic clearance of highly bound drugs and comparative assessment with existing calculation methods. *J Pharm Sci,* 101**,** 838-51.

Powley, M.W. & Carlson, G.P., 2002. Benzene metabolism by the isolated perfused lung. *Inhal Toxicol,* 14**,** 569-84.

Price, R.J., Renwick, A.B., Beamand, J.A., Esclangon, F., Wield, P.T., Walters, D.G. & Lake, B.G., 1995. Comparison of the metabolism of 7-ethoxycoumarin and coumarin in precision-cut rat liver and lung slices. *Food Chem Toxicol,* 33**,** 233-7.

Price, R.J., Renwick, A.B., Walters, D.G., Young, P.J. & Lake, B.G., 2004. Metabolism of nicotine and induction of CYP1A forms in precision-cut rat liver and lung slices. *Toxicol In Vitro,* 18**,** 179-85.

Pushparajah, D.S., Umachandran, M., Plant, K.E., Plant, N. & Ioannides, C., 2007. Evaluation of the precision-cut liver and lung slice systems for the study of induction of CYP1, epoxide hydrolase and glutathione S-transferase activities. *Toxicology,* 231**,** 68-80.

Quane, P.A., Graham, G.G. & Ziegler, J.B., 1998. Pharmacology of benzydamine. *Inflammopharmacology,* 6**,** 95-107.

Rau, J.L., 2005. The inhalation of drugs: advantages and problems. *Respir. Care Clin. N. Am.,* 50**,** 367-82.

Raunio, H., Hakkola, J., Hukkanen, J., Lassila, A., Päivärinta, K., Pelkonen, O., Anttila, S., Piipari, R., Boobis, A. & Edwards, R.J., 1999. Expression of xenobiotic-metabolizing CYPs in human pulmonary tissue. *Experimental and Toxicologic Pathology,* 51**,** 412-417.

Rawden, H.C., Kokwaro, G.O., Ward, S.A. & Edwards, G., 2000. Relative contribution of cytochromes P-450 and flavin-containing monoxygenases to the metabolism of albendazole by human liver microsomes. *Br J Clin Pharmacol,* 49**,** 313-22.

Ridgway, D., Tuszynski, J.A. & Tam, Y.K., 2003. Reassessing models of hepatic extraction. *J Biol Phys,* 29**,** 1-21.

Ripp, S.L., Itagaki, K., Philpot, R.M. & Elfarra, A.A., 1999. Species and sex differences in expression of flavin-containing monooxygenase form 3 in liver and kidney microsomes. *Drug Metab. Dispos.,* 27**,** 46-52.

Roberts, M.S. & Rowland, M., 1986a. A dispersion model of hepatic elimination: 1. Formulation of the model and bolus considerations. *J Pharmacokinet Biopharm,* 14**,** 227-60.

Roberts, M.S. & Rowland, M., 1986b. A dispersion model of hepatic elimination: 2. Steady-state considerations-influence of hepatic blood flow, binding within blood, and hepatocellular enzyme activity. *Journal of Pharmacokinetics and Biopharmaceutics,* 14**,** 261-288.

Roth, R.A. & Vinegar, A., 1990. Action by the lungs on circulating xenobiotic agents, with a case study of physiologically based pharmacokinetic modeling of benzo(a)pyrene disposition. *Pharmacol Ther,* 48**,** 143-55.

Roth, R.A. & Wiersma, D.A., 1979. Role of the lung in total body clearance of circulating drugs. *Clin Pharmacokinet,* 4**,** 355-67.

Saladin, K.S., Gan, C.A. & Cushman, H.N., 2018. *Anatomy & physiology : the unity of form and function*.

Saleh, S., Becker, C., Frey, R. & Muck, W., 2016. Population pharmacokinetics of single-dose riociguat in patients with renal or hepatic impairment. *Pulm Circ,* 6**,** S75-85.

Samuel, J.J., Nick, A., Doug, B., Ilaria, B., James, G., Lamia, H., Alan, H., Judy, L., Anja, P., Paul, P., Andrew, R., Alison, R., Michelle, S., Carol, S., Mark, Y. & Kathryn, C., 2016. Does age matter? The impact of rodent age on study outcomes. *Laboratory Animals,* 51**,** 160-169.

Sanderink, G.-J., Bournique, B., Stevens, J., Petry, M. & Martinet, M., 1997. Involvement of Human CYP1A Isoenzymes in the Metabolism and Drug Interactions of Riluzole In Vitro . *Journal of Pharmacology and Experimental Therapeutics,* 282**,** 1465-1472.

Sanderson, M.J., 2011. Exploring lung physiology in health and disease with lung slices. *Pulm. Pharmacol. Ther.,* 24**,** 452-65.

Schmitz, A., Portier, C.J., Thormann, W., Theurillat, R. & Mevissen, M., 2008. Stereoselective biotransformation of ketamine in equine liver and lung microsomes. *J Vet Pharmacol Ther,* 31**,** 446-55.

Segre, G. & Hammarstrom, S., 1985. Aspects of the mechanisms of action of benzydamine. *Int J Tissue React,* 7**,** 187-93.

Sharan, S. & Nagar, S., 2013. Pulmonary metabolism of resveratrol: in vitro and in vivo evidence. *Drug Metab Dispos,* 41**,** 1163-9.

Shehata, H., 2010. Chapter Twelve - Drugs and drug therapy. *In* P. Bennett & C. Williamson (eds.) *Basic Science in Obstetrics and Gynaecology (Fourth Edition).* Churchill Livingstone, 259-277.

Siminski, J.T., Kavanagh, T.J., Chi, E. & Raghu, G., 1992. Long-term maintenance of mature pulmonary parenchyma cultured in serum-free conditions. *American Journal of Physiology-Lung Cellular and Molecular Physiology,* 262**,** L105-L110.

Simionescu, M., 1980. Ultrastructural organization of the alveolar-capillary unit. *Ciba Found Symp,* 78**,** 11-36.

Sly, P.D. & Collins, R.A., 2008. Chapter 7 - Applied Clinical Respiratory Physiology A2 - Taussig, Lynn M. *In* L.I. Landau (ed.) *Pediatric Respiratory Medicine (Second Edition).* Philadelphia: Mosby, 73-88.

Smith, G.B.J., Harper, P.A., Wong, J.M.Y., Lam, M.S.M., Reid, K.R., Petsikas, D. & Massey, T.E., 2001. Human Lung Microsomal Cytochrome P4501A1 (CYP1A1) Activities. *Cancer Epidemiol Biomarkers Prev,* 10**,** 839-853.

Smith, P.F., Gandolfi, A.J., Krumdieck, C.L., Putnam, C.W., Zukoski, C.F., 3rd, Davis, W.M. & Brendel, K., 1985. Dynamic organ culture of precision liver slices for in vitro toxicology. *Life Sci.,* 36**,** 1367-75.

Smith, P.F., Krack, G., Mckee, R.L., Johnson, D.G., Gandolfi, A.J., Hruby, V.J., Krumdieck, C.L. & Brendel, K., 1986. Maintenance of adult rat liver slices in dynamic organ culture. *In Vitro Cell Dev. Biol.,* 22**,** 706-12.

Somers, G.I., Lindsay, N., Lowdon, B.M., Jones, A.E., Freathy, C., Ho, S., Woodrooffe, A.J., Bayliss, M.K. & Manchee, G.R., 2007. A comparison of the expression and metabolizing activities of phase I and II enzymes in freshly isolated human lung parenchymal cells and cryopreserved human hepatocytes. *Drug Metab. Dispos.,* 35**,** 1797-805.

Sourial, M., Cheng, C. & Doering, L.C., 2013. Progress toward therapeutic potential for AFQ056 in Fragile X syndrome. *Journal of Experimental Pharmacology,* 5**,** 45-54.

Stone, K.C., Mercer, R.R., Gehr, P., Stockstill, B. & Crapo, J.D., 1992. Allometric relationships of cell numbers and size in the mammalian lung. *Am J Respir Cell Mol Biol,* 6**,** 235-43.

Stormer, E., Roots, I. & Brockmoller, J., 2000. Benzydamine N-oxidation as an index reaction reflecting FMO activity in human liver microsomes and impact of FMO3 polymorphisms on enzyme activity. *Br J Clin Pharmacol,* 50**,** 553-61.

Testa, B. & Clement, B., 2015. Chapter 24 - Biotransformation Reactions and their Enzymes. *In* C.G. Wermuth, D. Aldous, P. Raboisson & D. Rognan (eds.) *The Practice of Medicinal Chemistry (Fourth Edition).* San Diego: Academic Press, 561-584.

Thomsen, R., Rasmussen, H.B., Linnet, K. & Consortium, I., 2014. In vitro drug metabolism by human carboxylesterase 1: focus on angiotensin-converting enzyme inhibitors. *Drug Metab. Dispos.,* 42**,** 126-33.

Tillement, J.P. & Tremblay, D., 2007. 5.02 - Clinical Pharmacokinetic Criteria for Drug Research. *In* J.B. Taylor & D.J. Triggle (eds.) *Comprehensive Medicinal Chemistry II.* Oxford: Elsevier, 11-30.

Tolson, A.H. & Wang, H., 2010. Regulation of drug-metabolizing enzymes by xenobiotic receptors: PXR and CAR. *Advanced drug delivery reviews,* 62**,** 1238-1249.

Tronde, A., Norden, B., Jeppsson, A.B., Brunmark, P., Nilsson, E., Lennernas, H. & Bengtsson, U.H., 2003. Drug absorption from the isolated perfused rat lung--correlations with drug physicochemical properties and epithelial permeability. *J Drug Target,* 11**,** 61-74.

Uchaipichat, V., Mackenzie, P.I., Guo, X.-H., Gardner-Stephen, D., Galetin, A., Houston, J.B. & Miners, J.O., 2004. Human UDP-Glucuronlytransferases: Isoform selectivity and kinetics of 4-Methylumbellifferone and 1-Naphtol Glucuronidation, effects of organic solvents, and inhibition by Diclofenac and Probenecid. *Drug Metab. Dispos.,* 32**,** 413-423.

Umachandran, M., Howarth, J. & Ioannides, C., 2004. Metabolic and structural viability of precision-cut rat lung slices in culture. *Xenobiotica,* 34**,** 771-80.

Umachandran, M. & Ioannides, C., 2006. Stability of cytochromes P450 and phase II conjugation systems in precision-cut rat lung slices cultured up to 72 h. *Toxicology,* 224**,** 14-21.

Van Bezooijen, C.F.A., Horbach, G.J.M.J. & Hollander, C.F., 1986. The Effect of Age on Rat Liver Drug Metabolism. *In* D. Platt (ed.) *Drugs and Aging.* Berlin, Heidelberg: Springer Berlin Heidelberg, 45-55.

Van De Kerkhof, E.G., De Graaf, I.A., Ungell, A.L. & Groothuis, G.M., 2008. Induction of metabolism and transport in human intestine: validation of precision-cut slices as a tool to study induction of drug metabolism in human intestine in vitro. *Drug Metab Dispos,* 36**,** 604-13.

Walles, M., Wolf, T., Jin, Y., Ritzau, M., Leuthold, L.A., Krauser, J., Gschwind, H.P., Carcache, D., Kittelmann, M., Ocwieja, M., Ufer, M., Woessner, R., Chakraborty, A. & Swart, P., 2013. Metabolism and disposition of the metabotropic glutamate receptor 5 antagonist (mGluR5) mavoglurant (AFQ056) in healthy subjects. *Drug Metab. Dispos.,* 41**,** 1626-41.

Walsh, A.A., Szklarz, G.D. & Scott, E.E., 2013. Human cytochrome P450 1A1 structure and utility in understanding drug and xenobiotic metabolism. *J Biol Chem,* 288**,** 12932-43.

Wang, L.Q., Falany, C.N. & James, M.O., 2004. Triclosan as a substrate and inhibitor of 3'-phosphoadenosine 5'-phosphosulfate-sulfotransferase and UDP-glucuronosyl transferase in human liver fractions. *Drug Metab. Dispos.,* 32**,** 1162-9.

Whetstine, J.R., Yueh, M.F., Mccarver, D.G., Williams, D.E., Park, C.S., Kang, J.H., Cha, Y.N., Dolphin, C.T., Shephard, E.A., Phillips, I.R. & Hines, R.N., 2000. Ethnic differences in human flavin-containing monooxygenase 2 (FMO2) polymorphisms: detection of expressed protein in African-Americans. *Toxicol Appl Pharmacol,* 168**,** 216-24.

Winkler, J., Hochhaus, G. & Derendorf, H., 2004. How the Lung Handles Drugs. *Proceedings of the American Thoracic Society,* 1**,** 356-363.

Wohak, L.E., Krais, A.M., Kucab, J.E., Stertmann, J., Ovrebo, S., Seidel, A., Phillips, D.H. & Arlt, V.M., 2016. Carcinogenic polycyclic aromatic hydrocarbons induce CYP1A1 in human cells via a p53-dependent mechanism. *Arch Toxicol,* 90**,** 291-304.

Woo, M.S. & Szmuszkovicz, J.R., 2009. Chapter 4 - Pulmonary Manifestations of Cardiac Diseases A2 - Turcios, Nelson L. *In* R.J. Fink (ed.) *Pulmonary Manifestations of Pediatric Diseases.* Philadelphia: W.B. Saunders, 79-97.

Woods, H.F., Meredith, A., Tucker, G.T. & Shortland, J.R., 1980. Methods for the study of lung metabolism. *Ciba Found Symp,* 78**,** 61-83.

Wynalda, M.A., Hutzler, J.M., Koets, M.D., Podoll, T. & Wienkers, L.C., 2003. In vitro metabolism of clindamycin in human liver and intestinal microsomes. *Drug Metab Dispos,* 31**,** 878-87.

Yamamoto, Y., Tanaka, A., Kanamaru, A., Tanaka, S., Tsubone, H., Atoji, Y. & Suzuki, Y., 2003. Morphology of aging lung in F344/N rat: Alveolar size, connective tissue, and smooth muscle cell markers. *The Anatomical Record Part A: Discoveries in Molecular, Cellular, and Evolutionary Biology,* 272A**,** 538-547.

Yang, J., Jamei, M., Yeo, K.R., Rostami-Hodjegan, A. & Tucker, G.T., 2007. Misuse of the Well-Stirred Model of Hepatic Drug Clearance. *Drug Metabolism and Disposition,* 35**,** 501-502.

Yilmaz, Y., Umehara, K., Williams, G., Faller, T., Schiller, H., Walles, M., Kraehenbuehl, S., Camenisch, G. & Manevski, N., 2017. Assessment of the pulmonary CYP1A1 metabolism of mavoglurant (AFQ056) in rat. *Xenobiotica***,** 1-11.

Yilmaz, Y., Williams, G., Manevski, N., Walles, M., Krahenbuhl, S. & Camenisch, G., 2018. Functional assessment of rat pulmonary flavin-containing monooxygenase activity. *Xenobiotica***,** 1-10.

Yuan, R., Madani, S., Wei, X.X., Reynolds, K. & Huang, S.M., 2002. Evaluation of cytochrome P450 probe substrates commonly used by the pharmaceutical industry to study in vitro drug interactions. *Drug Metab. Dispos.,* 30**,** 1311-9.

Zhang, J.Y., Wang, Y. & Prakash, C., 2006. Xenobiotic-metabolizing enzymes in human lung. *Curr. Drug Metab.,* 7**,** 939-48.